11-2015

Challenges in the Pharmacokinetics of Therapeutic Proteins

Wararat Limothai
University of Tennessee Health Science Center

Challenges in the Pharmacokinetics of Therapeutic Proteins

Abstract

Due to the complex structure and complicated disposition pattern of therapeutic macromolecules, their pharmacokinetic interpretation has many challenges. Two of these challenges were investigated in this dissertation: 1) the error of classical bioavailability assessment observed during subcutaneous (SC) administration of therapeutic macromolecules that undergo target-mediated drug disposition (TMDD) and 2) the ontogeny of the neonatal Fc receptor (FcRn) expression along with its effect on the pharmacokinetics of monoclonal antibodies (mAbs) during development.

TMDD often well describes the pharmacokinetics of therapeutic proteins that have high specificity and affinity of binding to their target receptors. The target receptors can be saturated by therapeutic proteins under therapeutic concentration due to their limited expression and availability in the body. Consequently, clearance through this pathway will reach its maximum and nonlinear pharmacokinetics will be observed upon further increasing dose if TMDD is a major elimination process. This, in turn, will impact the bioavailability estimation. Bioavailability estimations based on the classic AUC approach can be erroneous in this situation, mainly due to the incorrect assumption of dose-independent constant clearance that cannot be applied to therapeutic proteins that undergo TMDD. To shed light on this issue, a simulation study was performed with two model drugs: filgrastim and denosumab. Their published structural pharmacokinetic models and model parameters were employed in the simulations of plasma concentration-time profiles at different IV and SC doses. The bioavailability was calculated as the ratio of dose-normalized AUC after SC administration to that after IV administration.

The overestimation was extreme when high SC and low IV doses of both protein drugs were used for the estimations, whereas excessive underestimation was observed with the combination of low SC and high IV doses. These biases in the bioavailability estimation resulted from the transition from low plasma concentration (at low doses) to high plasma concentration (at high doses), which shifted the major elimination pathway from TMDD to the unspecific linear clearance pathway. The changes in clearance resulted in parallel changes in dosenormalized AUCs and were very dynamic in the dose range of 0.1 – 5 μg/kg for filgrastim and below 60 mg for denosumab; thus caution is necessary when bioavailability of these two therapeutic proteins is estimated in these dose ranges using conventional method. To minimize the error of conventional bioavailability estimation of protein drugs that undergo TMDD, the bioavailability should be estimated at similar IV and SC doses or the assessment should be performed in dose ranges that yield constant dose-normalized AUCs (0.01 – 0.1 μg/kg or 5 – 10000 μg/kg for filgrastim, and 60 – 210 mg for denosumab). Moreover, an alternative estimation method could be applied, which determines the ratio of IV and SC doses that generate equally shaped concentration-time profile by applying a variable rate IV infusion, thereby resulting in equal AUCs as suggested by others.

FcRn has been evidenced as a salvage pathway from lysosomal clearance for mAbs and Fc conjugated proteins; thus it can prolong the existence of these protein drugs in systemic circulation. The ontogeny of FcRn expression and its effect on the pharmacokinetics of mAbs should be of special concern if therapeutic mAbs are used in both pediatrics and adults. The down-regulation of FcRn during the development may shortened the half-life of therapeutic mAbs observed in adults. To address this problem, FcRn expression was quantified in various organs of C57BL/6J mice from postnatal days 2 through 70, the pharmacokinetics of AMG589 were studied in different age groups of C57BL/6J mice, and the correlation between the FcRn expression levels and the pharmacokinetics of AMG589 at various developmental stages of mice were explored using a nonlinear-mixed effects modeling-based population pharmacokinetic approach.

FcRn showed ontogenetic changes in liver, lungs, and kidneys. Two-fold increases in FcRn expression

were observed in liver and lungs of 10-day-old mice, whereas FcRn expression in the kidneys was doubled in 10- and 42-day-old mice. However, the ontogeny of FcRn expression could not be correlated to the prolonged persistence of AMG589 observed in 42 day old mice. A population pharmacokinetic approach revealed that after accounting for the effect of body weight by allometric scaling, age and FcRn expression in skin influenced the pharmacokinetics of AMG589 in different age groups of mice. Decreasing volume of distribution of AMG589 was observed during development. Interestingly, clearance of AMG589 was negatively correlated with the expression of FcRn in the skin, even though FcRn expression in skin did not show any ontogeny. These results suggest that body weight, age, and FcRn expression in skin could affect the pharmacokinetics of fully-human mAbs. However, regardless of the species difference in physiology, body weight should be considered during dosage regimen design, especially for pediatric patients who show a highly dynamic change in body size at early age.

In summary, the findings in this dissertation have pointed out the weakness of the classical bioavailability estimation for protein drugs that undergo TMDD and have determined the factors that should be considered for dose adjustments of therapeutic mAbs in different-aged populations.

Document Type
Dissertation

Degree Name
Doctor of Philosophy (PhD)

Program
Pharmaceutical Sciences

Research Advisor
Bernd Meibohm, Ph.D., FCP

Keywords
Bioavailability, FcRn, Neonatal Fc receptor, Ontogeny, Target-mediated drug disposition, TMDD

Subject Categories
Medicinal and Pharmaceutical Chemistry | Medicine and Health Sciences | Pharmacy and Pharmaceutical Sciences

Challenges in the Pharmacokinetics of Therapeutic Proteins

A Dissertation
Presented for
The Graduate Studies Council
The University of Tennessee
Health Science Center

In Partial Fulfillment
Of the Requirements for the Degree
Doctor of Philosophy
From The University of Tennessee

By
Wararat Limothai
December 2015

DEDICATION

I would like to dedicate this dissertation work to my family and friends. A special feeling of gratitude to my loving parents and my lovely sister, Waralak, for their love, understanding, and support. A special appreciation to the McDonald's family for making my stay in Memphis a warmly memorable experience. A special thanks to my best friends, Sumalee Thitinan, and Bancha Chuasuwan, for their words of encouragement and supportive suggestions throughout these years of the doctorate program. I also want to thank all my friends in Memphis for making my stay in Memphis a wonderful experience. Finally, I would like to convey my gratitude to all friends and colleagues in Thailand for their understanding and supportive environment during my writing period.

ACKNOWLEDGEMENTS

This dissertation would not have been possible and completed without the support of many people. First and foremost, I would like to express my deepest gratitude to my advisor, Dr. Bernd Meibohm, for his excellent counseling, patience, and providing me an opportunity and excellent atmosphere for doing research. He has widened my perspectives and introduced me to the world of pharmacometrics. His incredible profession has guided me through all the conundrums I experienced during completion of my dissertation.

I would like to thank all of my current committee members, Dr. Sarka Beranova, Dr. Marc Gastonguay, Dr. George C. Wood, and Dr. Charles R. Yates, for their advice and guiding my research for the past several years. I would like to give my special thanks to Dr. Gastonguay for his input regarding the population pharmacokinetic modeling. I also would like to thank my former committee member, Dr. Ram Mahato, for his advice during his serving as my committee member.

I would like to express my appreciation to the staff of the animal facility, especially Dr. David Hamilton, Ernestine Hayes, and Dr. Yada Akkhawattanangkul for their professional support with the newborn mouse study. I also owe a special thanks to Dr. Dora Babu Madhura for his professional help with the mouse study for FcRn extraction. I would like to express my sincere gratitude to Amgen, Inc. especially Dr. Vibha Jawa and Dr. Theingi Thway for providing me the model drug for the pharmacokinetic study, the analysis of the serum samples, and the ELISA results.

I would like to thank all my friends, former and current colleagues, Dr. Yi Zhang, Dr. Margaret Thomson, Dr. Ashit Trivedi, Chetan Rathi, Dr. Josiah Ryman, Dr. Dora Babu Madhura, Jordan Toutounchian, Dr. Pavan Vaddady, Dr. Nathaniel Dirks, Dr. Satyendra Suryawanshi, Dr. Lei Diao, Dr. Sumit Rawal, and Dr. Chaela Presley for their friendship, helpful discussion, and support. I would like to give my special thanks to Dr. Yi Zhang, Dr. Ashit Trivedi, and Chetan Rathi who always offered their help and always provided me with some helpful suggestions.

I also would like to thank all administrative staff, Benita Williams, Brenda Thornton, Corliss Finlay, Cynthia Crowe, and former staff members Faith B. Barcroft and Felicia Martin for their suggestions and administrative help to make my work go smoothly.

Finally, I would like to thank the Government Pharmaceutical Organization in Thailand for their financial support of my Ph.D. study.

Without all this support, I would not have reached this point of accomplishment.

ABSTRACT

Due to the complex structure and complicated disposition pattern of therapeutic macromolecules, their pharmacokinetic interpretation has many challenges. Two of these challenges were investigated in this dissertation: 1) the error of classical bioavailability assessment observed during subcutaneous (SC) administration of therapeutic macromolecules that undergo target-mediated drug disposition (TMDD) and 2) the ontogeny of the neonatal Fc receptor (FcRn) expression along with its effect on the pharmacokinetics of monoclonal antibodies (mAbs) during development.

TMDD often well describes the pharmacokinetics of therapeutic proteins that have high specificity and affinity of binding to their target receptors. The target receptors can be saturated by therapeutic proteins under therapeutic concentration due to their limited expression and availability in the body. Consequently, clearance through this pathway will reach its maximum and nonlinear pharmacokinetics will be observed upon further increasing dose if TMDD is a major elimination process. This, in turn, will impact the bioavailability estimation. Bioavailability estimations based on the classic AUC approach can be erroneous in this situation, mainly due to the incorrect assumption of dose-independent constant clearance that cannot be applied to therapeutic proteins that undergo TMDD. To shed light on this issue, a simulation study was performed with two model drugs: filgrastim and denosumab. Their published structural pharmacokinetic models and model parameters were employed in the simulations of plasma concentration-time profiles at different IV and SC doses. The bioavailability was calculated as the ratio of dose-normalized AUC after SC administration to that after IV administration.

The overestimation was extreme when high SC and low IV doses of both protein drugs were used for the estimations, whereas excessive underestimation was observed with the combination of low SC and high IV doses. These biases in the bioavailability estimation resulted from the transition from low plasma concentration (at low doses) to high plasma concentration (at high doses), which shifted the major elimination pathway from TMDD to the unspecific linear clearance pathway. The changes in clearance resulted in parallel changes in dose-normalized AUCs and were very dynamic in the dose range of 0.1 – 5 μg/kg for filgrastim and below 60 mg for denosumab; thus caution is necessary when bioavailability of these two therapeutic proteins is estimated in these dose ranges using conventional method. To minimize the error of conventional bioavailability estimation of protein drugs that undergo TMDD, the bioavailability should be estimated at similar IV and SC doses or the assessment should be performed in dose ranges that yield constant dose-normalized AUCs (0.01 – 0.1 μg/kg or 5 – 10000 μg/kg for filgrastim, and 60 – 210 mg for denosumab). Moreover, an alternative estimation method could be applied, which determines the ratio of IV and SC doses that generate equally shaped concentration-time profile by applying a variable rate IV infusion, thereby resulting in equal AUCs as suggested by others.

FcRn has been evidenced as a salvage pathway from lysosomal clearance for mAbs and Fc conjugated proteins; thus it can prolong the existence of these protein drugs

in systemic circulation. The ontogeny of FcRn expression and its effect on the pharmacokinetics of mAbs should be of special concern if therapeutic mAbs are used in both pediatrics and adults. The down-regulation of FcRn during the development may shortened the half-life of therapeutic mAbs observed in adults. To address this problem, FcRn expression was quantified in various organs of C57BL/6J mice from postnatal days 2 through 70, the pharmacokinetics of AMG589 were studied in different age groups of C57BL/6J mice, and the correlation between the FcRn expression levels and the pharmacokinetics of AMG589 at various developmental stages of mice were explored using a nonlinear-mixed effects modeling-based population pharmacokinetic approach.

FcRn showed ontogenetic changes in liver, lungs, and kidneys. Two-fold increases in FcRn expression were observed in liver and lungs of 10-day-old mice, whereas FcRn expression in the kidneys was doubled in 10- and 42-day-old mice. However, the ontogeny of FcRn expression could not be correlated to the prolonged persistence of AMG589 observed in 42 day old mice. A population pharmacokinetic approach revealed that after accounting for the effect of body weight by allometric scaling, age and FcRn expression in skin influenced the pharmacokinetics of AMG589 in different age groups of mice. Decreasing volume of distribution of AMG589 was observed during development. Interestingly, clearance of AMG589 was negatively correlated with the expression of FcRn in the skin, even though FcRn expression in skin did not show any ontogeny. These results suggest that body weight, age, and FcRn expression in skin could affect the pharmacokinetics of fully-human mAbs. However, regardless of the species difference in physiology, body weight should be considered during dosage regimen design, especially for pediatric patients who show a highly dynamic change in body size at early age.

In summary, the findings in this dissertation have pointed out the weakness of the classical bioavailability estimation for protein drugs that undergo TMDD and have determined the factors that should be considered for dose adjustments of therapeutic mAbs in different-aged populations.

TABLE OF CONTENTS

LIST OF TABLES

LIST OF FIGURES

LIST OF ABBREVIATIONS

θ	Typical value of parameter estimate
β_2m	β_2 microglobulin
ε_{ij}	Residual error
λ_z	Elimination rate constant obtained from non-compartmental analysis
η	Between-subject variability
σ^2	Variance
ω^2	Between-subject variance estimate
τ	Transit time for drug from lymph system to systemic circulation
A_{abs}	Amount of G-CSF absorbed
AAD	Age at dosing
A_C	Amount of denosumab in central compartment
A_D	Amount of denosumab in depot compartment
ADA	Anti-drug antibodies
A_p	Amount of denosumab in peripheral compartment
AR	Amount of free receptors for G-CSF
ARC	Amount of G-CSF-receptor complex
AR_0	Endogenous amount of G-CSF receptors in blood and bone marrow
ARC_0	Pre-treatment amount of G-CSF bound receptor complexes
A_s	Amount of G-CSF in the serum
A_{tot}	Total amount of denosumab in the serum
AUC	Area under the concentration-time curve

AUC_D	Dose normalized AUC
AUC_{IV}	Area under the concentration-time curve obtained from intravenous administration
AUC_{SC}	Area under the concentration-time curve obtained from subcutaneous administration
b	Allometric exponent
BLQ	Below limit of quantitation
BMD	Bone mineral density
BSA	Body surface area
BSV	Between-subject variability
BW	Body weight
C	The central compartment for denosumab
C_{free}	Serum free denosumab concentration
CI	Confidence interval
CL	Average clearance
CL/F	Apparent clearance
CL_{lin}	Linear clearance pathway
CL_{tot}	Total clearance of denosumab
C_{max}	Peak plasma concentration
COV	Covariate of interest
C_p	Drug concentration in plasma
C_s	Concentration of G-CSF in the serum
$C_{s,0}$	Endogenous serum concentration of G-CSF
C_t	Drug concentration in tissue

CYP	Cytochrome P450
D	The depot compartment for denosumab
D_{IV}	Intravenous dose
D_{PO}	Oral dose
DR	Drug-receptor complex
D_{SC}	Subcutaneous dose
D_2	Duration of zero-order absorption of r-metHuG-CSF
F	Absolute bioavailability
Fab	Antigen-binding fragment
Fc	Crystallizable fragment
FcRn	Neonatal Fc receptor
FOCE	First-order conditional estimation
F_{ref}	Reference bioavailability
F_{sim}	Bioavailability calculated from the simulated data
F_1	Bioavailability of the first-order absorption of r-metHuG-CSF
F_2	Bioavailability of zero-order absorption of r-metHuG-CSF
GAPDH	Glyceraldehyde 3-phosphate dehydrogenase
G-CSF	Granulocyte colony stimulating factor
GFR	Glomerular filtration rate
IgA	Immunoglobulin A
IgD	Immunoglobulin D
IgE	Immunoglobulin E
IgG	Immunoglobulin G

IgM	Immunoglobulin M
IM	Intramuscular
IV	Intravenous
K_a	First-order absorption rate constant
K_D	The equilibrium dissociation constant
kDa	Kilodaltons
K_{deg}	First-order degradation rate constant
K_e	First-order elimination rate constant
K_{int}	First-order internalization rate constant
$K_{G\text{-}CSF}$	Zero-order production rate of G-CSF
K_{lymph}	Elimination rates during lymphatic transport
K_m	Concentration at half-maximum elimination rate
K_{pt}	First-order distribution rate constant from plasma to tissue
K_{off}	First-order dissociation rate constant
K_{on}	Second-order association rate constant
K_{ss}	The quasi-steady-state dissociation constant
K_{syn}	Zero-order synthesis rate constant
K_{tp}	First-order distribution rate constant from tissue to plasma
K_0	Infusion rate
LDL	Low-density lipoprotein
LLOQ	Lower limit of quantitation
LRP	LDL-receptor-related protein
mAbs	Monoclonal antibodies

MHC	Major histocompatibility
OFV	Objective function value
P	The peripheral compartment for denosumab
PBS	Phosphate-buffered saline
PK/PD	Pharmacokinetics and pharmacodynamics
Q	Intercompartmental clearance
R	RANKL free ligand
R_0	Baseline RANKL level
RANKL	Receptor activator of nuclear factor κ-B ligand
RC	Denosumab-RANKL complex
RES	Reticuloendothelial system
r-metHuG-CSF	Recombinant methionyl human granulocyte colony stimulating factor
RSD	Relative standard deviation
RSE	Relative standard error
R_{tot}	Total amount of RANKL receptors which include free and bound receptors
SC	Subcutaneous
TAD	Time after dosing
t_{inf}	Infusion duration
TMDD	Target-mediated drug disposition
$t_{1/2}$	Half-life
V or V_d	Volume of distribution
V/F	Apparent volume of distribution

V_{max}	Maximum elimination rate
V_{ss}	Volume of distribution at steady-state
V_1	Central volume of distribution
V_2	Peripheral volume of distribution
W_{max}	Maximum body weight

CHAPTER 1. BACKGROUND

Advances in biotechnology have created a new era of therapeutic molecules, transitioning from chemically-defined small molecules to biotechnologically-derived large proteins. The application of biotechnologically-derived products as therapeutics has gained much attention due to several advantages they have over small molecule drugs. These advantages include a highly-specific and complex set of functions that cannot be mimicked by simple chemical compounds, a low propensity of adverse events due to their oftentimes highly-specific effect on a defined target with limited or no off-target activity, and far-reaching patent protection as a consequence of the unique forms and functions defined by their complex *in vivo* production process [1]. These superiorities have resulted in the expanded use of therapeutic proteins in clinical therapy.

Similar to small molecule drugs, successful therapy with therapeutic proteins can only be achieved with an effective dosage regimen that has been designed with the appreciation and application of pharmacokinetic and pharmacodynamic principles. The challenges in the pharmacokinetics and pharmacodynamics of protein drugs arise from some of their specific properties, including the structural similarity to endogenous proteins and nutrients, their intimate involvement in physiologic processes on the molecular level that often include regulatory feedback mechanisms, and their large molecular weight and macromolecule character [2, 3]. To gain insight into the pharmacokinetic properties of protein therapeutics, all relevant processes are described in general in this chapter as background for further discussion in subsequent chapters. Further interest in the pharmacokinetics of therapeutic proteins should be referred to several extensive reviews that were used as a basis for this chapter [2-8].

Pharmacokinetics of Protein Therapeutics

The *in vivo* disposition of protein drugs can be predicted to a large extent from their physiological function. The short elimination half-life can be expected from small proteins with hormone activity, which is desirable for close regulation of endogenous levels and thus function. In contrast, long half-lives of several days are usually observed for proteins with transport function (such as albumin) and long-term immune function (such as immunoglobulins) to ensure the continuous maintenance of physiologically-necessary concentrations in systemic circulation [2, 3]. Similar to small-molecule compounds, the processes involved in the pharmacokinetics of protein drugs generally include absorption, distribution, and elimination. However, the special processes entailed in the disposition of protein drugs may involve target receptor-mediated drug disposition, and interaction with Fc receptors. These two pathways play major roles in the pharmacokinetics of monoclonal antibodies (mAbs).

Absorption

The susceptibility of proteins to the digestive enzymes in the gastrointestinal tract, along with their physicochemical properties such as size and charge, hampers their absorption process through the gastrointestinal membranes and creates challenges in delivering protein therapeutics in oral dosage forms. Because of this limitation, the currently available dosages for protein therapeutics is injection or infusion via intravenous (IV), subcutaneous (SC), or intramuscular (IM) administration.

However, these administration routes have many drawbacks. Although IV administration such as bolus injection or infusion is preferred as a means to directly deliver peptides and proteins into the systemic circulation, it is inconvenient and might not provide the desired concentration-time profile. Moreover, the potentially decreased bioavailability with SC and IM injections is a disadvantage that has to be considered. The decreased bioavailability is due to variables such as local blood flow, injection trauma, protein degradation at the site of injection or in the lymphatic system, and limitations of uptake into the systemic circulation related to effective capillary pore size, convection**,** and diffusion.

After SC administration, proteins may enter the systemic circulation via blood capillaries or lymphatic vessels. The primary pathways for systemic absorption include diffusion across blood vessels distributed near the injection site and convective transport through lymphatic vessels and into the blood. There appears to be a linear relationship between molecular weight and the proportion of the dose entering the lymphatic system. The absorption into the systemic circulation after SC or IM administration is slow and it generally takes a few days to one week to reach peak plasma concentrations. The absolute bioavailability of mAbs is generally reported between 50 and 100% [5, 6]. The bioavailability of mAbs depends on the rates of extravascular degradation (e.g., proteolysis), antibody endocytosis (e.g., receptor-mediated or fluid-phase endocytosis), and recycling through interaction with the neonatal Fc-receptor (FcRn).

Other extravascular administration routes through nasal, buccal, rectal, vaginal, transdermal, ocular, and pulmonary drug delivery have also been shown promising results and are under development to improve bioavailability through improved systemic absorption.

Distribution

Similar to conventional small-molecule drugs, protein drugs have to extravasate across the endothelial walls of vascular capillaries, pass through the interstitium, and reach the target sites in order to exert their pharmacological activity. The extravasation of protein drugs to the target site can involve convection or transcytosis. The rate and extent of protein extravasation are determined largely by their size and molecular weight, physiochemical properties (e.g. charge, lipophilicity), protein binding, and their dependency on active transport processes. Biological factors including regional

differences in capillary structures, the disease state of an organ or tissue, and the flow rate of blood can also affect the extravasation and distribution of macromolecules. Due to their high molecular weight and large size, the distribution of most proteins is limited to the extracellular space. This leads to small apparent volumes of distribution for most proteins. Protein drugs with higher molecular weights will distribute in smaller distribution volumes than protein drugs with lower molecular weights, resulting in lower interstitial concentrations with increasing molecular weights. However, active tissue uptake and binding to extravascular proteins and other structures can substantially increase the apparent volume of distribution of protein drugs.

In contrast to small-molecule drugs, convection rather than diffusion is the main process that transports proteins from the vascular space into the interstitial space of tissues. The convection process occurs as a unidirectional fluid flux from the vascular space through paracellular pores into the interstitial tissue space. This process is the main pathway of protein transport and is largely determined by the rate of fluid movement from blood to tissue and by the sieving effect of paracellular pores in the vascular endothelium. The sieving effect is mainly determined by the size and tortuosity of membrane pores and by the size, shape, and charge of protein drugs. As pore size decreases and the tortuosity increases, there is an increased resistance to the movement of macromolecules. Proteins in the interstitial tissue space are subsequently removed by convective transport via lymph drainage back into the systemic circulation. Compared to extravasation, lymph drainage is a much more efficient process due to the much larger size of paracellular pores in lymphatic vessels compared to the vascular endothelium. As a consequence of the difference in the efficiency of convective uptake into tissue and convective drainage of proteins from tissue, protein concentrations in tissue interstitial fluid are substantially lower than protein concentration in plasma. However, higher concentrations of proteins can be observed in tissues with leaky vasculature (e.g. bone marrow and spleen).

In addition to the size-dependent sieving of macromolecules through the capillary walls, the charge may also play an important role in the biodistribution of proteins. Due to the abundance of glycosaminoglycans in the extracellular matrix that impart a negative charge on most cell surfaces, the rate and extent of distribution into tissues is increased by the electrostatic attraction between negatively-charged cell membranes and proteins that are positively charged.

Another pathway for the transfer of protein molecules from the vascular to the interstitial space is transcytosis**,** which is a transcellular transport pathway that couples endocytosis and exocytosis on the opposite plasma membranes of cells. However, for most proteins, convection is quantitatively more important than transcytosis in terms of extravasation of protein drugs from the systemic circulation.

Protein binding is another factor that can affect the volume of distribution and cause an inhibitory or stimulatory effect on the biological activity of protein therapeutics. Upon binding, endogenous binding proteins can serve as the storage depot for therapeutic proteins that result in prolonged plasma concentration-time profiles; alternately, they can

enhance protein clearance. Moreover, cellular uptake processes may be facilitated by interaction with specific binding proteins and thus affect the pharmacodynamics.

Besides physicochemical properties and protein binding, site-specific receptor-mediated uptake can also substantially affect the distribution of protein therapeutics. Elimination and pharmacodynamics can also be influenced by this receptor-mediated uptake process, which can be explained by target-mediated drug disposition (TMDD) pharmacokinetics. This is normally observed for therapeutic mAbs that are designed to bind membrane-standing target antigens with high affinity, which will affect the distribution of the drug and result in low volumes of distribution (approximately equal to the plasma volume). This is due to the tight binding of mAbs to cells near the sites of antibody extravasation, which is known as the "binding-site barrier" hypothesis. However, antibody fragments consisting of only an antigen-binding portion (Fab fragments) or single-chain variable fragments can cross the blood-tissue barrier more easily and are less hindered by the binding-site barrier.

After IV administration, proteins usually follow a bi-exponential plasma concentration-time profile well described by a two-compartmental model. The central compartment in this two-compartmental model principally represents the vascular space and the interstitial space of well-perfused organs such as liver and kidneys, which have permeable capillary walls. The peripheral compartment illustrates the interstitial space of the poorly-perfused organs with the slow equilibrium of the drug concentration [2, 3, 7].

Elimination

Protein therapeutics use the same catabolic pathways as endogenous or dietary proteins, which feeds into an amino acid pool that can be reused for the biosynthesis of structural or functional body proteins. The elimination processes of proteins include proteolysis, renal elimination, hepatic elimination, or receptor-mediated endocytosis. However, non-metabolic elimination pathways such as renal or biliary excretion are negligible for most proteins. If biliary excretion occurs, it is usually followed by metabolic degradation in the gastrointestinal tract. The metabolic rate for protein degradation generally increases with decreasing molecular weight from large to small proteins to peptides. The degradation rate also depends on other factors, such as size, charge, lipophilicity, functional groups, and glycosylation pattern as well as secondary and tertiary structure.

Proteolysis. Protein therapeutics can be metabolized throughout the body because of the ubiquitous availability of proteolytic enzymes. Thus, locations of intensive peptide and protein metabolism are not only limited to liver, kidney, and gastrointestinal tract but can also include blood and other body tissues. Proteases and peptidases are also located within cells; thus, intracellular uptake per se is more an elimination than a distribution process. There are two major mechanisms by which proteins are degraded intracellularly —the lysosomal pathway and the ubiquitin-mediated pathway. These two pathways work

together in the degradation of intracellular proteins and exogenous proteins. While peptidases and proteases in the gastrointestinal tract and in lysosomes are relatively nonspecific, soluble peptidases in the interstitial space and exopeptidases on the cell surface have a higher selectivity and determine the specific metabolism pattern of an organ.

Renal Elimination [2, 3, 7]**.** The kidneys are a major site of metabolism for smaller-sized proteins that undergo glomerular filtration. The cut-off size for glomerular filtration is approximately 60 kDa with the effective molecule diameter (based on molecular weight and conformation) or hydrodynamic radius as a potential limiting factor. However, glomerular filtration is most efficient for proteins that are smaller than 30 kDa.

Peptides and small proteins (<5 kDa) are filtered very efficiently, and their glomerular filtration clearance reaches the maximal glomerular filtration rate (GFR, ~ 120 mL/min in humans). In contrast, the filtration rate of proteins greater than 30 kDa abruptly declines. In addition to size, charge selectivity has also been observed for glomerular filtration. Anionic macromolecules pass through the filtration membranes less readily than neutral macromolecules, which in turn pass through less readily than cationic macromolecules.

Renal elimination of small proteins can occur through one of three routes, resulting in negligible amounts of intact molecules detected in urine. The first route involves glomerular filtration of larger, complex peptides and proteins followed by reabsorption into endocytic vesicles in the proximal tubule, and subsequent hydrolysis into small peptide fragments and amino acids. The second major route entails glomerular filtration followed by intraluminal metabolism by brush border membrane enzymes located on the luminal membrane of the proximal tubule. The resulting peptide fragments and amino acids are reabsorbed into the systemic circulation. The third route is the peritubular extraction of proteins from postglomerular capillaries with subsequent intracellular metabolism.

For the first two mechanisms, glomerular filtration is the rate-limiting step as subsequent degradation processes are unsaturated under physiologic conditions. Due to this limitation, the renal contribution to the overall elimination of proteins is dependent on the proteolysis that occurs in other regions of the body. If proteolysis is high in other body regions, renal contribution to total clearance will be limited, and becomes negligible in the presence of nonspecific degradation throughout the body. If metabolic activity for proteins is low in other tissues, or distribution to the extravascular space is limited, the renal contribution to the overall clearance may reach 100%. In general, mAbs are not eliminated by this pathway due to their large size, preventing renal filtration. However, Fab fragment-based therapeutics can be excreted to some extent by the kidneys.

Hepatic Elimination [2, 3]. A prerequisite for hepatic metabolism of proteins is the uptake into one of three cell types in the liver: hepatocytes, Kupffer cell, and endothelial cells.

Hydrophobic small peptides can either cross the hepatocyte membrane via simple passive diffusion if they have sufficient hydrophobicity or be taken up by the hepatocytes via a carrier-mediated transport. After internalization into the cytosol, these peptides are usually metabolized by microsomal enzymes. Peptides that enter the liver via carrier-mediated transport are typically excreted into the bile by active export transporters.

Uptake of larger peptides and proteins is facilitated via various carrier-mediated, energy-dependent transport processes such as receptor-mediated endocytosis. In receptor-mediated endocytosis, circulating peptides and proteins are recognized by specific hepatic receptor proteins, which are usually integral membrane glycoproteins with an exposed binding domain on the extracellular side of the cell membrane. For glycoproteins, if a critical number of exposed sugar groups (such as mannose, galactose, fucose, N-acetylglucosamine, N-acetylgalactosamine, or glucose) is exceeded, receptor-mediated endocytosis through sugar-recognizing receptors is an efficient hepatic uptake mechanism. Important carbohydrate receptors in the liver are the asialoglycoprotein receptor in hepatocytes and the mannose receptor in Kupffer and hepatic endothelial cells. Moreover, low-density lipoprotein (LDL)-receptor-related protein (LRP) is a member of the LDL receptor family, responsible for endocytosis of several important lipoproteins, proteases, and protease-inhibitor complexes in the liver and other tissues.

Uptake of proteins by hepatic cell types is followed by transport to an intracellular compartment for metabolism. Proteins internalized into vesicles via an endocytotic mechanism undergo intracellular transport towards the lysosomal compartment near the center of the cell. The endocytotic vesicles then fuse with or mature into lysosomes, which are specialized acidic vesicles that contain a variety of hydrolases capable of degrading all biological macromolecules. The hepatic metabolism of glycoproteins may occur more slowly than with naked proteins because protecting oligosaccharide chains need to be removed first. Peptide and protein metabolites in lysosomes from hepatocytes, hepatic sinusoidal cells, and Kupffer cells may be released into the systemic circulation. Degraded proteins in hepatocyte lysosomes can also be delivered to the bile canalicul and excreted by exocytosis.

Another intracellular, usually minor elimination pathway for proteins is the direct shuttle or transcytotic pathway. The endocytotic vesicle formed at the cell surface traverses the cell to the peribiliary space, where it fuses with the bile canalicular membrane, releasing its contents by exocytosis into bile.

Receptor-Mediated Metabolism/Target-Mediated Drug Disposition (TMDD). Unlike conventional small molecule drugs, receptor-mediated metabolism is a substantial elimination pathway for many therapeutic proteins. This is due to their high binding affinity to their target receptors along with the significant amount of protein drugs that is

normally involved in the target binding. The binding can lead to cellular uptake by receptor-mediated endocytosis and subsequent intracellular lysosomal degradation. This high-affinity, low-capacity binding process can occur in any organ and tissue that expresses specific receptors for the therapeutic protein, and thus contributes to the elimination of therapeutic proteins throughout the body. Thus, the process of receptor-mediated endocytosis contributes significantly not only to the pharmacodynamics but also to the pharmacokinetics of protein drugs.

For therapeutic proteins that have their target receptors on the cell surfaces, the elimination that occurs through receptor-mediated endocytosis can be described by target-mediated drug disposition pharmacokinetics. For mAbs, this process occurs via the interaction between the Fab portion of mAbs and the target epitopes on the cell surface. Since the number of target receptors is limited, this process can be saturated with therapeutic concentrations. As a consequence, the clearance of therapeutic proteins that go through this process is not constant but dose-dependent and decreases with increasing dose. Thus, receptor-mediated elimination constitutes a major source of the nonlinear pharmacokinetic behavior of numerous protein drugs that show over-proportional increases in systemic exposure with increasing dose.

Elimination via the Reticuloendothelial System (RES). For mAbs, the phagocytic cells in the immune system, such as macrophages and monocytes, are expected to play a role in the elimination as key factors in the effector functions of endogenous IgG. After the Fc portion of the antibody binds to the Fcγ-receptors expressed on the phagocytic cells, the internalization and subsequent degradation of IgG by lysosomes generally occurs. Unlike receptor-mediated metabolism, this route is not expected to be saturated by therapeutic mAb doses, because therapeutic mAb concentrations are generally a small fraction of total endogenous IgG. However, there is evidence that suggests that Fcγ-receptor-mediated elimination has limited influence or a merely minor effect on the plasma and tissue disposition of monomeric IgG [9-12]. This process might be a significant and perhaps dominant pathway when antibody is able to form soluble immune complexes containing three or more IgG molecules, and might play an important role when antibody binds to suspended cells in blood or other body fluids such as viruses, bacteria, platelets, erythrocytes, and leukocytes [9, 13, 14].

Polymorphisms in *FCGR3A*, which encodes FcγRIIIa, a Fcγ-receptor expressed by macrophages and natural killer cells, have no influence on the pharmacokinetics of horse anti-lymphocyte globulin in renal transplant patients [10]. 2.4G2, an antibody directed against the murine FcII receptor on macrophages, is able to clearly reduce the rate of clearance of immune complexes but does not alter the rate of clearance of monomeric IgG anti-HSA [9]. With ~ 85-fold reduction in HAE2-IgE complex binding to FcγRI, II, and III relative to wild-type IgG1, high-affinity anti-IgE antibody-2 (HAE2) reduces clearance of HAE2-IgE complex and decreases distribution to the liver [13]. Moreover, mAb blockade of the Fcγ-receptor is shown to prolong the systemic exposure of IgG-sensitized red blood cells *in vivo* [14]. Recent studies also suggest that Fcγ-receptors play only a minor role in the elimination of murine IgG1 mAb and endogenous

IgGs [11, 12]. However, the mechanism of this nonspecific elimination pathway for mAbs is still not fully understood and may differ across different mAbs.

Target-Mediated Drug Disposition

The pharmacokinetics of numerous protein therapeutics are characterized by target-mediated drug disposition (TMDD), which occurs when binding to the pharmacodynamic target molecule affects the pharmacokinetics of a drug compound and results in capacity-limited, saturable processes. These saturable processes are caused by the limited availability of enzymes, receptors, or other target protein structures with which the drug is interacting. This results in nonlinear pharmacokinetics that show a disproportional change in plasma concentration with increasing dose. Most notably, TMDD is the result of receptor-mediated protein metabolism, which is a frequently-encountered elimination pathway for many therapeutic proteins that often show saturation at therapeutic dosage regimens. However, TMDD can affect distribution as well as elimination processes.

To describe the processes that occur in TMDD, the general TMDD model is used [15]. Drugs administered via various routes get into the body and appear in the blood circulation (central compartment). The free drug in the blood circulation can distribute to the tissues (peripheral compartment) with the first-order rate constant K_{pt}, and free drug in the tissue can distribute back to the blood circulation with the first-order rate constant, K_{tp}. The free drug in the blood circulation can also be eliminated by linear clearance pathways such as proteolysis, with the first-order rate constant K_e. The drug in the blood circulation can also bind to free receptors at the target site, which are synthesized with the zero-order K_{syn} rate and degraded with the first-order rate constant K_{deg}. Drug and receptor will form the drug-receptor complexes with the second-order rate constant K_{on}. The drug-receptor complexes can dissociate back to generate the free drug with the first-order constant K_{off}, or they will be internalized with the first-order rate constant K_{int} and subsequently degraded. This general TMDD model can be modified to incorporate additional compartments or factors.

For many mAbs, target-mediated elimination is probably a more important elimination pathway than proteolysis by cells in the RES [4]. It occurs when the Fab-portion of mAbs binds to the target antigen and causes internalization and subsequent intracellular degradation in lysosomes. This process is often referred to as ‘antigen sink’ and is saturable because of the limited amount of the target antigen. As a consequence, nonlinear pharmacokinetics has often been reported. However, not all mAbs show concentration-dependent elimination. Linear elimination, in which the elimination rate does not depend on the dose or the plasma concentration, has been reported in some mAbs, especially for those that target a soluble antigen (not bound to cells) such as vascular endothelial growth factor or TNFα. The reason might be that the concentrations in plasma and tissues after therapeutic dose administration do not saturate the target antigen, or the target-mediated clearance is of less importance when compared to other elimination pathways.

The Neonatal Fc Receptor (FcRn)

The neonatal Fc receptor (FcRn) or Brambell receptor is involved in a physiological process that functions as a protective mechanism against metabolism and elimination of IgG and albumin [4-7, 16]. Through this process, IgGs show the longest elimination half-life compared to other isotypes of immunoglobulins (IgA, IgD, IgE, and IgM) [4, 7]. Intact IgGs have a molecular weight of ~ 150 kDa and a valence of 2 (each molecule of IgG contains two identical antigen-binding domains). Based on the heavy chain structure, the IgG family can be divided into four subclasses, including IgG1, IgG2, IgG3, and IgG4 [5, 6]. The structural difference in IgG heavy chains among the subclasses leads to the differences in the binding to Fc receptors, and results in subclass-specific differences in processes mediated by Fc receptors (e.g., activation of complement, or antibody-dependent cell-mediated cytotoxicity) [5]. Among the IgG family members, IgG3 has a much shorter elimination half-life (7 days) than those of the other IgG isotypes (20-21 days) [4, 7].

The salvage pathway by FcRn is a pH-dependent process since binding of IgG and albumin to the FcRn occurs in acidic (pH 6.0 – 6.5) but not in neutral (pH 7.0 – 7.5) environments. After nonspecific pino- or endocytosis, in which the molecule is engulfed by the cell membrane and taken up into the cell, the Fc portion of IgG binds to the FcRn in the slightly acidic environment of the endosomes. The IgG-FcRn complex is then transported back to the cell surface and released into the systemic circulation at neutral pH, whereas unbound IgG and other proteins are degraded to amino acids by intracellular lysosomes (**Figure 1-1**).

FcRn can transport IgG across cell monolayers in both the apical- to basolateral and basolateral- to apical directions. The FcRn protective mechanism has an influence on the pharmacokinetics of endogenous IgG and albumin. The long elimination half-life (21 days) of endogenous IgG and albumin compared to other plasma proteins can be explained by this mechanism. Saturation of FcRn can occur at high concentrations of IgG that demolish the salvation pathway. However, this is generally not expected at the therapeutic dose of mAbs as the usual therapeutic dose of a few hundred milligrams is small compared to the endogenous IgG amount of 12 g/L (~50-100 g in an adult). To saturate this protective mechanism, very high doses of therapeutic mAbs would be needed.

The saturation of FcRn occurs in the treatment of autoimmune diseases. High-dose intravenous immunoglobulin (IVIG) therapy with pooled human IgG at a dose of 2 g/kg can sufficiently increase IgG plasma concentrations, leading to an approximately threefold increase in IgG clearance [5, 17]. This increase in IgG clearance results in a decrease in the plasma concentrations of endogenous, pathogenic autoantibodies. However, IVIG therapy is very expensive due to the requirement of high doses for the therapy. To achieve a similar effect to that of IVIG therapy, anti-FcRn antibodies can be administered at a ~100-fold lower dose than IVIG therapy [5, 18]. These anti-FcRn antibodies are specifically directed against FcRn or have a modified Fc portion that can form more stable complexes with FcRn. As a result, an increase in the elimination rate of

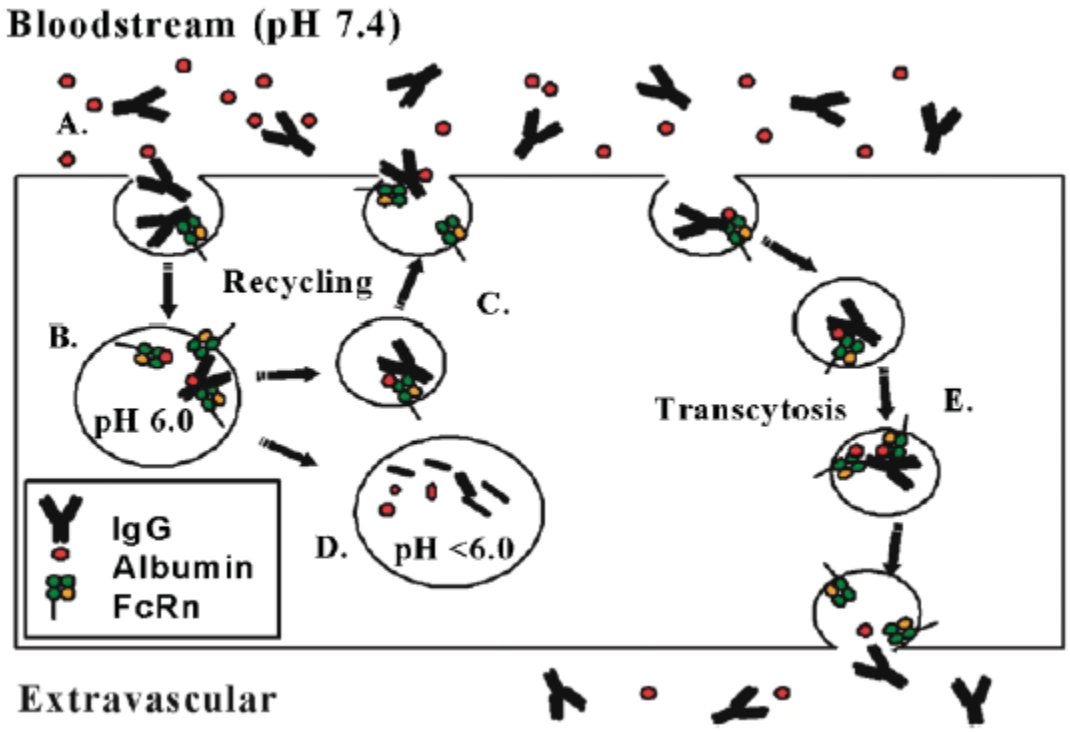

Figure 1-1. Schematic illustration of the FcRn mediated recycling pathway
(A) IgG and albumin circulating in the bloodstream are continuously taken up by fluid phase pinocytosis and enter early endosomes where FcRn predominantly resides. (B) The acidified milieu herein facilitates binding of IgG and albumin to FcRn. (C) The ternary complex is then recycled to the cell surface where exposure to physiological pH of the bloodstream triggers release of IgG and albumin into the circulation. (D) When the concentrations of IgG and albumin are high, FcRn is saturated and unbound ligands undergo lysosomal degradation. (E) FcRn may also transcytose IgG and albumin to the basolateral side of the cell for release into extravascular space.
Source: Reprinted with permission from The Japanese Society for the Study of Xenobiotics (JSSX). Andersen, J.T. and I. Sandlie, *The versatile MHC class I-related FcRn protects IgG and albumin from degradation: implications for development of new diagnostics and therapeutics.* Drug Metab Pharmacokinet, 2009. **24**(4): p. 318-32.

mAbs and endogenous IgG can be achieved after the administration of anti-FcRn antibodies [4].

The binding affinity between IgG and FcRn is species specific. High binding affinity is observed between human FcRn and human IgG as well as guinea pig and rabbit IgG [19]. However, human FcRn has a very low affinity to mouse, rat, bovine, and sheep IgG. As a result, the very rapid elimination of murine mAbs in human is observed. In contrast, mouse FcRn binds to IgG from all aforementioned species. Moreover, mouse FcRn has higher binding affinity to human IgG1 than that observed between human FcRn and human IgG1 [19, 20]. The difference in promiscuity for IgG-FcRn interaction between mouse and human has raised the concerns regarding the validity of using mice as a model to predict the pharmacokinetics of therapeutic mAbs in humans. The suitability of mouse models for the pharmacokinetic evaluation of therapeutic mAbs has been further called into question by another study when engineered human IgG1 was tested in murine and human systems and exhibited different pharmacokinetics and FcRn recycling behaviors [21]. As a consequence, a humanized FcRn transgenic mouse has been developed and has proved to be an effective surrogate for studying the pharmacokinetics of therapeutic mAbs and Fc-fusion proteins [22-24].

Effect of Immunogenicity on the Pharmacokinetics of Therapeutic Proteins

The origin of therapeutic proteins is important since xenogenic proteins can trigger immune responses (immunogenicity) that cause anti-drug antibodies (ADA) to be produced. Immunogenicity can occur when animal-derived proteins are applied in human clinical studies as well as when human proteins are administered to animals during preclinical studies [3]. ADAs that recognize epitopes on therapeutic proteins that are not essential for their bioactivity are referred to as non-neutralizing antibodies (binding antibodies) and usually result in fewer clinical consequences [8]. In contrast, ADAs that neutralize the biological activity of therapeutic proteins by binding to their active sites (neutralizing antibodies) frequently cause loss of efficacy. Immunogenicity can influence the pharmacokinetics of peptide and protein drugs by altering distribution and clearance. The direction of the immunogenic effect on pharmacokinetics is difficult to predict. The elimination rate can be either increased or decreased, depending on the number of antigenic sites on the exogenous proteins against which the endogenous antibodies are directed and the size of the resulting immune complexes [4-6]. In case, only one or two endogenous anti-drug IgGs bind to exogenous peptides or proteins, the half-life of those exogenous peptides or proteins can approach that of endogenous IgGs that act as a depot for therapeutic peptides or proteins. A prolonged duration of pharmacological action can occur in this case if the antibody is not neutralized. On the other hand, simultaneous binding of three or more anti-drug IgGs to the exogenous peptides and proteins can lead to the very rapid elimination of the immune complex through phagocytosis by the RES. This pharmacokinetic change resulting from the formation of antibodies against administered proteins can affect therapeutic efficacy.

In addition to the similarity between exogenous and endogenous proteins, the degree of aggregation of therapeutic protein products, along with the duration of therapy, dose, and route of administration**,** also have an influence on the occurrence and degree of immunogenicity [3, 5, 6]. Immunogenicity can increase because of the quantity of aggregates in the dosing formulation. The degree of immunogenicity can also increase with the duration of therapy. This might be due to the increasing exposure to exogenous proteins during prolonged therapy, which can lead to an increasing probability of anti-drug antibody development against multiple antigenic sites. This in turn may result in the rapid elimination of the therapeutic protein. The relationship between dose and immunogenicity is difficult to predict. The clearance of drug-antibody complexes may be delayed at low doses and increase at high doses due to the formation of aggregates that trigger clearance through the RES. However, the inverse relationship between immunogenicity and dose can also be observed. This inverse relationship might be due to the presence of high amounts of protein drugs in the samples, causing assay interference by masking the detection of anti-drug antibodies or due to the consumption of low-level ADA by high protein drug concentrations. The route of administration may also influence on the immunogenicity. Administration by the SC and IM route can lead to greater immunogenicity than that observed following IV administration. The increasing incidence of immunogenicity after extravascular administration is probably caused by a higher numbers of protein aggregates and precipitates formed at the injection sites, which activate immune cells and stimulate clearance through the RES.

Effect of Developmental Physiology on the Pharmacokinetics of Therapeutic Proteins

Special considerations should be taken when using therapeutic proteins in pediatric patients. This is due to the substantial differences between children and adults in terms of disease etiology, the time course of the disease, disease complications or prognosis, use of concomitant medications, immune and vaccination status, and eventually clinical responses (including therapeutic effects and adverse drug reactions) [8]. In addition, developmental changes in physiology that result in dynamic age-associated changes in body composition and organ function, along with receptor ontogeny, can affect the pharmacokinetics of protein drugs in populations of different ages [25]. Consequently, age-associated changes in the absorption, distribution, elimination, and immunogenicity of therapeutic proteins may be observed in pediatric patients.

Absorption

Since therapeutic peptides and proteins are mostly administered through the IV or SC route, developmental skin alterations may be a factor that should be considered when protein drugs are administered to children. Compared to adults, the presence of a thinner stratum corneum in the preterm neonate and the greater extent of cutaneous perfusion and hydration of the epidermis throughout childhood might contribute to enhanced

percutaneous absorption of drugs during infancy [25]. The higher ratio of total body surface area to body mass in infants and young children compared to adults is another factor that might affect the absorption of drugs. However, it is still inconclusive whether differences between adults and children in the thickness of SC tissue and local lymphatic flow at the injection site affect the absolute bioavailability of a therapeutic protein after SC administration [8, 26].

Distribution

Developmental changes in body composition may not have a significant impact on the biodistribution of therapeutic proteins [8]. However, a considerable alteration in the distribution of protein drugs may be caused by changes in the composition and amount of circulating plasma proteins and tissue targets [8, 25]. Steady-state levels of the target antigen may differ between adult and pediatric populations due to differences in either the production or degradation rate of the targeted antigens, which can result in differences in the biodistribution of the therapeutic protein upon dosing [8]. Nevertheless, the target antigens are usually overwhelmed by therapeutic proteins about a hundred- or thousand-fold at therapeutic concentrations. Thus, the biodistribution of therapeutic proteins at steady state might not be significantly altered by developmental changes in antigen production or degradation rates. Instead, such differences would more likely lead to inequalities in the elimination of therapeutic proteins if TMDD is the main pathway of clearance.

Elimination

For many protein drugs, proteolysis occurring throughout the body is considered to be the main pathway of clearance. Thus developmental changes in hepatic drug metabolizing enzyme systems such as CYP have a negligible impact on the metabolism and clearance of therapeutic proteins. Maturation in renal function may have some influence on the excretion and elimination of small peptides that can pass through glomerular filtration. However, the impact of developmental changes in renal function may be negligible depending on the contribution of renal elimination to the overall clearance that occurs in the other parts of the body.

For antibody-based therapeutic proteins, non-specific Fc receptor-mediated disposition (through Fcγ-receptors in RES and FcRn receptors) and target receptor-mediated metabolism are considered to be major elimination pathways. The elimination through RES after binding to Fcγ-receptors has been shown to have a limited effect on the clearance of monomeric mAbs. However, this pathway can accelerate the elimination of antigen-antibody complexes. Thus the difference in Fcγ-receptor distribution between adults and children, if it exists, might become problematic when immunogenicity occurs. In contrast to Fcγ-receptors, FcRn has been shown to play a significant role in extending the presence of mAbs in the systemic circulation after binding to this receptor. Due to its considerable role as a salvage pathway from clearance, potential differences in FcRn

expression during pediatric development might result in unequal pharmacokinetic profiles of therapeutic mAbs across different age groups. Unlike non-specific Fc receptor-mediated disposition, target receptor-mediated clearance is a specific process that occurs when a therapeutic protein binds to its specific receptor at the target site. The efficiency of this mechanism depends on the target receptor expression levels and the turnover rates of the target receptors. As a consequence, differences in the target receptor levels and turnover rates between adults and children might be a major concern if therapeutic proteins are mainly eliminated through this specific pathway [8, 26].

Immunogenicity

The incidence of immunogenicity from therapeutic proteins may differ between children and adults due to variation in patient-related factors that may predispose an individual to an immune response [8, 26]. These patient-related factors include underlying disease, genetics, immune status, concomitant use of immunomodulators, and previous experience using protein therapeutics. Currently, the similarities and dissimilarities in immunogenicity between pediatrics and adults are still inconclusive. This is due to the limited availability of immunogenicity data in pediatric populations along with substantial shortcomings of the current technologies for ADA evaluation and quantification. To gain insight into this matter, the improvement of assay technologies and standardized evaluation of immunogenicity across clinical trials will be needed.

Dose Optimization of Therapeutic Proteins in Pediatric Development

Currently, the application of therapeutic proteins in pediatrics is often based on the extrapolation of clinical findings in adults [8, 26]. The extrapolation approach may be useful in the case that no pediatric data are available. However, this approach may significantly compromise the efficacy and safety of pediatric patients if the differences between children and adults are not explicitly determined. The potential considerable differences between children and adults in terms of disease etiology, time course of disease, disease complications or prognosis, use of concomitant medications, immune and vaccination status, and eventually, clinical responses (including therapeutic effects and unwanted adverse events caused by a given therapy) should all be considered in the dosage regimen optimization. Moreover, the fundamental comprehension of the similarities and dissimilarities in the pharmacokinetics and pharmacodynamics between children and adults can assist in determining the rational use of therapeutic proteins in pediatric populations.

A number of potential covariates, including target antigen levels, serum albumin levels, disease activity, concomitant medications, and development of ADA may affect the pharmacokinetics of protein drugs. However, the effect of body size more often warrants dose adjustment in pediatric patients compared relative to other covariates. This is due to the differential growth rates during development that create much larger variability in body size for children than for adults. Because of this, the effect of body

size is a major determinant of the pharmacokinetics of therapeutic macromolecules in pediatrics. As a consequence, several dosing approaches that account for size alterations during pediatric development have been successfully used in children.

To account for the size difference, weight-based (mg/kg) dosing, body surface area (BSA)-based (mg/m^2) dosing, tiered fixed dosing (i.e., a fixed dose for patients in a specified narrow weight range), and hybrid dosing (fixed dosing for older children and body size-based dosing for younger children) have been successfully applied. However, both weight- and BSA-based dosing may not satisfactorily correct the body size effect, as clearance of antibody-based therapeutic proteins is often not proportional to either weight or BSA. To attain more physiologically-based and more accurate dose adjustment, allometric scaling approaches have been used for dosage extrapolation from adults to pediatric patients.

After accounting for the effect of body size, age itself has rarely been identified as a covariate that influences the pharmacokinetics of therapeutic proteins. The available data show that the proper correction for body size-related pharmacokinetic differences is essential for appropriate dose selection of antibody-based therapeutic proteins for pediatric patients. However, the body size-based dosing approach might be inefficient for designing the dosage regimen of therapeutic proteins that are mainly eliminated through target receptor-mediated metabolism. For these therapeutic macromolecules, differences in the target antigen expression levels and turnover rates of the target antigens during development may become another major determinant of pharmacokinetics. The target receptor levels and turnover rates of the target antigen may not always increase with body size. As a consequence, physiologically-based dose adjustment may become a better approach to achieve a successful therapy in pediatric populations. Only very limited clinical data are available for the use of mAbs in very young pediatric patients, including term and preterm neonates, and further age-related adjustments beyond body size may be warranted in this patient group.

Summary

Because susceptibility to digestive enzymes in the gastrointestinal tract, along with limitations due to their physiochemical structure, most therapeutic proteins are administered via the IV or SC route. The absorption of protein drugs after SC administration occurs via convection through lymphatic vessels and diffusion across blood capillaries. The distribution of therapeutic proteins is limited by their size and physiochemical properties such as charge, which result in their confinement predominantly in the vascular space. Convection and transcytosis are the two main pathways that facilitate the distribution of protein drugs. Generally, therapeutic proteins exhibit bi-exponential plasma concentration-time profiles upon IV administration. Hepatic and renal excretion are negligible for therapeutic proteins. Instead, protein drugs are usually degraded by proteolysis, which can occur throughout the body. Moreover, target receptor-mediated catabolism is the main clearance pathway for most therapeutic proteins that have high binding specificity to their targets. The pharmacokinetics of

protein drugs that follow such an elimination pathway can be well described by TMDD. For monomeric mAbs, elimination via the RES may be negligible; however, RES becomes the main pathway of clearance of antigen-antibody complexes during when immunogenicity occurs. The prolonged existence of mAbs in the systemic circulation can be explained by the salvage pathway via the FcRn-mediated recycling mechanism. Administration of therapeutic proteins can cause immunogenicity, which may lead to prolonged exposure or abruptly-increased clearance. The occurrence of immunogenicity can result in toxicity or lack of efficacy upon administration of protein drugs. Several factors are responsible for the prevalence of immunogenicity, but the occurrence remains difficult to predict in the individual patient.

Due to the physiological difference between adults and pediatric patients, the pharmacokinetics of protein drugs may be altered during child development. Immunogenicity reactions may also be different between adults and children. However, current data on these differences are limited and further studies are needed in order to elucidate differences between adults and pediatric patients in the pharmacokinetics and immunogenicity of therapeutic proteins. Although body size-based dosing is currently widely used for therapeutic proteins in pediatric patients, physiologically-based dosage regimen design may be necessary for some therapeutic proteins that are influenced by additional physiological factors such as target density and turnover.

CHAPTER 2. INTRODUCTION

As discussed in **Chapter 1**, there are many factors that contribute to the regulation of drug disposition for protein therapeutics. As a result, the interpretation of the pharmacokinetics for protein therapeutics presents a complex challenge. Two challenges in the pharmacokinetic assessment of therapeutic proteins were explored in this study.

The assessment and prediction of bioavailability after SC administration for protein therapeutics becomes an important challenge, especially if these drugs exhibit target-mediated drug disposition (TMDD) – a clearance process that is dependent upon the expression patterns and turnover rates of its target receptor. As a consequence, the clearance of protein drugs may vary with respect to dose. With increasing dose, the clearance through TMDD can become saturated and plateaus. However, current bioavailability estimations use the approach of comparing dose normalized AUC from non-intravenous routes to that of IV administration with the assumption of a dose-independent clearance. Due to failure in this assumption, an error in bioavailability estimation may be observed for protein drugs that undergo TMDD. I hypothesized that there is a dose-dependent error in the bioavailability assessment for therapeutic proteins that undergo TMDD if the classical approach of dose-normalized AUC is used. The error becomes apparent when different doses of IV and SC administration are used for bioavailability estimations since the clearances at different IV and SC doses are not equal. To test this hypothesis and to evaluate the errors of bioavailability estimation, I selected two model drugs filgrastim and denosumab that undergo TMDD. Based on their published pharmacokinetic models, the plasma concentration-time profiles of filgrastim and denosumab were simulated in Phoenix® WinNonlin 6.3 and their bioavailabilities were subsequently estimated. With the current bioavailability estimation approach, the bioavailabilities of filgrastim and denosumab were determined at theoretical doses ranging from 0.01 – 10000 μg/kg for filgrastim and 0.66 – 210 mg for denosumab. The errors of bioavailability assessments at different doses were subsequently determined. All findings are described in **Chapter 3**.

The second challenge investigated in this study was the pharmacokinetics of human monoclonal antibodies (mAbs) with respect to age and development. Published studies have shown that neonatal Fc receptor (FcRn) expression is detectable up to 3 weeks postpartum in mouse intestines. Additionally, it was also postulated that a functional role of FcRn is to salvage mAbs and Fc-fusion proteins from the degradation or elimination pathways. Therefore, an ontogenic pattern of expression of FcRn may exist in different organs and could potentially alter the pharmacokinetic profile of protein therapeutics during pediatric development. These findings suggest that there is a critical need for better predictions and assessments of PK profiles for protein therapeutics in pediatric patients. Therefore, I conducted *ex vivo* analyzes of the ontogeny of FcRn expression and described the *in vivo* pharmacokinetics of a model human mAb, AMG589, in C57BL/6J mice during the post-natal developmental stages (Day 2 – Day 70). Based on the current published evidence, my central hypothesis is that a reduced

expression of FcRn during early postnatal development will result in a shortened half-life of monoclonal antibody AMG589 in adult mice compared to newborn mice.

To test the main hypothesis regarding the effect of the ontogeny of FcRn expression on the pharmacokinetics of mAbs, three experimental aims were framed. In the first aim I examined the levels of FcRn expression in organs of C57BL/6J mice from postnatal day 2 through day 70 (these results are described and discussed in **Chapter 4)**. In my second aim, I analyzed and characterized the pharmacokinetics of AMG589 in different age groups of C57BL/6J mice (**Chapter 5)**. Finally, in the third aim I attempted to correlate the FcRn expression levels with the pharmacokinetics of AMG589 in the differently aged mice using a population pharmacokinetic approach. I hypothesized that a decrease in half-life of AMG589 in adult mice is strongly correlated to the reduced levels of FcRn during development. To delineate the effect of FcRn expression on the pharmacokinetics of AMG589 in different age groups of C57BL/6J mice, body size effect was first evaluated by an allometric scaling approach, after which the effect of the ontogeny of FcRn expression was subsequently evaluated. The results of these analyses and their discussion are presented in **Chapter 5**.

The integration of my findings with the TMDD and pharmacokinetic challenges of monoclonal antibodies in the early stages of development are summarized and discussed in **Chapter 6**. The findings may help to elucidate the challenges faced in developing and optimizing dosing regimens of mAbs for pediatric patients. The presented studies strive to make better predictions of the pharmacokinetic profile for protein therapeutics in order to achieve a more desirable therapeutic effects while limiting toxicity – this is especially important when considering the highly vulnerable pediatric population.

CHAPTER 3. CHALLENGES IN THE APPARENT BIOAVAILABILITY ESTIMATION FOR THERAPEUTIC PROTEINS THAT UNDERGO TARGET-MEDIATED DRUG DISPOSITION

Introduction

Target-mediated drug disposition (TMDD), the process that was first described by Levy in 1994 [27], is the most common pathway that can well describe the pharmacokinetics of therapeutic proteins that exert specific binding with high affinity to pharmacological targets or receptors. Upon binding to the cell surface targets or receptors, the internalization of the ligand-receptor complex is usually followed by lysosomal degradation. This process causes the irreversible elimination of biotech drugs from the body and is often the main pathway of clearance when the number of pharmacological targets or receptors is in the same magnitude or larger than the number of drug molecules [28]. Through this pathway, the saturable target-binding is responsible for observable nonlinear pharmacokinetic behavior [6, 15, 27-32].

The evaluation of pharmacokinetic profiles and dose selections for these therapeutic proteins are complicated due to this nonlinear pharmacokinetic behavior as it results in a dose-dependent effect on the overall distribution and/or elimination parameters [15, 29-32]. As a consequence, the rule of superposition cannot be applied [30]. One area in which this has resulted in challenges in drug development is the assessment of systemic bioavailability after extravascular, particularly subcutaneous administration. For classic bioavailability assessments, dose-normalized areas-under-the-plasma concentration-time curves are compared under the assumption that clearance is constant and independent of time and route of administration. This assumption of invariant clearance is not valid for therapeutic proteins that undergo TMDD as their clearance mediated by the TMDD pathway is highly dependent on the degree of saturation of this pathway and thus the concentration of the therapeutic protein. An over-proportional increase in systemic exposure with increasing dose is usually observed when elimination through receptor-mediated endocytosis starts to become saturated [28]. As a result, an apparently dose-dependent bioavailability is frequently observed in many therapeutic proteins including interferon-β1a (27 – 71%) [31], filgrastim (62 – 72%) [33] and denosumab (36 – 78%) [34, 35]. However, much of this apparent dose-dependency is likely only the consequence of using bioavailability assessment methodology with the invalid assumption of a constant clearance. The potential bias of using the standard methodology of bioavailability estimation for therapeutic proteins that exhibit TMDD has so far not been evaluated.

Currently, other than the full TMDD model that was first proposed by Mager et al. [15], there are several simplified mechanistic models have been proposed to describe the pharmacokinetic profiles of therapeutic proteins that undergo TMDD including quasi-equilibrium approximation, quasi-steady-state approximation, and Michaelis-Menten models [36-39]. The difference among these simplified models is the assumption associated with models which can specifically well describe the pharmacokinetics of

individual therapeutic proteins in different scenarios. With the quasi-equilibrium model, very rapid binding between drugs and target receptors that leads to an instantaneous equilibrium of the system is assumed. In this case, the binding process is considered very rapid when compare to other processes. Thus, binding (K_{on}) and dissociation (K_{off}) rate constants in the full TMDD model are difficult to obtain and are replaced by the equilibrium dissociation constant (K_D) in the quasi-equilibrium model to describe the concentration-time profiles of drugs. However, if the rate of the internalization or elimination of the complexes is high and cannot be negligible, quasi-steady-state approximation model may be preferable since this model incorporates internalization rate (K_{int}) in a new parameter, K_{ss}, for describing the time course of drug concentration. For the Michaelis-Menten model, all parameters involving the binding and internalization processes are replaced by K_m and V_{max} parameters that describe capacity limitation. With different mechanistic models, the different parameter values are obtained and these can have the impact on the time course of drug concentration and bioavailability estimation [40, 41].

To quantify the error that can possibly occur from the currently used bioavailability estimation for therapeutic proteins, two model drugs, filgrastim, and denosumab, were selected that undergo TMDD and for which a mechanistic TMDD model had been used to quantify bioavailability. With the full TMDD model for filgrastim and quasi-steady-state approximation of TMDD model for denosumab, the plasma concentration-time profiles of filgrastim and denosumab were simulated at different doses. The bioavailability was calculated using the standard AUC approach and the effect of dose on the bias in bioavailability assessment was determined.

Method

Structural Pharmacokinetic Model

The structural models for filgrastim and denosumab were obtained from the literature [34, 42]. A full target-mediated drug disposition (TMDD) model well described the pharmacokinetics of filgrastim in healthy adults whereas the pharmacokinetics of denosumab in healthy subjects and postmenopausal women with osteopenia or osteoporosis was reasonably well described with the quasi-steady-state approximation of the TMDD model.

TMDD Model for Filgrastim

The TMDD model for filgrastim, a recombinant methionyl human granulocyte colony stimulating factor (r-metHuG-CSF), was developed by Wiczling and colleagues for a population pharmacokinetic study in healthy adults [42]. This protein is used to treat inherited and acquired neutropenia that can occur during the chemotherapy as well as to mobilize the hematopoietic stem cells and progenitors for transplantation. The developed

TMDD model well described the pharmacokinetics of intravenously (IV) and subcutaneously (SC) administered filgrastim in healthy adults.

After IV and SC administration, filgrastim enters the body and is distributed throughout the central compartment with the assumption that free G-CSF in the serum (A_s) is in instantaneous equilibrium with the bone marrow and can bind to the G-CSF receptors on neutrophilic granulocytes in blood and bone marrow. The absorption of filgrastim after SC administration appears to follow parallel zero- and first-order processes that concurrently occur for 6.6 hours (D_2). Thereafter, there is only the first-order absorption process present. The bioavailability associated with the first- and zero-order absorption processes are F_1 and F_2, respectively. The overall bioavailability is the summation of the bioavailability from zero- and first- order processes. In addition to G-CSF from filgrastim, G-CSF is naturally synthesized at the zero-order rate which is described by $K_{G\text{-}CSF}$. Free G-CSF in the serum is eliminated with the first-order rate constant K_e or bound to G-CSF receptors (AR) that are synthesized at the zero-order rate K_{syn} and degraded by the first-order process K_{deg}. The binding process is a second-order process with the rate constant K_{on}. Upon binding, the G-CSF-receptor complex is internalized by a first-order process described by K_{int} or dissociates with the first-order rate constant K_{off} generating free G-CSF.

Mathematically, the pharmacokinetics of filgrastim is described by the following differential equations (**Equations 3-1** to **3-3**):

$$\frac{dA_s}{dt} = Input + K_{G-CSF} - K_e \times A_s - \frac{K_{on}}{V_d} \times AR \times A_s + K_{off} \times ARC$$

(Eq. 3-1)

$$\frac{dAR}{dt} = K_{syn} - K_{deg} \times AR - \frac{K_{on}}{Vd} \times AR \times A_s + K_{off} \times ARC$$

(Eq. 3-2)

$$\frac{dARC}{dt} = \frac{K_{on}}{V_d} \times AR \times A_s - K_{off} \times ARC - K_{int} \times ARC$$

(Eq. 3-3)

where A_s is the quantity of G-CSF in the serum, AR is the quantity of free receptor, and ARC is the quantity of filgrastim-receptor complex. K_{on}, the association constant, is determined by $\frac{K_{off}}{K_D}$ in which K_D is an equilibrium dissociation constant. The input process can be specified by **Equation 3-4**.

$$Input = \begin{cases} \frac{Dose}{t_{inf}} & ,for\ t\ \leq t_{inf}; IV \\ 0 & ,for\ t > t_{inf}; IV \\ K_a\ \times F_1\ \times Dose\ \times e^{-K_a t} + F_2\ \times \frac{Dose}{D_2} & ,for\ t\ \leq D_2; SC \\ K_a\ \times F_1\ \times Dose \times e^{-K_a t} & ,for\ t\ > D_2; SC \end{cases}$$

(Eq. 3-4)

where t_{inf} is the infusion duration (0.5 hours), K_a is the first-order absorption rate constant, F_1 is the bioavailability of the first-order absorption process, F_2 is the bioavailability of the zero-order absorption process, D_2 is the duration of zero-order absorption, IV is the intravenous administration, and SC is the subcutaneous administration. The absolute bioavailability equals (**Equation 3-5**):

$$F = F_1 + F_2$$

(Eq. 3-5)

The system is assumed to be in a steady-state condition prior to the administration of the drug. Thus the relationships at baseline can be implied as (**Equations 3-6** to **3-8**):

$$K_{G-CSF} = K_e\ \times C_{s,0}\ \times V_d + K_{on}\ \times AR_0\ \times C_{s,0} - K_{off}\ \times ARC_0$$

(Eq. 3-6)

$$K_{syn} = K_{deg}\ \times AR_0 + K_{on}\ \times AR_0\ \times C_{s,0} - K_{off}\ \times ARC_0$$

(Eq. 3-7)

$$ARC_0 = \frac{K_{on}\ \times AR_0\ \times C_{s,0}}{K_{off} + K_{int}}$$

(Eq. 3-8)

where $C_{s,0}$ is the endogenous serum concentration of G-CSF, AR_0 is the endogenous amount of G-CSF receptors in blood and bone marrow, and ARC_0 is the pre-treatment amount of G-CSF bound receptor complexes. The concentration of G-CSF in the serum, C_s, is determined by **Equation 3-9**.

$$C_s = \frac{A_s}{V_d}$$

(Eq. 3-9)

Quasi-Steady-State Approximation of the TMDD Model for Denosumab

An open, two-compartment pharmacokinetic model with a quasi-steady-state approximation of the TMDD model was developed by Sutjandra and colleagues to describe the pharmacokinetics of denosumab in healthy subjects and postmenopausal

women with osteopenia or osteoporosis [34]. Denosumab (AMG 162; Prolia®) is a fully human monoclonal antibody of the IgG2 subclass that has high affinity ($K_D = 3 \times 10^{-12}$ mol/L) and specificity for the receptor activator of nuclear factor κ-B ligand (RANKL). Upon binding of denosumab to RANKL, it prevents the binding between RANKL and its receptor, RANK, which is expressed on pre-osteoclasts and mature osteoclasts. Consequently, terminal differentiation, activation and survival of osteoclasts are hampered. This results in a reduction in bone resorption and an increase in bone mineral density (BMD).

After the SC administration of denosumab, the drug is absorbed with the first-order process K_a. Absolute bioavailability (F) is estimated by simultaneously analyzing the serum free denosumab concentration obtained after SC and IV administration. After IV bolus dosing or SC absorption, free denosumab is distributed into the central compartment that has the volume of distribution represented by V_1. The non-specific distribution from the central compartment into the peripheral compartment is characterized by intercompartmental clearance (Q) and the peripheral volume of distribution (V_2). The free denosumab in the central compartment is eliminated by a linear pathway quantified by CL_{lin}, or by binding to RANKL (R) following a second-order process (K_{on}) to form the denosumab-RANKL (RC) complex. The denosumab-RANKL complex is dissociating according to a first-order process (K_{off}) and generates free denosumab and RANKL, or is internalized through a first-order process, represented by the rate constant K_{int}. RANKL is assumed to be produced following a zero-order process, characterized by K_{syn}, and degraded by a first-order process (K_{deg}).

However, the denosumab-RANKL association and dissociation processes are substantially faster than the change in denosumab disposition and elimination of the RANKL and denosumab-RANKL complex. Therefore, the quasi-steady-state approximation of the TMDD model is considered more suitable to describe the pharmacokinetics of denosumab with the assumption that the drug-receptor complex is at steady-state. Consequently, the binding rate is balanced by the sum of the dissociation and internalization rates. Moreover, the steady-state constant (K_{ss}), defined as $K_D + \frac{K_{int}}{K_{on}}$, is estimated since the denosumab –RANKL binding affinity (K_D), defined as $\frac{K_{off}}{K_{on}}$, cannot be estimated independently.

The differential equations that are used to describe the amount of denosumab and RANKL in the body are as follows (**Equations 3-10** to **3-12**):

$$\frac{dA_D}{dt} = -K_a \cdot A_D$$

(Eq. 3-10)

$$\frac{dA_{tot}}{dt} = K_a \cdot A_D - CL_{tot} \cdot C - Q \cdot \left(C - \frac{A_p}{V_2}\right)$$

(Eq. 3-11)

$$\frac{dR_{tot}}{dt} = \ K_{syn} - K_{deg} \cdot R_{tot} - \frac{\left(K_{int} - \ K_{deg}\right) \cdot \ R_{tot} \cdot C}{K_{ss} + C}$$

(Eq. 3-12)

where A_D, A_p, and A_C represent an amount of denosumab in the depot, peripheral, and central compartment, respectively. R_{tot} is the total amount of RANKL receptors which include free and bound receptors. The total amount of denosumab (A_{tot}) in the serum is introduced as the sum of serum free and bound denosumab and can be estimated by the differential **Equation 3-11**. The serum free denosumab concentration ($C_{free} = \frac{A_C}{V_1}$) and the denosumab-RANKL complex are calculated as followed (**Equations 3-13** to **3-14**):

$$C_{free} = \frac{1}{2}\left[\left(\left(\frac{A_{tot}}{V_1}\right) - R_{tot} - K_{ss}\right) + \sqrt{\left(\frac{A_{tot}}{V_1} - R_{tot} - K_{ss}\right)^2 + 4 \cdot K_{ss} \cdot \frac{A_{tot}}{V_1}}\right]$$

(Eq. 3-13)

$$RC = \frac{R_{tot} \cdot C_{free}}{K_{ss} + C_{free}}$$

(Eq. 3-14)

The total clearance in **Equation 3-11** can be estimated by **Equation 3-15**.

$$CL_{tot} = CL_{lin} + \frac{K_{int} \cdot V_1 \cdot R_{tot}}{K_{ss} + C_{free}}$$

(Eq. 3-15)

The initial conditions of these differential equations (**Equations 3-10** to **3-12**) are set as (**Equation 3-16**):

$$A_D(0) = F \cdot Dose_{SC}$$

$$A_{tot}(0) = Dose_{IV}$$

$$A_p(0) = 0$$

$$R_{tot}(0) = R_0 = \frac{K_{syn}}{K_{deg}}$$

(Eq. 3-16)

Data Simulation

By using the reported population pharmacokinetic parameters of filgrastim and denosumab that were estimated in the original studies (**Table 3-1**), the plasma concentration-time profiles for filgrastim and denosumab after IV and SC administration were reproduced in Phoenix® WinNonlin 6.3 from the sets of equations that were described in the structural pharmacokinetic model section. For denosumab, the population pharmacokinetic parameters estimated from the data set that includes BLQ data were used. The input bioavailability of SC administered filgrastim and denosumab were set to the values of the estimated bioavailability from the original study (0.691 and 0.638 for filgrastim and denosumab, respectively [34, 42]). Simulation was also performed with an absolute bioavailability of 1 for easier assessment of the deviation between nominal bioavailability and the bioavailability determined by comparing AUCs. To study dose effect on the bias of bioavailability estimation, simulations were performed to generate the plasma concentration-time profiles of filgrastim and denosumab at various IV and SC doses, 0.01 – 10000 μg/kg for filgrastim; and 0.66 – 210 mg for denosumab. These dose ranges were selected based on the evidence of usual therapeutic doses and doses that were studied for clinical evidence or pharmacokinetic profiles of filgrastim and denosumab. For filgrastim, the pharmacokinetic study was performed in the dose range of 2.5 – 10 μg/kg for SC administration and at 5 μg/kg for IV administration [42]. The usual therapeutic dose range for filgrastim is 1.2 - 10 μg/kg [43]. For denosumab, the population pharmacokinetic meta-analysis was implemented on the pooled data from 11 clinical studies which covered the dose range of 6 – 210 mg of denosumab [34]. The recommended therapeutic dose of denosumab is 120 mg via SC administration every 4 weeks [44]. However, the dose ranges that were used for simulation in this study were expanded to the extremes, especially for filgrastim, in order to capture the dynamic of the errors that possibly occur from the current approach of bioavailability estimation. All the parameter values used in the simulations to study the dose effect are summarized in **Table 3-1**.

To further evaluate the influence of other TMDD parameters on the bioavailability estimation of therapeutic proteins that undergo TMDD, the plasma concentration-time profiles of filgrastim in the dose range of 0.01 – 10 μg/kg were simulated with the variation of K_D (0.001 – 50 ng/mL), K_{int} (0.0001 – 50 h^{-1}), K_{off} (0.001 – 50 h^{-1}), and K_{on} (0.001 – 50 mL/ng·h). The respective parameter values and results for these estimations are listed as supplemental data to this dissertation.

Data Analysis

Non-compartmental analysis was performed in Phoenix® WinNonlin 6.3 to determine the area under the concentration-time curve (AUC) of the simulated profiles. The absolute bioavailability estimation was calculated from **Equation 3-17** under the assumption of a dose-independent, constant clearance.

Table 3-1. Summary of the estimated population pharmacokinetic parameters of filgrastim and denosumab following IV and SC administration that were used for simulation to determine the dose effect on bioavailability estimation

Model drug	Dose	Parameters	Fixed-effect estimate
Filgrastim	0.01, 0.05, 0.1, 0.5, 1, 2.5, 5, 10, 50, 100, 500, 1000, 1500, 5000, and 10000 µg/kg	F	0.691, 1.0
		K_a (h^{-1})	0.403
		F_2	0.586
		D_2	6.6
		K_e (h^{-1})	0.26
		V_d (L)	2.03
		K_D (ng/mL)	0.308
		K_{int} (h^{-1})	0.0438
		K_{deg} (h^{-1})	0.215
		AR_0 (µg)	12.7
		K_{off} (h^{-1})	0.389
		$C_{s,0}$ (ng/mL)	0.0253
Denosumab	0.66, 1.98, 6, 6.6, 14, 15, 19.8, 30, 60, 66, 100, 120, 198, and 210 mg	F	0.638
		K_a (d^{-1})	0.212
		CL_{lin} (mL/day/66 kg)[a]	73.44
		V_1 (mL/66 kg)	2490
		Q (mL/day/66 kg)[a]	909.6
		V_2 (mL/66 kg)	1360
		K_{ss} (ng/mL)	138
		K_{int} (d^{-1})[a]	0.1908
		K_{deg} (d^{-1})[a]	0.03552
		R_0 (ng/mL)	614

[a] The parameter values were converted to day base unit. 66 kg is the typical weight of postmenopausal women with osteoporosis in the original study [34].
NOTE: F = absolute bioavailability; K_a = first-order absorption rate constant; F_2 = bioavailability of the zero-order absorption process of filgrastim; D_2 = duration of zero-order absorption of filgrastim; K_e = first-order elimination rate constant; V_d = volume of distribution of filgrastim; K_D = equilibrium dissociation constant which equals to $\frac{K_{off}}{K_{on}}$; K_{int} = first-order internalization rate constant; K_{deg} = first-order degradation rate constant; AR_0 = pretreatment amount of G-CSF receptors in the blood and bone marrow; K_{off} = first-order dissociation rate constant; $C_{s,0}$ = pretreatment concentration of G-CSF; CL_{lin} = linear clearance; V_1 = central volume of distribution; Q = intercompartmental clearance; V_2 = peripheral volume of distribution; K_{ss} = quasi-steady-state constant; R_0 = baseline RANKL level
Source: a) Wiczling, P., P. Lowe, E. Pigeolet, F. Ludicke, S. Balser, and W. Krzyzanski, *Population pharmacokinetic modelling of filgrastim in healthy adults following intravenous and subcutaneous administrations.* Clin Pharmacokinet, 2009. **48**(12): p. 817-26.

Table 3-1. (Continued)

b) Sutjandra, L., R.D. Rodriguez, S. Doshi, M. Ma, M.C. Peterson, G.R. Jang*, et al.*, *Population pharmacokinetic meta-analysis of denosumab in healthy subjects and postmenopausal women with osteopenia or osteoporosis.* Clin Pharmacokinet, 2011. **50**(12): p. 793-807.

$$F = \frac{AUC_{SC}/D_{SC}}{AUC_{IV}/D_{IV}}$$

(Eq. 3-17)

where F is the absolute bioavailability, AUC_{SC} is the AUC from SC administration, AUC_{IV} is the AUC from IV administration, D_{SC} is the SC dose, and D_{IV} is the IV dose. To determine dose effect, F was calculated for the different combinations of doses after SC and IV administration of filgrastim or denosumab. Dose normalized AUCs (AUC_D) and average clearance (CL) at different doses were calculated to determine the effect of dose on these parameters by using **Equations 3-18** and **3-19** respectively.

$$AUC\_D = \frac{AUC}{Dose}$$

(Eq. 3-18)

$$CL = \frac{F \cdot Dose}{AUC}$$

(Eq. 3-19)

To quantify the error in the bioavailability assessment, %prediction error was calculated by **Equation 3-20**.

$$\%Prediction\ error = \frac{F_{sim} - F_{ref}}{F_{ref}} \times 100$$

(Eq. 3-20)

where F_{sim} is the bioavailability calculated from the simulated data, and F_{ref} is the reference bioavailability which is the absolute bioavailability that was used to simulate the plasma concentration-time profiles of filgrastim or denosumab. The reference values are 0.691 or 1.0 for filgrastim, and 0.638 or 1.0 for denosumab.

Results

With reported population pharmacokinetic parameters and models for filgrastim and denosumab, plasma concentration-time profiles at various IV and SC doses of both protein drugs were simulated and shown in **Figure 3-1**. Notably, the pattern of plasma concentration-time profile of both filgrastim and denosumab showed transition during variation of IV and SC doses.

Subsequently, with the combinations of different IV and SC doses of filgrastim at the reference bioavailability value of 0.691 (F_{ref} = 0.691), the dose variation from 0.01 – 10000 μg/kg yielded the bioavailability estimations presented in **Table 3-2**. The absolute bioavailability resulted from the dose effect varied from 0.172 – 2.74 showing the deviation from the reference bioavailability (F_{ref} = 0.691) that was used for the drug input in the TMDD model simulation. The corresponding prediction errors ranged from -75.1

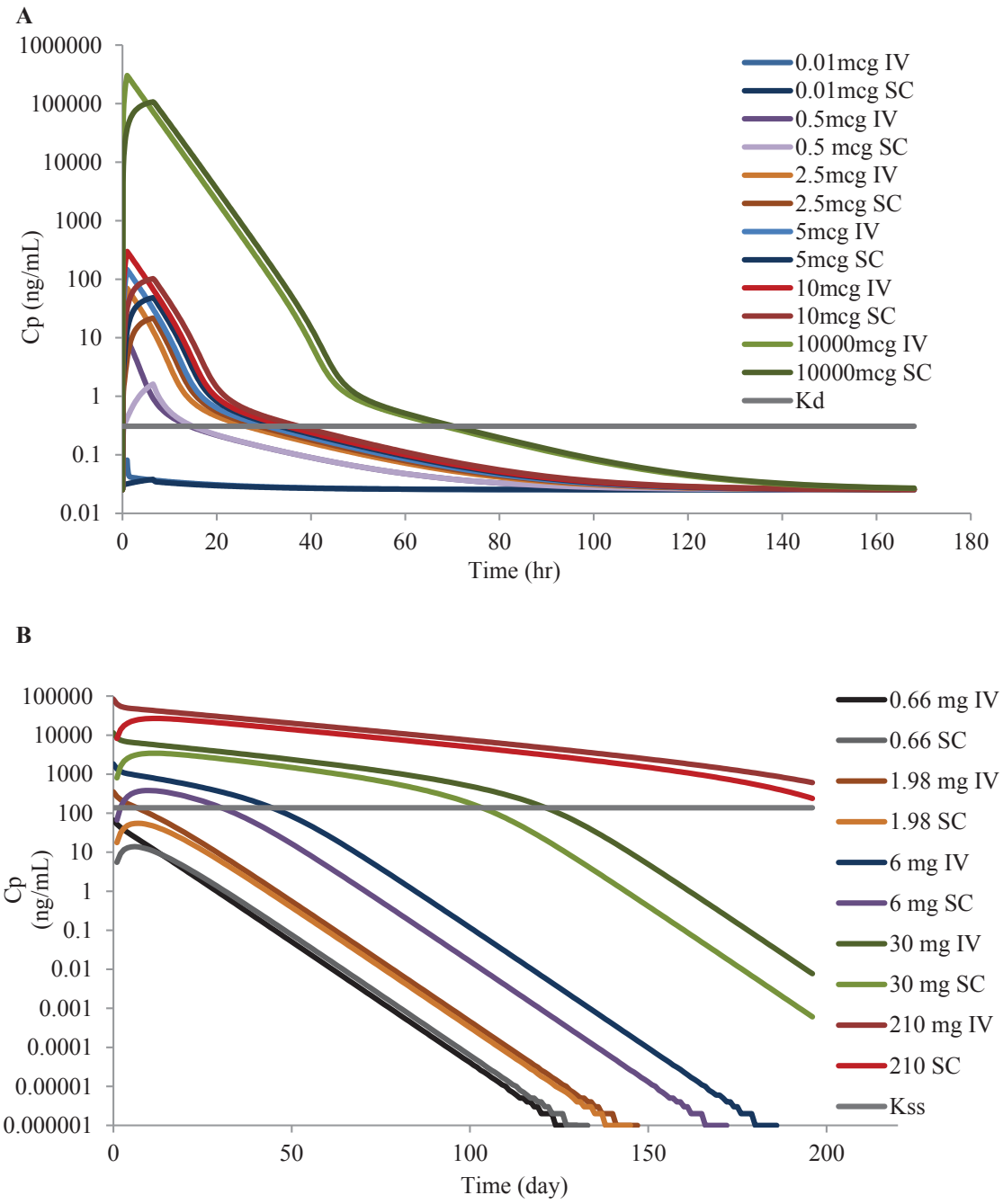

Figure 3-1. Simulated plasma concentration-time profiles of filgrastim and denosumab after IV and SC administration

Plasma concentration-time profiles were simulated in the dose range of 0.01 – 10000 µg/kg for filgrastim (A) and 0.66 – 210 mg for denosumab (B).

Table 3-2. Dose effect on the bioavailability estimation of filgrastim with reference bioavailability (F_{ref}) equals to 0.691[a]

IV dose	SC dose (µg/kg)														
(µg/kg)	**0.01**	**0.05**	**0.1**	**0.5**	**1**	**2.5**	**5**	**10**	**50**	**100**	**500**	**1000**	**1500**	**5000**	**10000**
0.01	0.683	**0.694**	0.711	0.929	1.32	1.94	2.26	2.46	2.67	2.70	2.73	2.73	2.74	2.74	2.74
	(-1.11)	**(0.462)**	(2.91)	(34.4)	(91.7)	(180.)	(227)	(256)	(287)	(290.)	(295)	(296)	(296)	(296)	(296)
0.05	0.663	0.674	**0.690**	0.901	1.29	1.88	2.19	2.39	2.59	2.62	2.65	2.65	2.65	2.66	2.66
	(-4.05)	(-2.52)	**(-0.141)**	(30.4)	(86.0)	(172)	(217)	(245)	(274)	(279)	(283)	(284)	(284)	(284)	(285)
0.1	0.627	0.637	**0.652**	0.852	1.22	1.78	2.07	2.26	2.44	2.48	2.50	2.51	2.51	2.51	2.51
	(-9.29)	(-7.85)	**(-5.60)**	(23.3)	(75.8)	(157)	(200.)	(226)	(254)	(258)	(262)	(263)	(263)	(263)	(264)
0.5	0.345	0.350	0.359	0.469	**0.668**	0.977	1.14	1.24	1.34	1.36	1.38	1.38	1.38	1.38	1.38
	(-50.1)	(-49.3)	(-48.1)	(-32.2)	**(-3.32)**	(41.3)	(64.7)	(79.5)	(94.5)	(97.0)	(99.2)	(99.5)	(99.7)	(99.9)	(99.9)
1	0.261	0.265	0.271	0.355	0.506	**0.739**	0.861	0.938	1.02	1.03	1.04	1.04	1.04	1.05	1.05
	(-62.3)	(-61.7)	(-60.7)	(-48.7)	(-26.8)	**(6.95)**	(24.7)	(35.8)	(47.2)	(49.1)	(50.8)	(51.0)	(51.1)	(51.3)	(51.3)
2.5	0.211	0.214	0.220	0.287	0.409	0.598	**0.697**	0.759	0.823	0.833	0.843	0.844	0.845	0.846	0.846
	(-69.5)	(-69.0)	(-68.2)	(-58.5)	(-40.8)	(-13.5)	**(0.851)**	(9.88)	(19.1)	(20.6)	(22.0)	(22.2)	(22.3)	(22.4)	(22.4)
5	0.194	0.197	0.201	0.263	0.375	0.549	0.639	**0.697**	0.755	0.765	0.773	0.775	0.775	0.776	0.776
	(-72.0)	(-71.5)	(-70.8)	(-61.9)	(-45.7)	(-20.6)	(-7.47)	**(0.811)**	(9.28)	(10.6)	(11.9)	(12.1)	(12.2)	(12.3)	(12.3)
10	0.184	0.187	0.192	0.250	0.357	0.522	0.608	0.663	**0.718**	0.727	0.735	0.737	0.737	0.738	0.738
	(-73.4)	(-72.9)	(-72.3)	(-63.8)	(-48.3)	(-24.5)	(-12.0)	(-4.12)	**(3.94)**	(5.23)	(6.44)	(6.62)	(6.68)	(6.78)	(6.80)
50	0.175	0.178	0.182	0.238	0.340	0.497	0.579	0.631	0.684	**0.692**	0.700	0.701	0.702	0.703	0.703
	(-74.6)	(-74.2)	(-73.6)	(-65.5)	(-50.8)	(-28.1)	(-16.2)	(-8.71)	(-1.04)	**(0.195)**	(1.34)	(1.51)	(1.58)	(1.67)	(1.69)
100	0.174	0.177	0.181	0.237	0.337	0.493	0.575	0.626	0.679	0.687	**0.695**	0.696	0.696	0.697	0.697
	(-74.8)	(-74.4)	(-73.8)	(-65.8)	(-51.2)	(-28.7)	(-16.9)	(-9.41)	(-1.80)	(-0.579)	**(0.560)**	(0.731)	(0.792)	(0.883)	(0.905)
500	0.173	0.175	0.180	0.235	0.335	0.489	0.570	0.621	0.674	0.682	0.690	**0.691**	0.691	0.692	0.692
	(-75.0)	(-74.6)	(-74.0)	(-66.0)	(-51.5)	(-29.2)	(-17.5)	(-10.1)	(-2.51)	(-1.30)	(-0.166)	**(0.00402)**	(0.0642)	(0.155)	(0.177)
1000	0.173	0.175	0.180	0.235	0.334	0.489	0.570	0.621	0.673	0.681	0.689	0.690	**0.691**	0.691	0.691
	(-75.0)	(-74.6)	(-74.0)	(-66.1)	(-51.6)	(-29.2)	(-17.5)	(-10.2)	(-2.61)	(-1.40)	(-0.272)	(-0.103)	**(-0.0427)**	(0.0483)	(0.0699)
1500	0.172	0.175	0.179	0.234	0.334	0.489	0.570	0.621	0.673	0.681	0.689	0.690	0.690	**0.691**	0.691
	(-75.0)	(-74.6)	(-74.0)	(-66.1)	(-51.6)	(-29.3)	(-17.6)	(-10.2)	(-2.65)	(-1.44)	(-0.310)	(-0.141)	(-0.0808)	**(0.0101)**	(0.0317)
5000	0.172	0.175	0.179	0.234	0.334	0.488	0.569	0.620	0.672	0.681	0.688	0.690	0.690	0.691	**0.691**
	(-75.1)	(-74.7)	(-74.0)	(-66.1)	(-51.6)	(-29.3)	(-17.6)	(-10.2)	(-2.71)	(-1.50)	(-0.368)	(-0.199)	(-0.139)	(-0.0481)	**(-0.0265)**
10000	0.172	0.175	0.179	0.234	0.334	0.488	0.569	0.620	0.672	0.681	0.688	0.690	0.690	0.691	**0.691**
	(-75.1)	(-74.7)	(-74.0)	(-66.1)	(-51.7)	(-29.3)	(-17.6)	(-10.3)	(-2.72)	(-1.51)	(-0.382)	(-0.213)	(-0.153)	(-0.0620)	**(-0.0404)**

[a] %Prediction errors are reported in the brackets. Bioavailabilities with minimum bias are reported in bold.
Light gray area demonstrates overestimated bioavailability with prediction error exceeds 20%.
Dark gray area demonstrates underestimated bioavailability with prediction error exceeds 20%.

to +296. The overestimations tended to appear in the right upper area of the table when high SC doses and low IV doses of filgrastim were used for bioavailability calculations; whereas the underestimations of bioavailability were observed in the left lower area of the table in which low SC doses and high IV doses of filgrastim were used for bioavailability estimations. The acceptable prediction errors considered as ±20% were attained when bioavailability was estimated from IV and SC filgrastim in the dose ranges of 0.01 – 0.1 μg/kg and 5 – 10000 μg/kg irrespective of the combination of IV and SC doses. The minimum biases tended to occur in the diagonal area of the table when the similar doses of IV and SC filgrastim were used for the bioavailability estimation. However, higher SC doses than IV doses were required in order to achieve the lowest bias of bioavailability estimation except for IV dose of 0.1 μg/kg that showed the minimum error when it was paired with the same dose of SC administration. A similar result was also observed when the input bioavailability for simulation was set to 1.0 (data is shown in **Table A-1** in the **Appendix A** section). However, the least deviation of bioavailability estimation seemed to be mostly achieved with the same doses of IV and SC administration when input bioavailability was set to 1.0.

Notably, even with the same doses of IV and SC filgrastim used for the bioavailability assessment, some bias still occurred in the dose range of 0.01 – 10 μg/kg, especially at 0.5 and 1 μg/kg that showed a prediction error greater than 20% in the case of input bioavailability was set to 0.691. In this dose range, the highest error of bioavailability estimation occurred at 0.5 μg/kg with prediction errors equaled to -32.2% and -19.6% when F_{ref} = 0.691 and F_{ref} = 1.0 respectively (**Figure 3-2**).

Similarly to the full TMDD model for filgrastim, estimation of absolute bioavailability for denosumab with the quasi-steady state approximation to the TMDD model was also affected by dose variation. The results for dose variation from 0.66 – 210 mg of IV and SC administered denosumab at F_{ref} = 0.638 are shown in **Table 3-3**. The absolute bioavailability varied from 0.0264 – 12.5, substantial deviation from F_{ref} = 0.638. The corresponding prediction errors ranged from -95.9 to +1862%. Most overestimation was observed in the upper right corner of **Table 3-3** when high SC and low IV denosumab doses were used for bioavailability estimation; whereas the absolute bioavailability was underestimated in the lower half left of **Table 3-3** when low SC and high IV doses were used for calculation. Bioavailability with acceptable prediction error (± 20%) was estimated in the dose range of 60 – 210 mg denosumab (lower right area of the table) regardless of the combination of IV and SC doses. The least bias tended to be presented along the diagonal area of the table when similar doses of IV and SC denosumab with mostly higher SC doses than IV doses were used for bioavailability estimation. Similar to filgrastim, simulation results of denosumab with F_{ref} = 1.0 also showed the same pattern and comparable magnitude of error (-95.5 – 1926% prediction error) as of those resulting from F_{ref} = 0.638 (**Table A-2** in **Appendix A** section). Moreover, as in the case of filgrastim, the least deviation of bioavailability estimation was achieved with mostly the same doses of IV and SC administered denosumab when F_{ref} = 1.0.

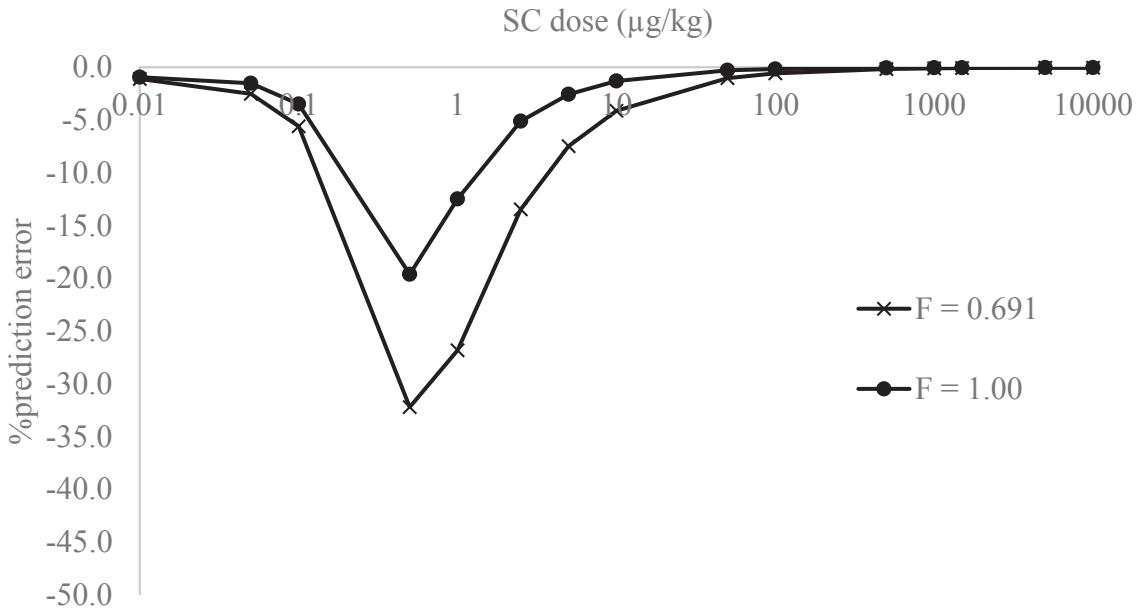

Figure 3-2. %Prediction error of bioavailability estimation by dose effect in filgrastim

Table 3-3. Dose effect on the bioavailability estimation of denosumab with the reference bioavailability (F_{ref}) equals to 0.638[a]

IV dose	SC dose (mg)													
(mg)	**0.66**	**1.98**	**6**	**6.6**	**14**	**15**	**19.8**	**30**	**60**	**66**	**100**	**120**	**198**	**210**
0.66	**0.535**	0.760	2.51	2.84	5.82	6.09	7.17	8.63	10.5	10.7	11.5	11.8	12.5	12.5
	(-16.1)	(19.1)	(294)	(344)	(812)	(855)	(1024)	(1252)	(1550)	(1583)	(1707)	(1752)	(1852)	(1862)
1.98	0.256	**0.364**	1.20	1.36	2.79	2.92	3.44	4.13	5.04	5.14	5.52	5.66	5.96	5.99
	(-59.8)	**(-43.0)**	(88.5)	(113)	(337)	(357)	(438)	(548)	(690.)	(706)	(766)	(787)	(835)	(839)
6	0.0750	0.107	0.352	0.398	**0.816**	0.855	1.01	1.21	1.48	1.51	1.62	1.66	1.75	1.75
	(-88.2)	(-83.3)	(-44.8)	(-37.7)	**(27.8)**	(33.9)	(57.7)	(89.6)	(131)	(136)	(153)	(160.)	(174)	(175)
6.6	0.0693	0.0984	0.325	0.367	**0.754**	0.790	0.930	1.12	1.36	1.39	1.49	1.53	1.61	1.62
	(-89.1)	(-84.6)	(-49.0)	(-42.4)	**(18.1)**	(23.8)	(45.7)	(75.2)	(114)	(118)	(134)	(140.)	(153)	(154)
14	0.0439	0.0624	0.206	0.233	0.478	0.500	**0.589**	0.708	0.865	0.882	0.947	0.970	1.02	1.03
	(-93.1)	(-90.2)	(-67.7)	(-63.5)	(-25.1)	(-21.6)	**(-7.68)**	(11.0)	(35.5)	(38.2)	(48.4)	(52.1)	(60.3)	(61.1)
15	0.0426	0.0605	0.200	0.226	0.463	0.486	0.572	**0.687**	0.839	0.856	0.919	0.942	0.992	0.997
	(-93.3)	(-90.5)	(-68.6)	(-64.6)	(-27.4)	(-23.9)	(-10.4)	**(7.74)**	(31.5)	(34.1)	(44.0)	(47.6)	(55.5)	(56.3)
19.8	0.0383	0.0544	0.180	0.203	0.417	0.437	0.514	**0.618**	0.755	0.770	0.826	0.847	0.892	0.897
	(-94.0)	(-91.5)	(-71.8)	(-68.2)	(-34.7)	(-31.5)	(-19.4)	**(-3.10)**	(18.3)	(20.6)	(29.5)	(32.7)	(39.9)	(40.6)
30	0.0339	0.0482	0.159	0.180	0.369	0.387	0.455	0.547	**0.668**	0.681	0.732	0.750	0.790	0.794
	(-94.7)	(-92.4)	(-75.0)	(-71.8)	(-42.2)	(-39.4)	(-28.7)	(-14.2)	**(4.70)**	(6.79)	(14.7)	(17.5)	(23.8)	(24.4)
60	0.0297	0.0421	0.139	0.157	0.323	0.338	0.398	0.479	0.584	0.596	**0.640**	0.656	0.691	0.694
	(-95.3)	(-93.4)	(-78.2)	(-75.3)	(-49.4)	(-47.0)	(-37.6)	(-25.0)	(-8.42)	(-6.59)	**(0.287)**	(2.78)	(8.31)	(8.85)
66	0.0293	0.0416	0.137	0.155	0.318	0.334	0.393	0.472	0.576	0.588	**0.631**	0.647	0.682	0.685
	(-95.4)	(-93.5)	(-78.5)	(-75.7)	(-50.1)	(-47.7)	(-38.4)	(-26.0)	(-9.65)	(-7.84)	**(-1.05)**	(1.41)	(6.86)	(7.40)
100	0.0279	0.0396	0.131	0.148	0.303	0.318	0.374	0.450	0.549	0.560	0.602	0.616	**0.650**	0.653
	(-95.6)	(-93.8)	(-79.5)	(-76.8)	(-52.4)	(-50.2)	(-41.3)	(-29.5)	(-13.9)	(-12.2)	(-5.72)	(-3.38)	**(1.82)**	(2.33)
120	0.0274	0.0390	0.129	0.145	0.298	0.313	0.368	0.443	0.540	0.551	0.591	0.606	**0.639**	0.642
	(-95.7)	(-93.9)	(-79.8)	(-77.2)	(-53.2)	(-51.0)	(-42.3)	(-30.6)	(-15.4)	(-13.7)	(-7.30)	(-4.99)	**(0.114)**	(0.620)
198	0.0265	0.0375	0.124	0.140	0.288	0.301	0.355	0.426	0.520	0.531	0.570	0.584	0.616	**0.619**
	(-95.9)	(-94.1)	(-80.5)	(-78.0)	(-54.9)	(-52.8)	(-44.4)	(-33.2)	(-18.4)	(-16.8)	(-10.7)	(-8.44)	(-3.52)	**(-3.03)**
210	0.0264	0.0374	0.124	0.140	0.286	0.300	0.353	0.425	0.519	0.529	0.568	0.582	0.613	**0.616**
	(-95.9)	(-94.1)	(-80.6)	(-78.1)	(-55.1)	(-53.0)	(-44.6)	(-33.4)	(-18.7)	(-17.1)	(-11.0)	(-8.77)	(-3.87)	**(-3.38)**

[a] %Prediction errors are reported in the brackets. Bioavailabilities with minimum bias are reported in bold.
Light gray area demonstrates overestimated bioavailability with prediction error exceeds 20%.
Dark gray area demonstrates underestimated bioavailability with prediction error exceeds 20%.

However, with the same doses of IV and SC denosumab, the bias of bioavailability estimation was more pronounced than for filgrastim, especially in the case of F_{ref} = 0.638 as can be observed in **Figure 3-3**. At F_{ref} = 0.638, a prediction error greater than 20% was observed in the dose range of 1.98 – 15 mg denosumab with the highest bias occurring at 6 mg. In contrast to filgrastim that showed the bias peaks at the same dose at different F_{ref}, the most error occurred at 1.98 mg denosumab when F_{ref} was set at 1.0.

The dose effect on dose-normalized AUC of filgrastim and denosumab were investigated and shown in **Figure 3-4**. For filgrastim, at both F_{ref} = 0.691 and F_{ref} = 1.0, dose-normalized AUC increased as the doses increased and exhibited the S-shaped curve which could be observed in **Figures 3-4A** and **3-4B** respectively. The rapid increase of dose-normalized AUC occurred in the dose range of 0.1 – 5 μg/kg filgrastim. Similarly, the same pattern of the dose effect on dose-normalized AUC were observed for denosumab at both F_{ref} = 0.638 (**Figure 3-4C**) and F_{ref} = 1.0 (**Figure 3-4D**). The slightly S-shaped curves showed an increasing of dose-normalized AUC as the doses increased in the range of 0.66 – 210 mg. The sharp increase of dose-normalized AUC occurred at the dose of 1.98 mg onward and seemed to reach a plateau at very high dose. Notably, dose-normalized AUC tended to level off at 60 mg IV and SC doses of denosumab.

The alteration of dose-normalized AUC during dose variation may imply the disproportional change in filgrastim and denosumab plasma concentrations at different doses resulted from the concentration-dependent clearance. The dynamic of clearance alteration at different doses was subsequently investigated and the results are shown in **Figures 3-5** and **3-6** for filgrastim and denosumab, respectively. Dose effect on clearance was linked by a peak plasma concentration (C_{max}) since the rate of elimination depends on available systemic concentration.

Upon increasing dose, C_{max} after IV and SC administration was increased. However, the increasing pattern of C_{max} after SC administration was slightly different from what was observed after IV administration with the extra reflection points in the dose range of 0.1 – 5 μg/kg for filgrastim (**Figure 3-5A**) and below 60 mg for denosumab (**Figure 3-6A**). Different degrees of clearance at various IV and SC doses of filgrastim and denosumab were subsequently correlated with the corresponding C_{max}. To truly represent clearance for protein drugs that undergo TMDD at various doses, average clearance determined from plasma concentration-time profiles after IV administration was used as a reference.

Due to the wrong assumption of dose-independent clearance that was used for bioavailability estimation for protein drugs that undergo TMDD, average clearances that were determined from plasma concentration-time profiles of SC administration showed bias with the deviation from average clearance after IV administration (**Figures 3-5B** and **3-6B** for filgrastim and denosumab, respectively). F that was used in the calculation for determining the average clearance after SC administration (**Equation 3-19**) only accounted for bias within apparent clearance that associated with dose- independent elimination. Thus, average clearance determined from concentration-time profile after SC

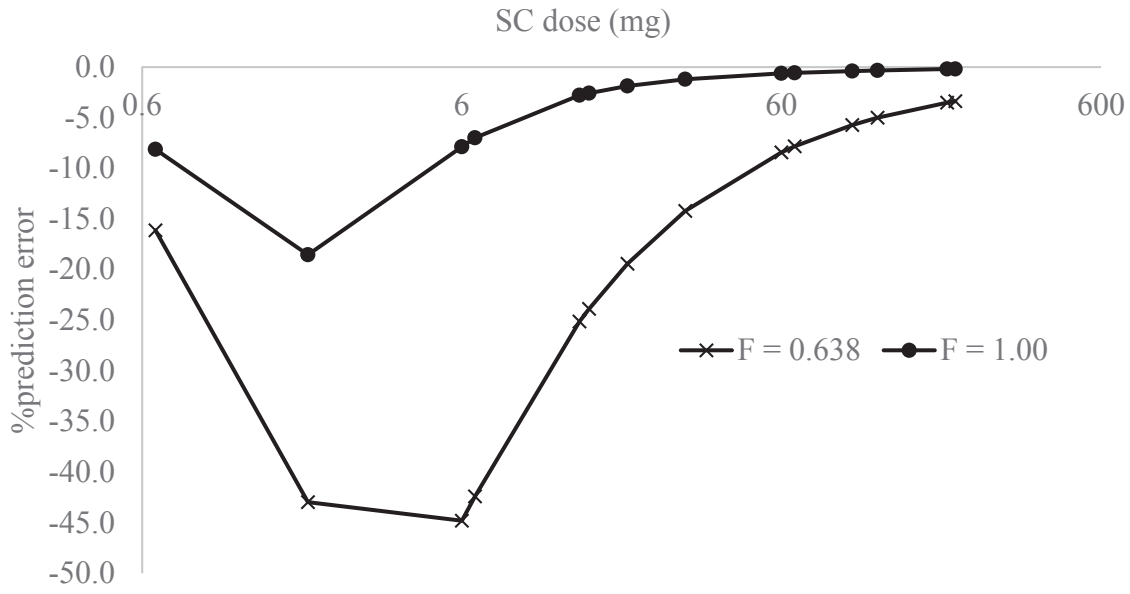

Figure 3-3. %Prediction error of bioavailability estimation by dose effect in denosumab

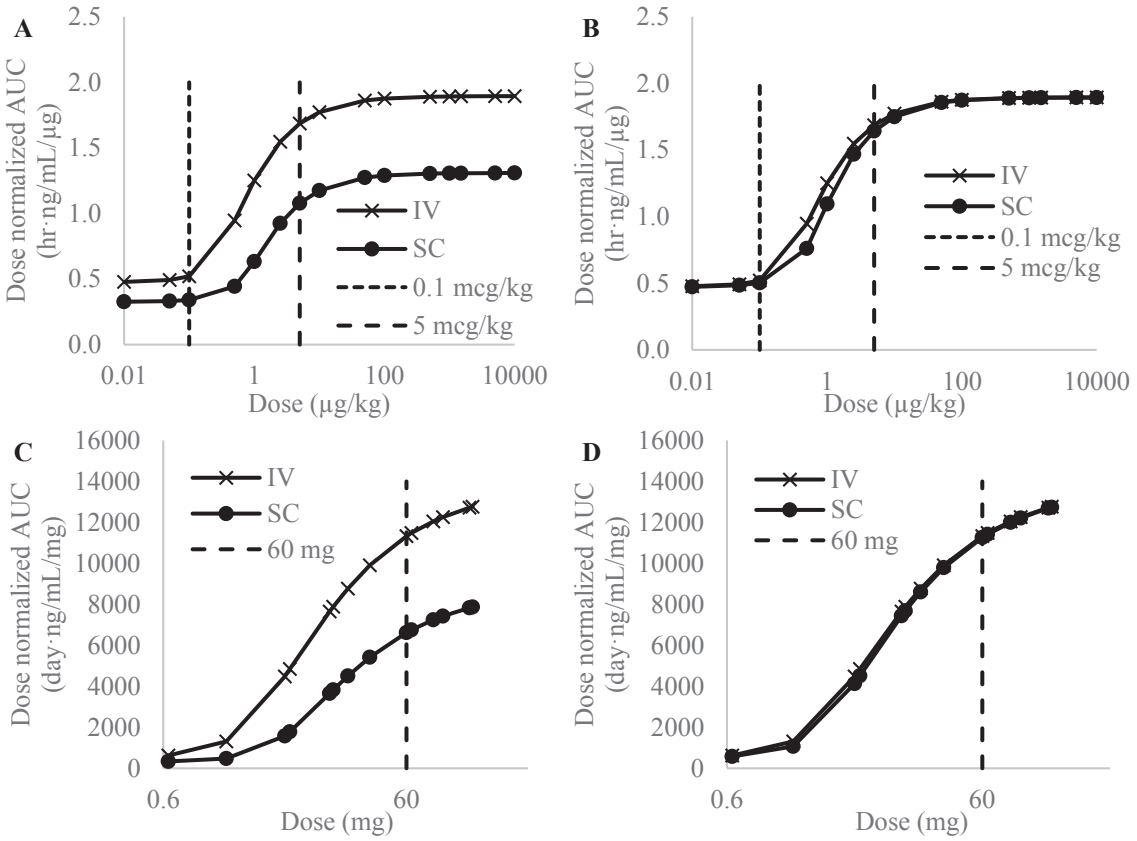

Figure 3-4. Dose effect on the dose normalized AUC of filgrastim and denosumab
The effect of dose on dose-normalized AUC of filgrastim exhibited an S-shaped curve with dose normalized AUC increased as dose increased in the range of 0.1 – 10 µg/kg at both F = 0.691 (A) and F = 1.0 (B). Similarly, the effect of dose on dose-normalized AUC of denosumab showed a slightly S-shaped curve with dose normalized AUC increased as dose increased in the range of 0.66 – 210 mg at both F = 0.638 (C) and F = 1.0 (D).

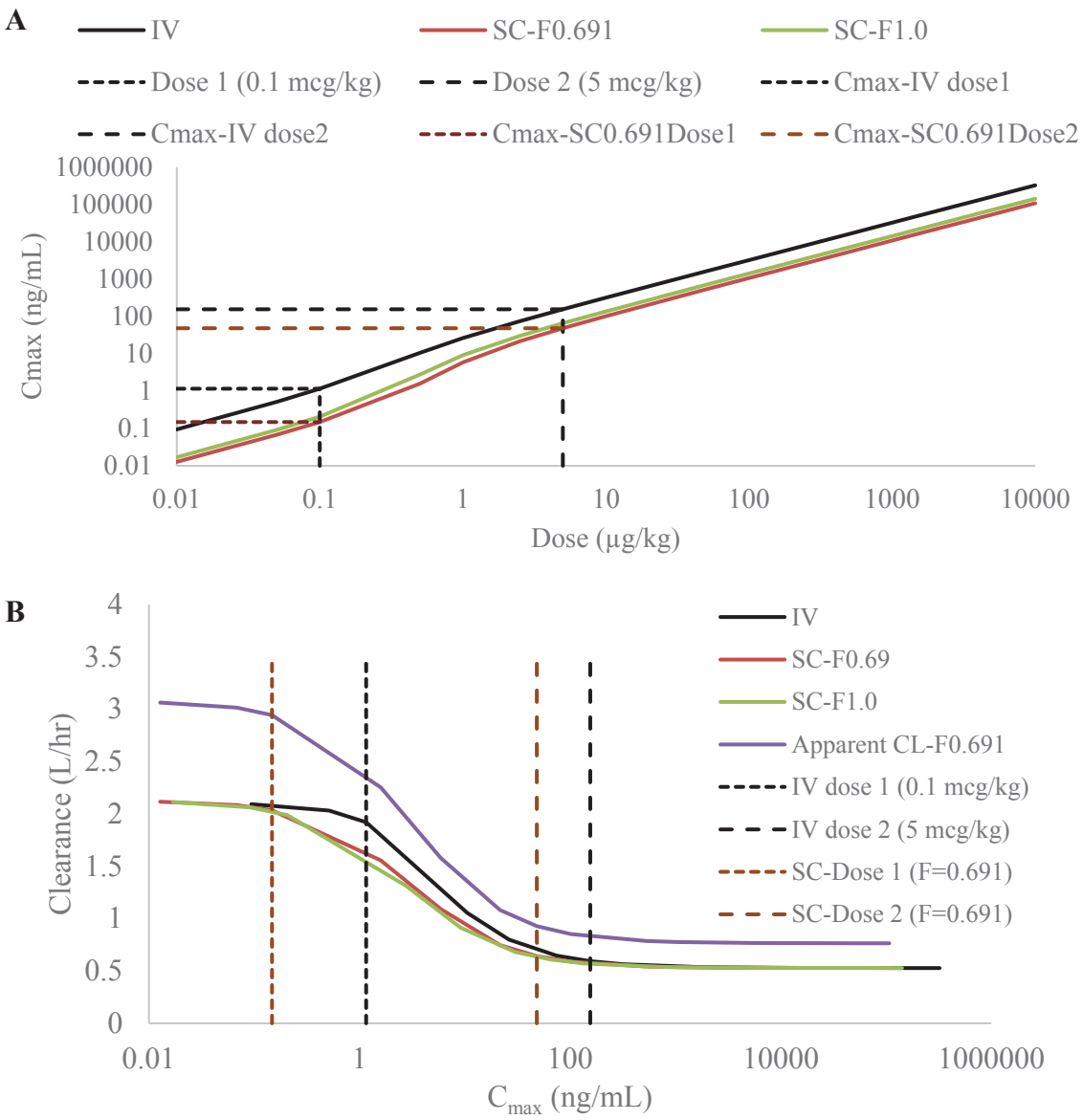

Figure 3-5. The correlation between dose and average clearance of filgrastim through the alteration of plasma concentration

Due to increasing dose, peak plasma concentration of IV and SC administered filgrastim (C_{max}) was increased (A). At various C_{max}, different degrees of clearance were observed (B).

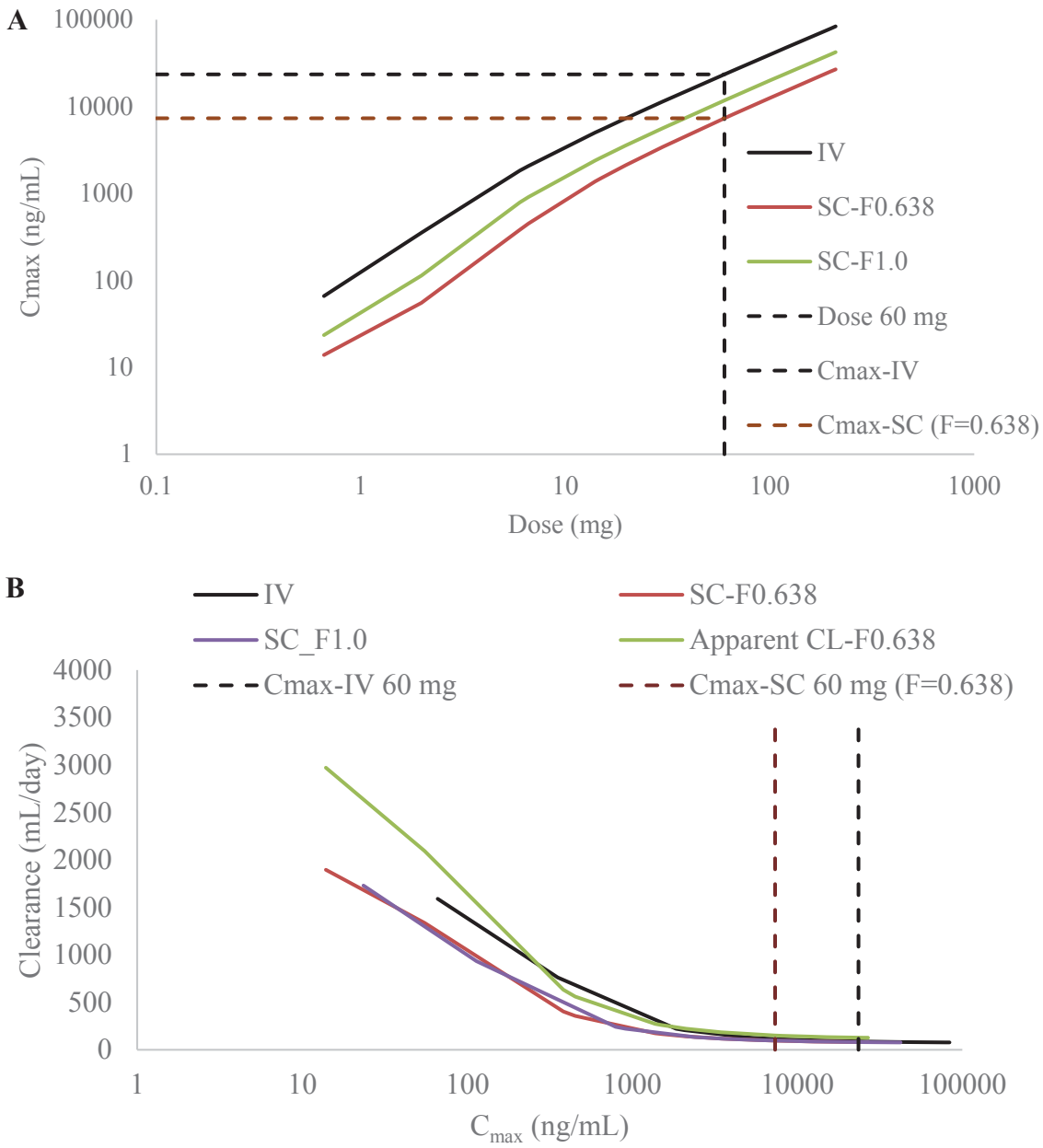

Figure 3-6. The correlation between dose and average clearance of denosumab through the alteration of plasma concentration
Due to increasing dose, peak plasma concentration of IV and SC administered denosumab (C_{max}) was increased (A). At various C_{max}, different degrees of clearance were observed (B).

administration may warrant at very low or very high doses when linear elimination process was dominated.

For filgrastim, clearance showed a perfect S-shaped correlation to the various degree of C_{max} with a high degree of constant clearance at low C_{max} and low invariant clearance at high C_{max} (**Figure 3-5B**). It should be noted that a very active dynamic in the alteration of clearance occurred in the plasma concentration range corresponding to 0.1 – 5 μg/kg filgrastim regardless of administration route. In contrast to filgrastim, clearance of denosumab did not show an S-shaped pattern (**Figure 3-6B**). However, similar to filgrastim, minimum constant clearance was achieved at the high dose. A dynamic change in clearance of denosumab was observed in the plasma concentration range that was corresponded to doses lower than 60 mg for both IV and SC administration.

Discussion

With dose-dependent clearance and subsequent non-linear pharmacokinetics, bioavailability estimations are difficult to perform for drugs that undergo a TMDD process since the standard methodology for bioavailability estimation is calculated under the assumption of dose-independent, constant clearance. As a consequence of an assumption violation, the dose-dependent bioavailability that is usually observed when the standard methodology is used in drugs that exhibit TMDD pharmacokinetics is misleading. This notion is supported by this simulation study when the bioavailability of filgrastim and denosumab were determined at various doses.

Although, the assumption and limitation of pharmacokinetic models can impact the simulated concentration-time profiles [41] in which they might deviate from the real pharmacokinetic profiles, the full TMDD model and the quasi-steady-state approximation of the TMDD model that were proven to adequately describe the pharmacokinetics of filgrastim [42] and denosumab [34], respectively, should be able to fairly reproduce the pharmacokinetic profiles of both protein drugs. Transition in the characteristics of plasma concentration-time profiles of filgrastim and denosumab during variation of doses is also observed in a study of the dynamics of TMDD by Peletier and Gabrielsson [41]. The nonlinear pharmacokinetics and dose-dependent bioavailability that were observed in both therapeutic proteins in this study have also been reported in other studies [33] and for several other protein drugs that undergo TMDD [29, 31].

Dose-dependent bioavailability that was observed in filgrastim and denosumab was a result from a change in dose-normalized AUC during dose alteration. Regardless of the assumed nominal bioavailability F_{ref} and the applied pharmacokinetic model, the dose had an effect on the dose normalized AUC of both therapeutic proteins, filgrastim, and denosumab. As doses increased, the dose-normalized AUCs tended to increase which were very obvious in the dose range of 0.1 – 5 μg/kg for filgrastim and 1.98 mg onward for denosumab. This dose effect on the dose normalized AUC was also observed in population pharmacokinetic-pharmacodynamic modeling of filgrastim in healthy volunteers [33] and during a population pharmacokinetic study of AMG 317, a fully

human monoclonal antibody against IL4 receptor [45] in which the increasing dose caused an increase in dose-normalized AUC during non-compartmental analysis.

The increment in dose-normalized AUC upon increasing dose of filgrastim and denosumab may indicate a disproportionate increase in plasma concentration, which may subsequently imply the alteration in clearance due to the variation of dose. The results showed that different degrees of clearance could be observed at various plasma concentrations (C_{max}) resulting from different IV doses of filgrastim and denosumab. The cooperation between two elimination pathways, a linear clearance and a target receptor-mediated elimination, may impart the dynamic in the alteration of clearance during dose variation. Similar to what is described in the dynamics of TMDD study [41], different plasma concentrations of ligand determine which elimination pathway becomes predominant. At low plasma concentration (low dose) of protein drugs, target receptors still have the capacity for the elimination of ligands, thus TMDD is considered as the main pathway of clearance. However, increasing plasma concentration upon increasing dose until target receptor becomes partially saturated, the contribution of TMDD to the overall clearance may decrease and protein drugs are more potentially eliminated via a linear clearance pathway. After all target receptors are saturated at very high plasma concentration (high dose) of therapeutic proteins, the linear clearance pathway is dominated. The transition between these two elimination pathways during dose variation may not only cause a change in the degree of clearance but also influence the transition in the characteristics of plasma concentration-time profile as could be observed in filgrastim and denosumab.

For both protein drugs, the average clearance tended to decrease as plasma concentration increased and this decreasing was very obvious in the corresponding dose range of 0.1 – 5 μg/kg for filgrastim and below 60 mg for denosumab. The dose-dependent or concentration-dependent clearance observed in this study was also observed in interferon-β1a [31], other several therapeutic monoclonal antibodies [29] such as tocilizumab [46], PF-04840082 (Dickkopt-1 antibody) [47], panitumumab, cetuximab [32], and concizumab [48], a bivalent humanized nanobody [49], and in the study of the dynamics of TMDD [40]. At very high doses of both protein drugs, the clearance reached the lowest plateau phase, which might be due to the saturation of the targets that are responsible for protein degradation. At this plateau phase after high dosing, the linear clearance pathway becomes predominant [29, 31, 32, 34, 40, 46, 48].

As a consequence of transition between two elimination pathways, change in the degree of clearance, and transition in the characteristics of plasma concentration-time profile, disproportional increased AUC upon increasing dose may contribute to the increment of dose-normalized AUC. Due to these artifacts, if different IV and SC dose levels are combined and used for bioavailability estimation, it may cause bias. The results showed the overestimation of bioavailability was observed with the combination of high SC doses and low IV doses, and the underestimation of bioavailability occurred when the combination of low SC doses and high IV doses was used.

In the original clinical study, the bioavailability of filgrastim was determined from three SC injections of 2.5, 5, and 10 μg/kg, and one IV infusion of 5μg/kg over half an hour. However, according to the results reported in **Table 3-2**, bioavailability estimation within this dose range could result in prediction error ranging from -20.6% to +0.811%. For denosumab, pooled data from 11 clinical studies with IV and SC dose range of 6 – 210 mg possibly resulted in the bias of bioavailability estimation in the range of -80.6 – +175% (**Table 3-3**). Thus, the bioavailability obtained for filgrastim and denosumab may not represent the true bioavailability.

However, the bioavailability of filgrastim and denosumab could be estimated with ±20% prediction error if the assessment was performed in the dose ranges of 0.01 – 0.1 μg/kg or 5 – 10000 μg/kg for filgrastim, and 60 – 210 mg for denosumab. Notably, any combination within these dose ranges could be used for bioavailability estimation. Interestingly, these dose ranges yielded constant dose normalized AUC. The constant dose-normalized AUC might result from a proportional increase in plasma concentration which was due to the concentration-independent clearance that concurrently occurred within these dose ranges. To minimize the bias of bioavailability estimation, similar or the same doses of IV and SC administration should be used. It should be noted that if F_{ref} was less than 1.0, slightly higher SC dose than IV dose should be combined in order to attain the least deviation. This may imply that similar plasma concentration after IV and SC administration may be required in order to achieve the minimum bias. It seems intuitively possible since similar plasma concentration after IV and SC administration may be eliminated with a similar degree through the same pathway of clearance. Nevertheless, with the same IV and SC doses, prediction error greater than 20% still occurred when bioavailability estimations were calculated in the dose range of 0.5 – 1 μg/kg filgrastim and 1.98 – 15 mg denosumab. The errors that occurred when bioavailability was estimated from an equal dose of IV and SC administration might result from other factors that affect the clearance of drugs that go through TMDD pathway which in turn can affect the drug concentration-time profiles and AUCs.

Other factors that possibly have an impact on the bioavailability assessments of drugs that undergo TMDD are the parameters specific for the TMDD process, the dissociation rate constant (K_D) which describes the binding (K_{on}) and dissociation (K_{off}) processes, and the internalization process described by K_{int} that occurs after drugs bind to their receptors. Moreover, for denosumab, the quasi-steady-state constant (K_{ss}) in the quasi-steady-state approximation to TMDD model can be an influential factor. The effects of all these parameters were shown to affect the drug concentration vs time profiles in the dynamics of TMDD study dependent on the dose of the ligands [40, 41]. The impact of these factors was further explored in the supplemental material.

It should be noted that the bioavailability of therapeutic proteins that follow a TMDD pathway should be carefully estimated, especially in the dose range in which the target sites are partially saturated and both elimination pathways have equal potential to contribute to the overall clearance, since dose-normalized AUC varies actively with dose at this state. To overcome this problem, a very low dose of protein drug within the capacity of target receptor can be used for bioavailability assessment. However, with the

limitation of the sensitivity of the analytical method, this may become problematic. Another solution is to perform bioavailability estimation at the high dose of therapeutic proteins that saturate all target sites and render the linear clearance pathway to become dominant. At this state, the bioavailability estimation is no longer dependent on dose. Thus, this saturation phase should be the suitable state for determining the true absolute bioavailability with the least bias. In many instances, however, these are supra-therapeutic doses that cannot practically administer to human subjects or animal.

Ideally, to get an accurate assessment of bioavailability of protein drugs that undergo TMDD, the IV doses should be administered at the amounts that will generate the exact same plasma concentration-time profiles as those from SC administrations. However, this might be difficult to accomplish since carefully monitoring the drug plasma concentration-time profile is required during IV infusion. Even in an ideal scenario in which nonlinearity through TMDD can be overcome by high doses (as outlined in the previous chapter), other factors can affect the bioavailability assessment of therapeutic proteins. One such factor that could result in true nonlinearity in bioavailability is the absorption process that occurs in the body. In a study by Zhao et al., bioavailability is shown to be sensitive and negatively related to transit time for the drug from lymph system to systemic circulation (τ) and elimination rate during lymphatic transport (K_{lymph}) [50]. Moreover, bioavailability is also found to be sensitive and positively related to the lymphatic flow rate when the lymphatic flow rate is set to less than 0.5 fold of original value.

Gibiansky et al suggest another way to determine the absolute bioavailability with a minimum bias for drugs that exhibit nonlinear pharmacokinetics , in which the ratio of IV and SC doses that provided equal AUCs are used for bioavailability estimation [51]. By this method, the approximation underestimates the true bioavailability by no more than 5 – 30% with more precision of approximation achieved when AUC at steady-state is used for calculation. Moreover, the bias decreases with the increase of SC absorption, true bioavailability, and SC dose. This finding may also imply that equal amount of protein drugs presented in the systemic circulation after IV and SC administration is required in order to achieve a minimum bias of bioavailability estimation. According to this finding, the bioavailability of filgrastim and denosumab may be more accurately estimated by determining the ratio of IV and SC doses that possessed equal AUCs.

In conclusion, with the current methodology and assumptions of bioavailability determination, the absolute bioavailability of drugs that undergo a TMDD pathway and exhibit nonlinear pharmacokinetics are estimated with bias. The bias is caused by a dose effect on the dose-normalized AUC, which is the result of concentration-dependent differences in clearance based on differences in the characteristics of the concentration-time profiles. To achieve more accurate bioavailability estimation, the absolute bioavailability should be determined, if possible, at low or high doses when the invariant clearance is observed or with the alternate estimation method suggested by Gibiansky et al [51]that determines the ratio of IV and SC doses that generate equal AUCs.

CHAPTER 4. THE ONTOGENY OF NEONATAL FC RECEPTOR (FCRN) EXPRESSION IN MICE

Introduction

The neonatal Fc receptor (FcRn) (reviewed in [16, 52-56]), also known as the Brambell receptor, is a major histocompatibility (MHC) class I-like molecule that is encoded by *Fcgrt*. It is a heterodimeric glycoprotein consisting of one heavy chain with a large extracellular part associated with one β_2 microglobulin (β_2m) subunit followed by a transmembrane segment and a short cytoplasmic tail. The extracellular part of the FcRn heavy chain is composed of three subunits denoted as α_1, α_2, and α_3 (**Figure 4-1**). The functions of FcRn include protection of IgG and albumin from catabolism, transportation of IgG across epithelial cells, and antigen presentation in immunoprotective systems. IgGs and albumins are found to bind noncompetitively and without cooperativity to the distinct FcRn binding site. Although FcRn can bind to IgG as a 1:1 complex, most studies have shown that two FcRn molecules bind to a single IgG with the stoichiometric ratio of 2:1 [52, 53, 55]. Mutational and crystallographic studies have revealed the Fc-FcRn complex structure, and proposed that FcRn uses the C-terminal portion of the α_2 domain, the first residue of β_2-microglobulin and carbohydrate to interact with the Fc C_H2-C_H3 interface [57, 58]. Upon the pH-dependent binding process, FcRn does not undergo a major conformational change. However, a slight rearrangement of the FcRn side chain and chemical alteration of the amino acid residues occurs at the binding interface.

As previously described in **Chapter 1**, FcRn resides mainly within acidic cytoplasmic vesicles inside the cells. The interaction with IgG is initiated when circulating IgG is taken up by receptor-mediated endocytosis or fluid-phase pinocytosis, and subsequently binds to FcRn in the endosomes (**Figure 1-2**). The acidic environment causes protonation of the histidine residues in the area between the C_H2 and C_H3 domains of the Fc region. The protonated histidine binds to the binding site on the FcRn heavy chain. After binding the IgG-FcRn complex returns to the apical or basolateral side of the cell surface membrane in the recycling and transcytosis processes, respectively. The exposure to physiological pH causes the release of IgG to the blood stream or the extracellular fluid. This process occurs in a strictly pH-dependent manner such that the binding takes place in an acidic environment (~ 6.0 – 6.5) and the release takes place in the physiological or neutral milieu (~ 7.4) [59-65]. This pH dependencyis the consequence of the presence of the conserved histidine residues on the Fc fragment of IgG that bind to the α_2 domain of FcRn [52].

FcRn expression has been detected in a variety of endothelial, epithelial, and hematopoietic cells in various organs throughout the body, including skin [64, 66, 67], muscle [66, 68], liver [63, 68-70], kidney [66, 71], spleen [66, 70], lung [70, 72], mammary gland [73], intestine [62, 66, 69, 70, 72, 74-79], stomach [69], brain [66, 80, 81], eye [82], immune cells [65, 83], and placenta [84-87] (**Table 4-1**). FcRn is expressed throughout life and differs across tissue types and species. However, a developmental downregulation of intestinal FcRn mRNA and protein are observed in adult rodents

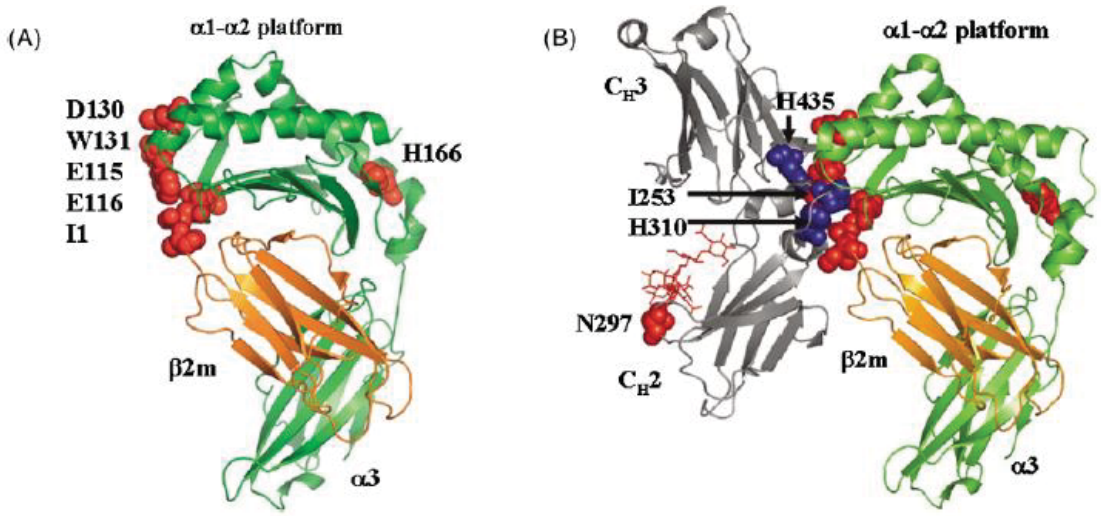

Figure 4-1. The crystal structures of human FcRn and rat FcRn-rat IgG Fc complex

(A) The crystal structure of human FcRn. The loci of the amino acids essential for IgG (E115, E116, D130, W131, L135 and I1) and albumin (H166) binding are highlighted. (B) The co-crystal structure of rat FcRn with a rat IgG Fc fragment. The amino acid residues (H310, H435, and I253) at the Fc elbow region involved in binding to FcRn are highlighted with numbers and arrows. The glycosylated amino acid residue N297 in the C_H2 domain of rat Fc is shown as a red spherical ball and numbered. The corresponding amino acid residues on rat FcRn involved in IgG Fc (E117, E118, E132, W133, D137, and I1) and albumin binding (H168) are indicated as red balls. In both figures, the FcRn heavy chain is shown in green and β2m in orange.

Source: Reprinted with permission from The Japanese Society for the Study of Xenobiotics (JSSX). Andersen, J.T. and I. Sandlie, *The versatile MHC class I-related FcRn protects IgG and albumin from degradation: implications for development of new diagnostics and therapeutics.* Drug Metab Pharmacokinet, 2009. **24**(4): p. 318-32.

Table 4-1. Distribution of FcRn expression in various organs and their functions

Organs	Cell types and tissues	Functions
Skin	Endothelial cell - Capillary endothelium [66] Epithelial cell - Stratum corneum, keratinocytes, melanocytes, sebaceous glands, and hair follicles [64, 67] Hematopoietic cell - Histiocytes	- Homeostasis of IgG [68]
Liver	Endothelial cell - Capillary endothelium [68] Epithelial cell - Hepatocyte [63, 66, 70], sinusoidal and canalicular membranes [63, 66, 68, 69] Hematopoietic cell - Kupffer cells [66, 69]	- Recycling of IgG [88]
Kidney	Epithelial cell - Podocytes, and proximal tubule cells [66, 71]	- Recycling of IgG to prevent accumulation in the kidney
Lung	Epithelial cell - Apical regions of large and small bronchiolar airways, and alveolar [72] Hematopoietic cell - Macrophages [66]	-Absorption of IgG and Fc fusion proteins [72] - Antigen presentation process
Intestine	Epithelial cell - Apical membranes of enterocyte villi, and crypts of small intestine [66, 75-79] Hematopoietic cell - Macrophages in intestinal lamina propria [65, 69, 77]	- Absorption of IgG and Fc-fusion proteins - Antigen presentation process
Muscle	Endothelial cell - Capillary endothelium [66, 68, 69] Epithelial cell - Endomysium [68]	
Stomach	Epithelial cell - Gastric mucosa [69]	

Table 4-1. (Continued)

Organs	Cell types and tissues	Functions
Spleen	Endothelial cell - Capillary endothelium [89] Hematopoietic cell - Macrophages [66, 89]	- Antigen presentation process
Eye	Endothelial cell - Capillary endothelium [82] - Corneal endothelium [82] Epithelial cell - Corneal, conjunctiva, non-pigmented ciliary, optic nerve, and lens epithelium [82]	- Blood-ocular barrier [82]
Central nervous systems	Endothelial cell - Capillary endothelium [66, 80, 81] Epithelial cell - Choroid plexus ependymal cells, and peripheral nerve perineurium [66, 80]	- Efflux of IgG from the brain to blood [81]
Reproductive organs	Endothelial cell - Placental endothelial cells [84] (inconsistently detected) Epithelial cell - Mucosa of uterine and vaginal tissues - Syncytiotrophoblasts of placenta [85, 87]	- Maternofetal immunity transfer
Mammary organs	Epithelial cell - Acinar epithelium of mammary glands [73]	- Maternofetal immunity transfer in rodent (Recycling of IgG)
Blood	Hematopoietic cell - Monocytes, monocyte-derived dendritic cells, and polymorphonuclear neutrophils (PMN) [65, 83, 89] - B cells [89](inconsistently detected)	- Recycling of IgG during homeostasis - Antigen presentation process
Lymph node	Hematopoietic cell - Macrophages, and dendritic cells [66]	- Antigen presentation process

relative to neonates [62, 74-76]. In the rat, reduction in FcRn mRNA and protein expression occurs in an age-dependent manner in the distal to proximal direction until FcRn-mediated IgG absorption is no longer detected at 3 weeks postpartum. Moreover, an upregulation of the expression of FcRn protein has been shown in mouse brain microvessels during aging [81]. These data suggest age-dependent differences in FcRn expression at different stages of development which might impact the pharmacokinetics of therapeutic proteins that bind to this receptor. To investigate the effect of ontogeny on the FcRn, FcRn protein expression in different organs was quantified relative to GAPDH expression, in different age groups of C57BL/6J mice in this study.

Due to preliminary results (data not shown) and information from the literature showing that expression of FcRn in adult rodent intestine [74, 75, 79], and stomach [66, 74] were undetectable, along with the low probability that these organs are involved in the homeostasis of therapeutic proteins that bind to this receptor, FcRn expression was not quantitated in these organs. Moreover, IgG is found to preferentially distribute to the lung, kidney, spleen, liver, and skin [55]. Thus, relative FcRn expression was quantified in these organs in 2, 10, 21, 42, and 70 day old animals. Although studies in adult mice reveal that FcRn is expressed in a functionally active form in the endothelium of small arterioles and capillaries of skin, muscle, liver, adipose tissues [68], and hematopoietic cells [66, 89], the potential of functional FcRn in other organs of neonates could not be precluded.

Materials and Methods

Animals

In order to obtain at least six animals at different ages including 2, 10, 21, 42, and 70 days of age, nine timed-pregnant C57BL/6J mice were purchased from The Jackson Laboratory (Bar Harbor, ME). Animals were shipped at 7 - 15 days of gestation and arrived at 10 - 18 days of gestation. All timed-pregnant mice were housed in the animal facility for 1 week before the delivery with free access to food and water. Pups delivered by pregnant mice were raised to pre-determined ages according to the study design and weaned at day 21. The day of birth was assigned as the first day of life (day 1). Males and females were housed separately in different cages at the weaning age (day 21) with ear tags for background tracking. All animals were housed in standard laboratory cages and had free access to food and water throughout the study period.

Organ Collection

At least one offspring from each timed-pregnant C57BL/6J mice was sacrificed for tissue collection at ages 2, 10, 21, 42, and 70 days. Each age group contained at least six animals, both males, and females. Euthanasia was performed with CO_2 and cervical dislocation in all age groups except mice at ages 2 and 10 days, which were sacrificed by

decapitation. The animal protocol was approved by the Institutional Animal Care and Use Committee (IACUC) at the University of Tennessee Health Science Center. All organs including skin, liver, kidneys, lung, spleen, heart, stomach, intestine, and pancreas were collected and preserved on ice. Blood was removed from all the organs using ice-cold phosphate-buffered saline (PBS). All organs were subsequently stored at -70°C until further processing.

Tissue Lysate and Total Protein Extract Preparation

Total protein extract from each organ was prepared using a commercial total protein extraction kit (Millipore, Billerica, MA). A 20 – 40-mg sample of tissue was excised from the whole organ and chopped into very small pieces. The tissue was then added into Eppendorf tubes containing 1×PI (a cocktail of protease inhibitor) in TM buffer (mixture of HEPES (pH 7.9), $MgCl_2$, KCl, EDTA, sucrose, glycerol, sodium deoxycholate, NP-40, sodium ortho-vanadate) at a gram of tissue per 2.5 mL solution, and were kept on ice for at least 5 minutes. The tissue was subsequently homogenized using a micro-homogenizer (Bio-Gen PRO200 model from Pro Scientific, Oxford, CT) at a minimum speed of 3 - 5 cycles of alternate homogenizing and resting on ice to minimize protein destruction. The tissue homogenate was rotated at 4°C for 20 minutes. Subsequently, the tissue lysate was centrifuged at 11,000 rpm at 4°C for 20 minutes. The supernatant was subsequently collected and stored at -20°C for further analysis.

Protein Quantification

Total protein in the supernatant from all samples was quantified by using the BCA protein assay kit (Novagen®, Billerica, MA). Different concentrations (0 – 1000 μg/mL) of bovine serum albumin (BSA) were prepared for a calibration curve. 25 μL of each BSA standard and protein sample were mixed with 200 μL BCA working reagent (a mixture of BCA solution and 4% cupric sulfate) on a 96-well plate. The mixture was then incubated at 60°C for 15 minutes before cooling to room temperature. The absorbance at 562 nm was measured on a plate reader (Beckman Coulter DTX880). The protein amount in the samples was determined based on the calibration curve of BSA.

Electrophoresis

Proteins in the isolated extracts were separated by gel electrophoresis. The electrophoresis was run for 90 minutes on ice in an XCell *SureLock*™ Mini-Cell (Invitrogen, Carlsbad, CA) system containing NUPAGE® MOPS SDS running buffer (Invitrogen, Carlsbad, CA) and 500 μL of NUPAGE® antioxidant (Invitrogen, Carlsbad, CA). The samples loaded on each gel comprise the following:

- Protein molecular weight markers: 5 µL of MagicMark™ XP (Invitrogen, Carlsbad, CA) + 5 µL of Novex® Sharp pre-stained protein standards (Invitrogen, Carlsbad, CA)
- Positive control: 25 ng of recombinant mouse FcRn (R&D Systems) + 1.5 µL of 10× NUPAGE® sample reducing agent (Invitrogen) + 3.75 µL of 4× NUPAGE® LDS sample buffer (Invitrogen)
- Negative control: 18 µg of bovine serum albumin + 1.5 µL of 10× NUPAGE® sample reducing agent (Invitrogen) + 3.75 µL of 4× NUPAGE® LDS sample buffer (Invitrogen)
- Unknown specimens: 20 and 40 µg of total protein extract from each organ in each age group + 1.5 µL of 10× NUPAGE® sample reducing agent (Invitrogen, Carlsbad, CA) + 3.75 µL of 4× NUPAGE® LDS sample buffer (Invitrogen, Carlsbad, CA)

The positive control, negative control, and unknown specimens were heated in a water bath at 70°C for 10 minutes before loading into 4 – 12% NUPAGE® bis-tris gels (Invitrogen, Carlsbad, CA). The electrophoresis condition was set to 150 V constant voltage with maximum current of 0.13 A.

Western Blot

After electrophoresis, separated proteins were transferred for 2 hours 15 minutes onto an Immobilon®-FL polyvinylidene fluoride (PVDF) 0.45 µm membrane (EMD Millipore, Billerica, MA) at 25 V and 0.17 A. The PVDF membrane was first pre-wetted in methanol for 1 minute and then rinsed with ultra-purified water followed by soaking in a mixture of NUPAGE® transfer buffer (Invitrogen, Carlsbad, CA) containing 20% methanol and NUPAGE® antioxidant (Invitrogen, Carlsbad, CA). The transfer process was run on ice in the XCell II™ Blot Module (Invitrogen, Carlsbad, CA) system that contained a mixture of NUPAGE® transfer buffer that was used to equilibrate the PVDF membrane.

The protein-transferred PVDF membrane was re-wetted for 1 minute in methanol, rinsed with ultra-purified water, and soaked in 1×PBS for 2 minutes. To prevent nonspecific binding of primary antibodies, the membrane was incubated in the Odyssey® blocking buffer (LI-COR, Lincoln, NE) for 1 hour at room temperature. An overnight incubation at 4°C was subsequently carried out in a mixture of 1:2000 goat anti-mouse FcRn polyclonal antibody (R&D Systems, Minneapolis, MN) and 1:10000 rabbit anti-mouse GAPDH monoclonal antibody (Cell Signaling, Beverly, MA) that was prepared in the Odyssey® blocking buffer containing 0.2%Tween 20. Protein transferred PVDF membrane was then rinsed and washed with 0.1% Tween 20 in PBS for four times,five minutes each. The incubation with a mixture of secondary antibodies in Odyssey® blocking buffer containing 0.2% Tween 20 and 0.01% sodium dodecyl sulfate (SDS) was subsequently performed for 1 hour at room temperature under light protection. The secondary antibodies in a mixture comprised 1:15000 donkey anti-goat IRDye® 800CW IgG (LI-COR, Lincoln, NE) and 1:15000 donkey anti-rabbit IRDye® 680RD IgG (LI-

COR, Lincoln, NE). After the incubation, rinsing and 5 minutes washing of the blot were completed for 4 times prior to rinsing with 1×PBS. Protein bands on the blot were detected and the intensity quantified by the Odyssey®Sa Infrared Imaging System (LI-COR, Lincoln, NE).

Data Analysis

FcRn expression was determined by the relative intensity of GAPDH band in the same sample. Within each individual sample set (20 and 40 μg loading), average relative expression of FcRn in each organ was compared across age groups by analysis of covariance (ANCOVA). Multiple comparisons with Bonferroni adjustment were performed to determine the difference of relative FcRn expression during development. Statistical analysis was performed in SAS 9.3 (SAS Institute Inc.). The difference in the relative FcRn expression between males and females in each age group was evaluated by t-test with unequal sample size.

Results

Relative FcRn protein expression in mouse organs was quantified by normalization of FcRn expression to the expression of the reference protein GAPDH within the same sample. The relative expression of FcRn protein was compared across 2, 10, 21, 42, and 70 day old mice. The Western blot scans of FcRn and GAPDH protein expression in mouse skin, liver, kidney, lung, and spleen from two sample sets (20 μg and 40 μg loading) are shown in **Figure 4-2**. The rationale for using two protein loading amounts was to assure that FcRn could be detected and quantified across all age groups since analytical sensitivity might be a problem with the down-regulation of FcRn. However, the results revealed that detection sensitivity was not an issue and FcRn in all age groups could be detected and quantified in both sample sets. Nevertheless, due to the limitations of protein abundance and the size of the organ, the 40-μg loading amount could not be performed in spleen samples from 2 day old mice.

Under reducing conditions of electrophoresis, native FcRn proteins in mouse tissues were detected at 45 – 55 kDa whereas recombinant mouse FcRn, a positive control, was consistently detected at a molecular weight ~ 45 – 47 kDa. This observation could be explained by the fact that the recombinant protein was synthesized as Ser22 – Val301 with no attached β_2m subunit. Moreover, additional modifications, such as a C-terminal 6-His tag, may contribute to the observed difference in the molecular weight. In contrast to other mouse organs, the Western blot scans showed double bands of FcRn protein at 45 – 55 kDa in mouse liver samples (**Figure 4-2B**). Broad bands of FcRn were observed in the range of 45 – 55 kDa in some samples, especially those from liver and kidney. In addition, an extra band at the molecular weight ~ 140 - 150 kDa was always present in mouse liver samples, which may be the result of the complex formation of FcRn monomers. Alternatively, cross-reactivity of the primary antibody with another

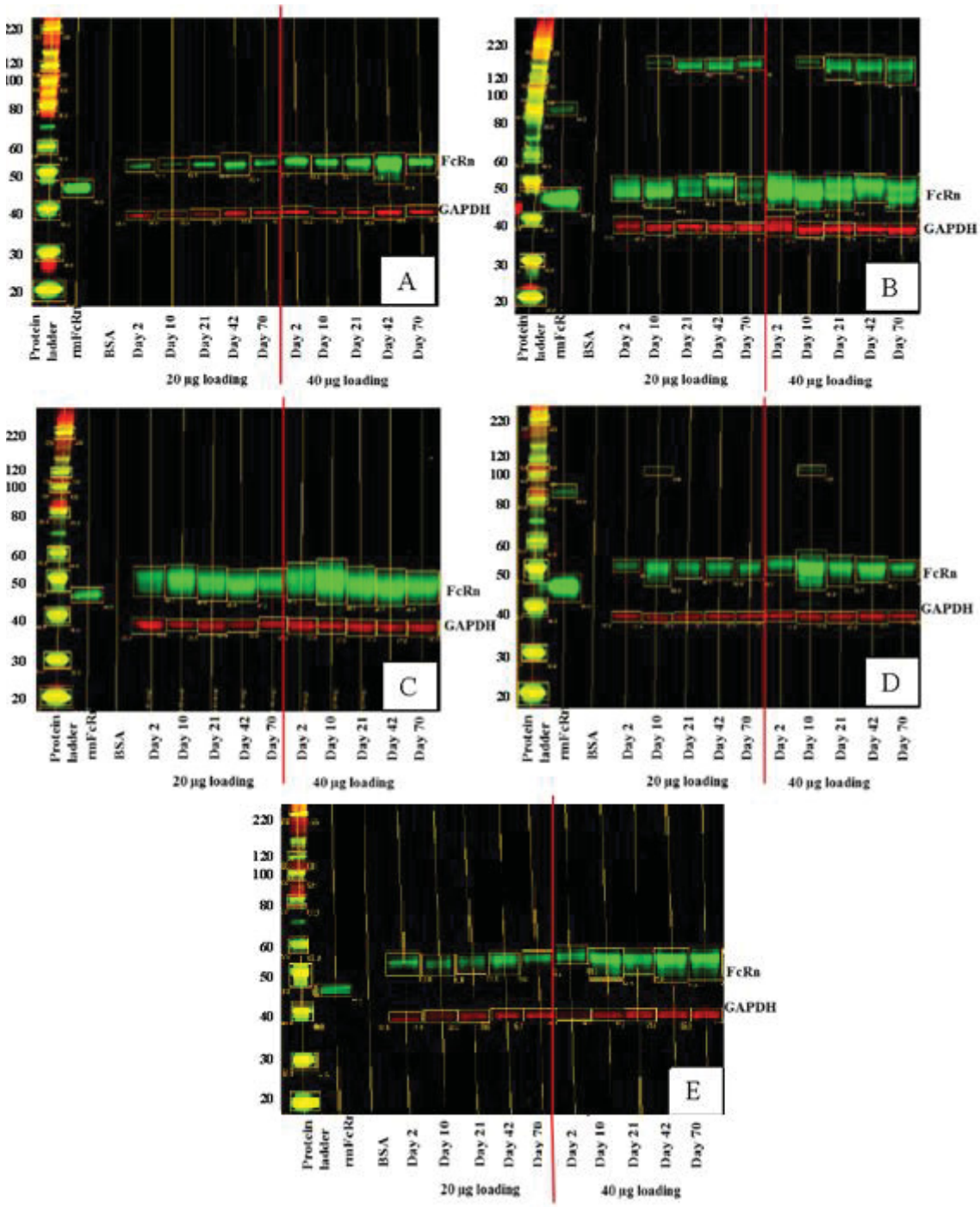

Figure 4-2. Western blot scan of FcRn and GAPDH protein expression in mouse skin (A), liver (B), kidney (C), lung (D), and spleen (E).
FcRn expression was quantified relative to GAPDH expression. The expression of FcRn was compared across all age groups within each loading sample set (20 µg and 40 µg loading amount) in each organ.

protein might have occurred. Due to this uncertainty, the relative expression of FcRn protein in mouse liver was quantitated based on the FcRn monomer at molecular weight 45 - 55 kDa and compared across all age groups.

Since there was no limitation of analytical sensitivity from loading protein at 20 μg but the scarcity of protein abundant arose from loading protein at 40 μg of spleen sample obtained from 2 day old mice, the results focused on the 20-μg loading sample set. The quantitation results of FcRn protein relative to GAPDH protein expression from the 20-μg loading samples are presented in **Figures 4-3** to **4-7** while the results of the 40-μg loading compared to those of the 20-μg loading are available in the **Appendix B** section (**Figures B-1** to **B-5**). Notably, there was a statistically significant difference between the relative amounts of FcRn protein expression in the 20-μg and 40-μg loading sample sets ($p < 0.05$). The relative FcRn expression was consistently higher in the 40-μg loading sample set than in the 20-μg loading sample set. Nevertheless, FcRn expression across all age groups showed the same pattern between two loading sample sets. As a result, the relative FcRn protein expression was compared among all age groups within each loading sample set.

In mouse skin, relative FcRn protein expression was not different among the investigated age groups, although the power to detect a difference was diminished due to lower than expected animal numbers in three age groups (**Figure 4-3**).

In mouse spleen (**Figure 4-7**), relative FcRn protein expression was also not statistically significantly different among the investigated age groups. Notably, the high variation observed in the relative FcRn protein expressions obtained from day 2 and day 10 animals may hinder the detection of significant difference.

In mouse liver; however, the relative FcRn protein expression significantly increased approximately two-fold at day 10 compared to other age groups (**Figure 4-4**). The other age groups seemed to express similar levels of FcRn proteins.

The two-fold increase of relative FcRn protein expression in 10-day old mice was also observed in mouse lung compared to 2- and 70- day old groups (**Figure 4-6**). Thus, for mouse lung, relative expression was similar in newborn and in adult animals but was approximately two-fold higher in 10-day old animals.

In mouse kidney, similar levels of relative FcRn protein expression was observed between 10- and 42-day old age groups. However, these two groups showed a two-fold increase in relative FcRn protein expression compared to other age groups (**Figure 4-5**).

The difference in the relative FcRn protein expression was also compared between males and females within each age group. The results of this analysis, however, showed that there was no significant sex difference in relative FcRn protein expression in any age group or tissue (**Figure 4-8**).

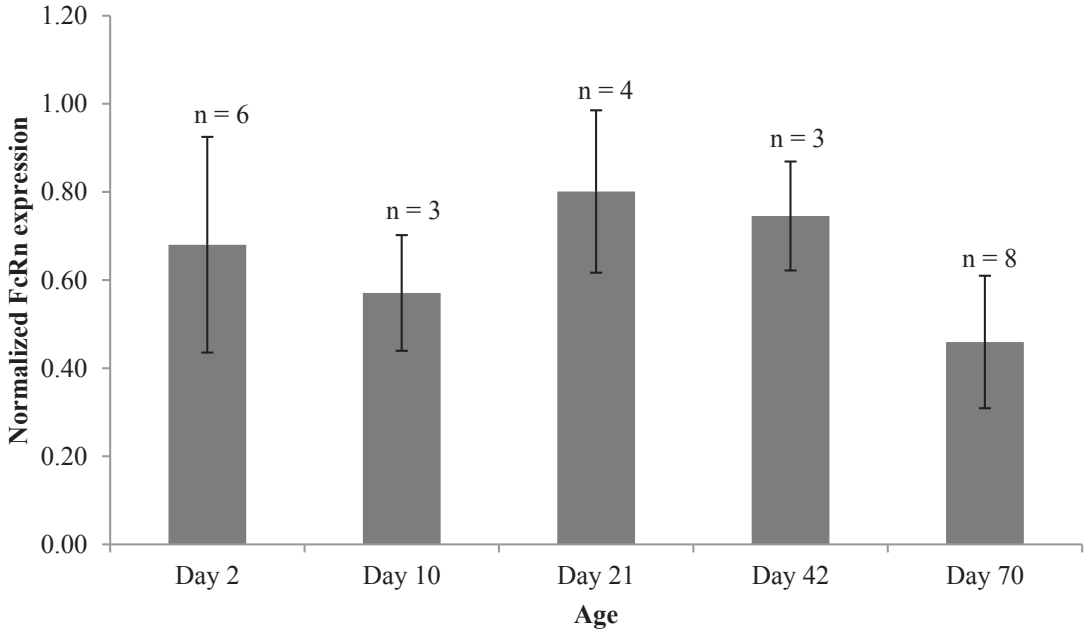

Figure 4-3. Ontogeny of FcRn protein expression in mouse skin
No significant difference in the relative FcRn protein expression was observed in the skin of 2-, 10-, 21-, 42-, and 70-day old mice.

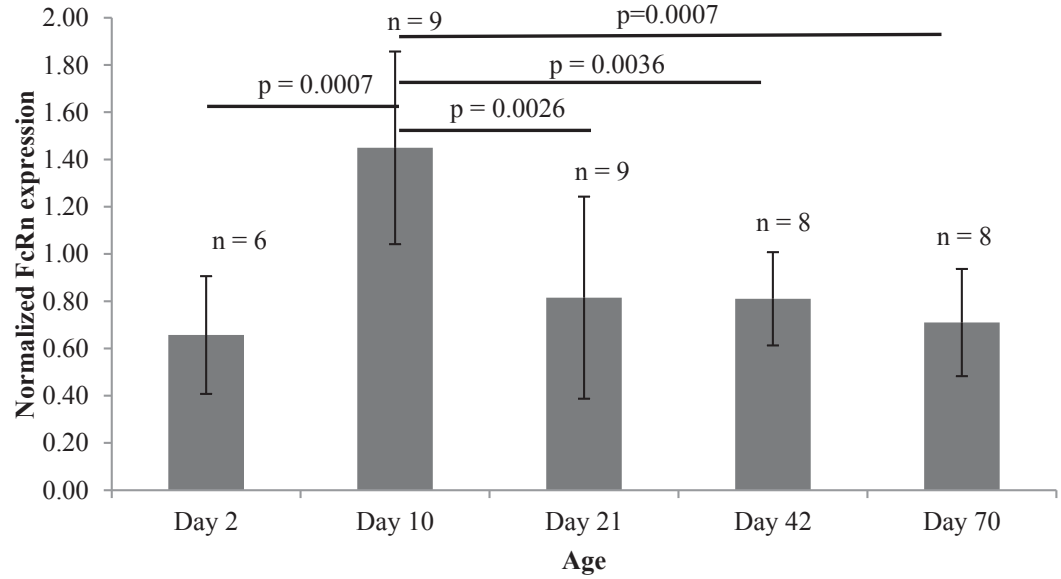

Figure 4-4. Ontogeny of FcRn protein expression in mouse liver
Relative expression of FcRn protein in mouse liver was significantly increased in 10-day old mice compared to other age groups. The p-values are reported above the lines associated with each paired comparison.

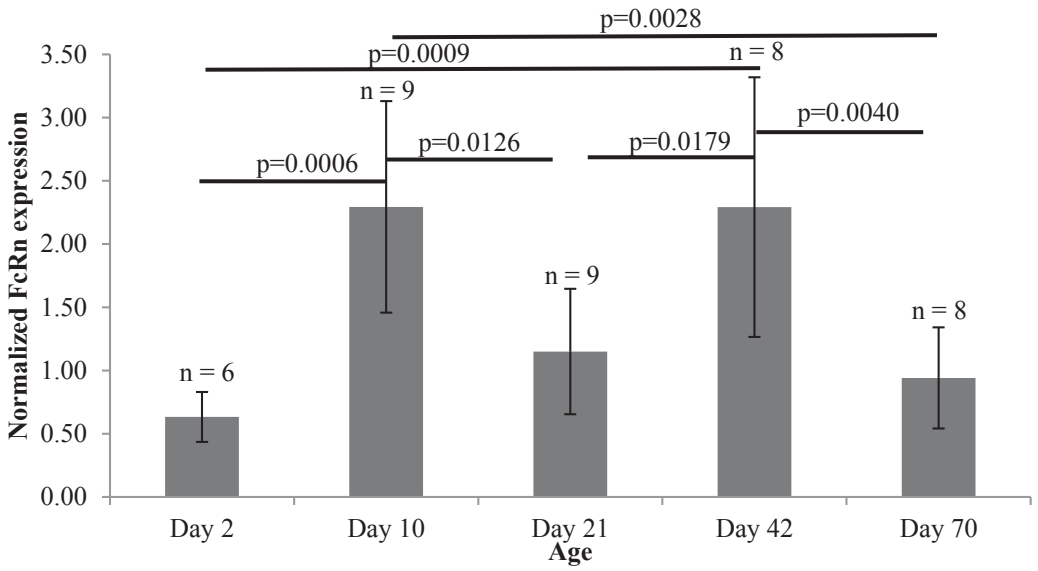

Figure 4-5. Ontogeny of FcRn protein expression in mouse kidney
Relative expression of FcRn protein in mouse kidney was significantly increased in 10- and 42-day old mice compared to other age groups. The p-values are reported above the lines associated with each paired comparison.

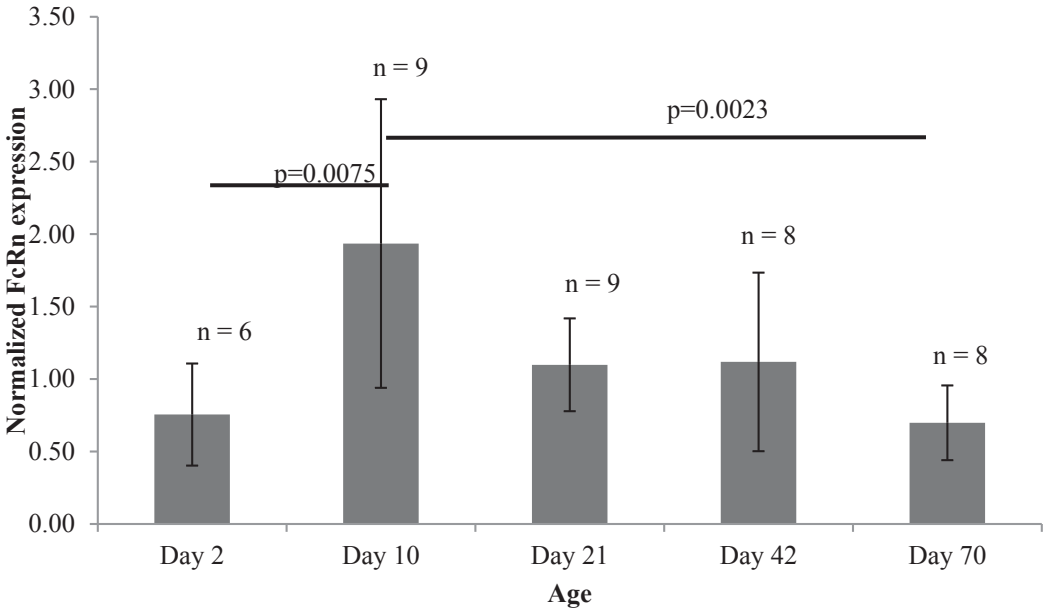

Figure 4-6. Ontogeny of FcRn protein expression in mouse lung
Relative expression of FcRn protein in mouse lung was significantly increased in 10-day old mice compared to 2- and 70-day old animals. The p-values are reported above the lines associated with each paired comparison.

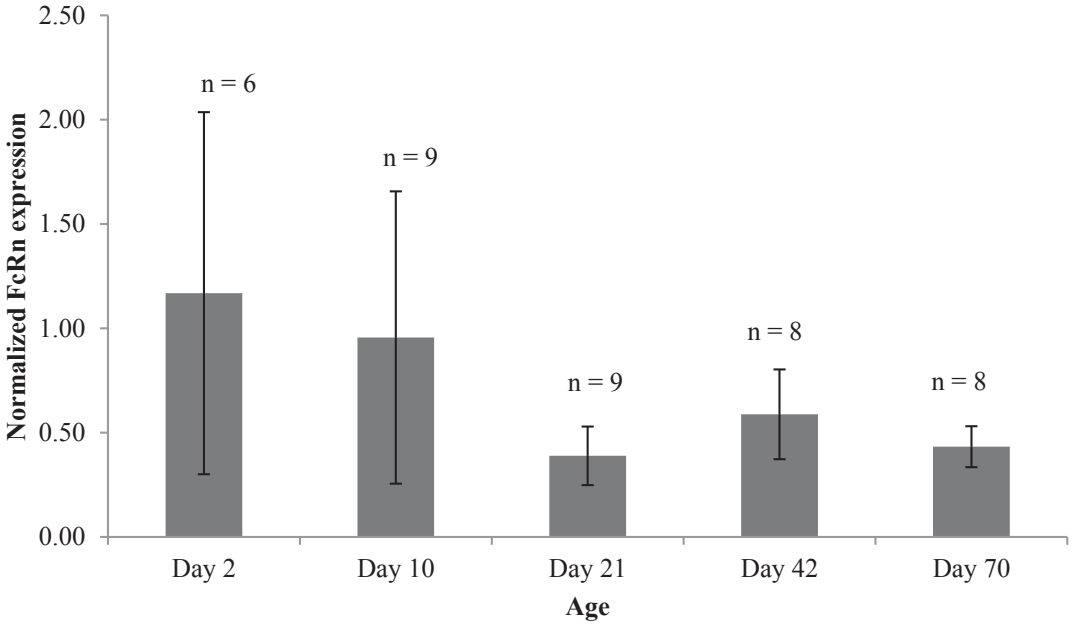

Figure 4-7. Ontogeny of FcRn protein expression in mouse spleen
There was no significant difference in the relative expression of FcRn protein in mouse spleen across age groups.

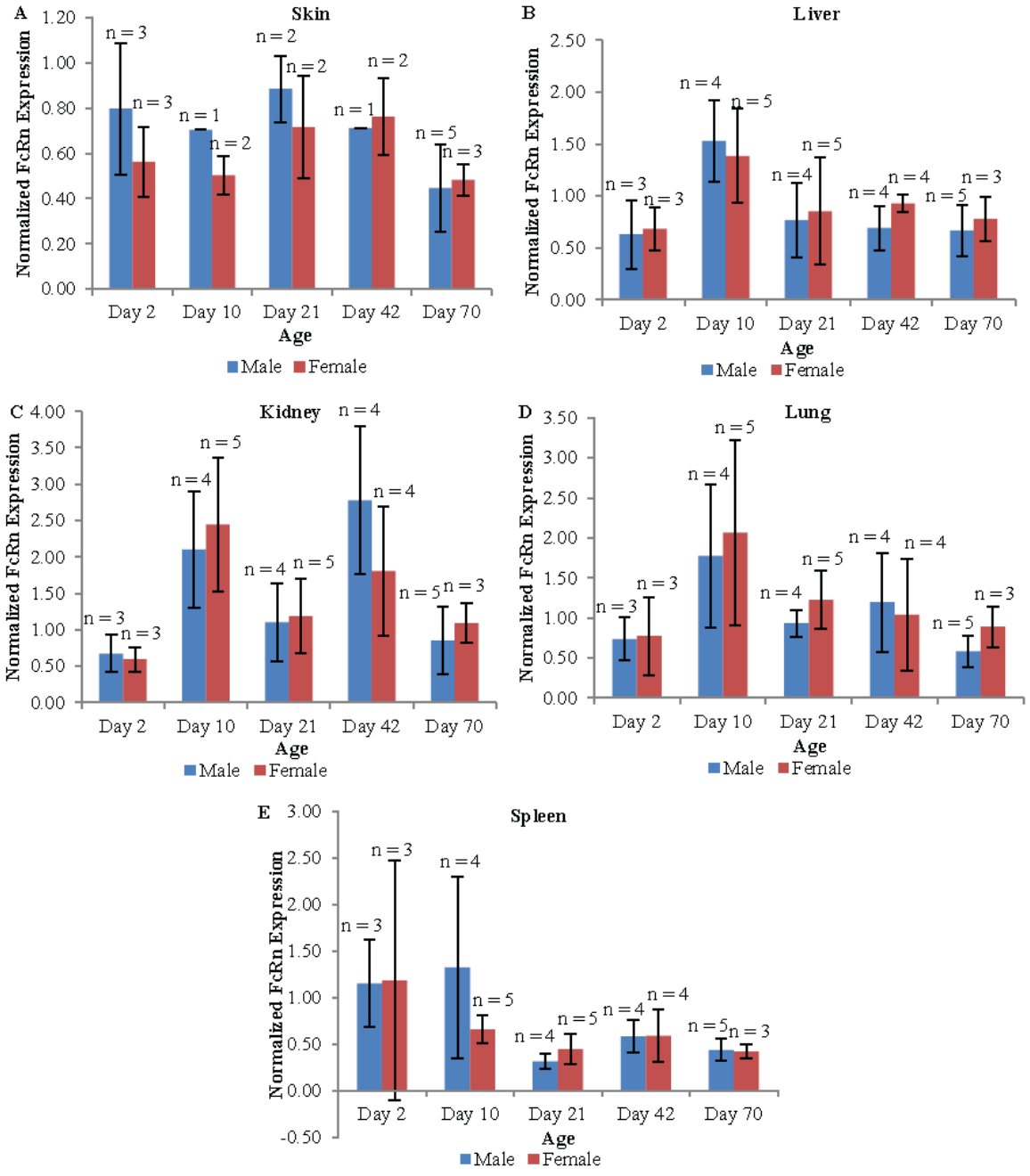

Figure 4-8. Sex-specific relative FcRn protein expression during postnatal development in mouse skin, liver, kidney, lung, and spleen

There was no significant difference in FcRn protein expression between males and females during development in mouse skin (A), liver (B), kidney (C), lung (D), and spleen (E).

Unfortunately, the difference in the relative quantitation of FcRn expression across various mouse tissues within each age group could not be determined due to the preliminary results that showed the different levels of GAPDH protein expression across the tissue observed in a 70-day old mouse (**Figure B-6**).

Discussion

Western blotting successfully determined the protein expression of FcRn relative to GAPDH in all organs and tissue samples. Under the reducing conditions of electrophoresis, double bands and broad bands of FcRn protein were observed at the molecular weight ~ 45 – 55 kDa in mouse liver samples. FcRn protein also produced broad bands in this molecular weight range in mouse kidney samples. This observation was not surprising, however, as detection of FcRn protein expression as double bands or broad bands hasbeen observed in other studies in rat small intestine and hepatocytes [61-63, 75, 76]. The broad band of FcRn protein expression was also detected in human glomerular extract [71]. The double bands and broad bands at 45 – 55 kDa may indicate various degrees of posttranslational modification of the FcRn receptor, such as glycosylation [62, 72, 75]. N-linked oligosaccharides were also shown to significantly contribute to the heterogeneity in molecular size of the IgE receptor that resulted in diffuse bands in the 45 – 62 kDa region [90]. In addition, dimerization of FcRn seemed to exist, as FcRn proteins from mouse liver could be detected at the molecular weight ~ 140 – 150 kDa. FcRn protein dimers were also observed in another study, but the molecular weight was described as 110 kDa [75].

According to the Western blot results, FcRn may be presented in various glycosylated species in some mouse organs such as liver and kidney. Moreover, the dimerization of FcRn may be more frequent in mouse liver since the bands related to FcRn dimers (~ 140 – 150 kDa) were very apparent even under the reducing condition of electrophoresis. Interestingly, the degree of dimerization seemed to show an ontogenic pattern with the lowest (~ 10%) observed in 10-day-old mice ($p < 0.005$ compared to 21- and 70-day old groups; **Table B-1**). The maximal level of FcRn dimers was reached at 21-day-old (~ 30%) and was constantly expressed later on in 42- and 70-day-old mice. Comparison of age-dependent expression of FcRn in mouse liver between FcRn monomers and total FcRn proteins (a mixture of monomers and dimers) across all age groups showed a similar pattern. However, a less-pronounced effect of ontogeny was observed when total FcRn protein expression was taken into account, resulting in a significant difference in total FcRn expression only between day 2 and day 10 age groups ($p < 0.005$; **Figure B-7**).

The current analysis assumed that FcRn was uniformly distributed throughout the organs and tissues. However, uneven FcRn mRNA and protein expressions have been reported in rat small intestine, with maximal expression in the proximal duodenum region and a gradual decline toward the distal small intestine [66, 74-76, 79, 91, 92]. This differential distribution of FcRn along the intestine may contribute to the negligible amount of immunoglobulin absorption in the distal small intestine [61, 79, 91-94]. A

differential distribution of FcRn also appears in the kidney, as high expression of FcRn was observed with a proximal to the distal gradient in the renal tubular system [66]. Moreover, the white pulp of the spleen was devoid of FcRn expression, whereas strong expression was detected in the sinusoids of splenic red pulp [66]. The regional variability of FcRn expression in organs may due to the differential distribution of endothelial cells in the organs and may be one of the factors that contributed to the variability of relative FcRn expression on the Western blots. If possible, these factors should be taken into account in the future studies.

The ontogeny of FcRn expression was investigated with C57BL/6J mice as a surrogate animal for the ontogeny of human FcRn. Animals of 2-, 10-, 21-, 42-, and 70-day postnatal age were selected as representative age groups for neonates, infants, children, adolescents, and adults. Our results showed a two-fold increase in relative expression of FcRn in liver and lung of 10-day old mice compared to neonates and adults. Similarly, relative expression of FcRn was doubled in the kidneys of 10- and 42-day-old mice. However, the ontogeny of FcRn expression did not seem to exist in mouse skin and spleen. These results suggested an organ-specific developmental expression of FcRn. These organ-specific developmental patterns of expression of FcRn are consistent with the observation of the different patterns of developmental FcRn expression in intestine and brain capillaries [74-76, 81]. Downregulation of FcRn expression during development is observed in mouse intestine [74-76], whereas upregulation occurs during aging in brain capillaries [81].

Relative FcRn expression in liver and lungs showed ontogenic development with low expression at birth, peak expression at 10 days, and diminishing expression to adult levels around weaning age (21 days). This developmental FcRn expression exhibits a similar pattern as in rat intestine [74-76]. The maximal level of duodenal FcRn mRNA expression exists between 1 and 19 days of age, but is undetectable during fetal life, at birth, and after weaning [74]. FcRn protein expression is also shown to disappear from the proximal small intestine of 23-day-old rats (weaning age) [75]. Thus, concordance between transcription and translation (i.e. mRNA vs. protein expression) seems to exist for this salvage receptor.

FcRn seems to have distinctive expression patterns in different species. Unlike in rodents, FcRn is also expressed in human fetal stomach and colon [78]. Moreover, the differential FcRn expression along the intestine in rodents does not seem to exist in humans [78]. In contrast, another study reported an increasing proximal-distal gradient of mucosal FcRn mRNA and protein expression in the adult human intestine, which translated to higher serum mAb levels after ileum-proximal colon infusion than after administration to the stomach or proximal small intestine [79]. The difference between these studies may be due to the ontogenic effect on the differential FcRn expression pattern along the intestine with the insignificant differential distribution of FcRn in the human fetus, but an increasing proximal-distal gradient observed in the adult human intestinal mucosa. The age-dependent expression of FcRn in human intestine and colon seems to show the reverse direction compared to rodents. Upregulation of FcRn

expression is observed in the small intestine as well as the colon in older child and adolescents compared to younger children [78].

The variability in the FcRn expression pattern in various mouse organs during development might indicate a complex regulatory system that controls the expression of this receptor. A possible factor that regulates developmental expression of FcRn may be *Fcgrt* transcription [95]. The selective temporal and spatial availability of specific transcription factors within the *Fcgrt* proximal promoter region may contribute to the developmental and tissue-specific regulation of *Fcgrt* expression, which can be observed as different age-dependent expression patterns of FcRn in different mouse organs. Although exogenous corticosteroids and thyroid hormone can downregulate FcRn expression, the endogenous forms of adrenal corticosteroids are assumed to not play a significant role in regulating the programmed pattern of FcRn expression [96].

Unfortunately, the level of FcRn protein expression could not be compared across various tissues within each age group of C57BL/6J mice. This was due to the observed inconsistent expression level of GAPDH that was used as a reference protein in various tissues. GAPDH has been reported as an inappropriate housekeeping gene for relative quantitation using RT-PCR or northern blot in, due to variation in expression in various mouse tissues [97]. However, different levels of endothelial cells expressed across various organs may result in the variation of FcRn expression in various mouse tissues.

A correlation between the ontogenic pattern of FcRn mRNA expression and IgG absorption has been described [74]. Postnatal absorption of IgG via FcRn is limited to the suckling phase in rodents and abruptly decreases at weaning [74, 94]. This alteration coincides with a significant induction of FcRn mRNA expression during the first day of life and a substantial decline in expression at the age of weaning [74]. Thus, the developmental alterations in the relative expression of FcRn may have an impact on the pharmacokinetics of therapeutic proteins that bind to this receptor. A prolonged half-life might be observed during the ages of high expression if liver, lung, and/or kidneys are the major organs of drug disposition. However, the endothelial cells in skin, muscle, and liver, along with the hematopoietic cells, have been shown to be the primary sites of functional FcRn expression in adult mice. This may indicate that these organs are the major sites of serum IgG homeostasis [68]. The primary sites of FcRn that are responsible for maintaining the IgG levels in adult mice have been shown to be endothelial cells and hematopoietic cells [89]. Moreover, based on physiologically based pharmacokinetic modeling, the contribution of various organs to the elimination of endogenous IgG was estimated to be 33%, 24%, 16%, and 12% for skin, muscle, liver and gut tissue, respectively [4]. Consequently, the ontogenic patterns of FcRn expression observed in mouse liver, kidney, and lung might not have a significant impact on the pharmacokinetics of therapeutic proteins that can bind to this salvage receptor. To further elucidate this question, a pharmacokinetic study using a therapeutic protein with its disposition largely affected by FcRn in different age groups of mice is needed. This pharmacokinetic study was performed and the results are reported and discussed in the next chapter.

CHAPTER 5. PHARMACOKINETICS OF A HUMAN MONOCLONAL ANTIBODY DURING THE POSTNATAL DEVELOPMENT PROCESS IN MICE

Introduction

In recent years, there is an increasing number of antibody-based therapeutic proteins have been approved for pediatric use, spanning from intact mAbs to IgG Fc-fusion proteins. However, the application of therapeutic proteins in pediatrics has often been based on the extrapolation of clinical findings from adults. This is frequently due to the lack of evidence of the efficacy and safety in pediatric populations, the difficulties in conducting pediatric clinical trials, a lack of financial incentives, and no mandatory regulatory requirements for pediatric development in the past [8, 26]. Although extrapolation may be useful when lacking pediatric data, this approach may significantly compromise the prediction of efficacy and safety in pediatric patients if the dissimilarities between children and adults are not well understood. Thus, the rational application of therapeutic mAbs in children requires a fundamental understanding of the similarities and differences in disease pathophysiology, pharmacokinetics, and pharmacodynamics (PK/PD) between children and adults, and informative clinical trials to define the optimal dosage regimens for children and evidence-based pediatric treatment guidelines.

As a first step toward achieving a better understanding of the pharmacokinetics of therapeutic mAbs in growth and maturation, the pharmacokinetics of AMG589, a fully-human mAb, was studied in various age groups of C57BL/6J mice. AMG589 was in this context solely used as a model compound for a mAb and does not bind to a specific target in mice. The effect of several factors, including weight and age, were explored and evaluated in this study to determine their impact on the pharmacokinetics of mAbs during postnatal development in mice. Due to the rapid growth of mice during the early phase of their development relative to the long half-life of mAbs, body size measures such as weight are expected to be the major factor that affects the pharmacokinetics of AMG589. Because of the significant influence of FcRn on the half-life of mAbs, the effect of developmental changes in FcRn expression level in various organs on the pharmacokinetics of AMG589 is one potential covariate affecting mAb disposition and was investigated across all age groups of mice. Other factors that needed to be considered are the promiscuity in the binding of mouse FcRn to human IgG and potential immunogenic events, such as the formation of anti-drug antibodies that might occur during the study.

The results of the relative quantification of FcRn expression in various organs of 2, 10, 21, 42, and 70 day old C57BL/6J mice as described in **Chapter 4** showed no difference in the relative FcRn protein expression across age groups in skin and spleen. However, the relative FcRn protein expression exhibited organ-specific ontogenic patterns in liver, lung, and kidney. Two-fold increases in FcRn expression were observed in liver and lung of 10-day old mice, whereas FcRn expression in kidney showed two-fold increases in 10 and 42 day old mice. This organ-specific pattern in the ontogeny of

FcRn expression may have an effect on the pharmacokinetics of AMG589 in the contribution of the organ to the overall clearance of mAbs.

The skin has been shown to contribute most to the homeostasis and the elimination of IgG [68]. Recent reports suggest FcRn may play a role in subcutaneous absorption and degradation of mAbs [55]. Although the presence of FcRn in subcutaneous tissue has not been reported beyond endothelial and some immune cells, FcRn expression has been detected in the epidermis, dermis, and skeletal muscle. Because quantitation of FcRn expression in skin in **Chapter 4** did not reveal any ontogenic pattern, the pharmacokinetics of AMG589 should not be affected by FcRn expression in the skin across age groups.

FcRn expression in bronchial and/or alveolar epithelial cells has been shown to enhance the pulmonary absorption of IgG and Fc-fusion proteins [55]. However, AMG589 was administered via a subcutaneous route in this study. Thus, intuitively, the increased expression of FcRn in the lungs of 10 days old C57BL/6J mice should not have any influence on the pharmacokinetics of AMG589 in this study if the lungs are not a major elimination organ for IgG.

FcRn has been shown to facilitate transport of IgG across both the glomerular and proximal tubule membranes. This provides an efficient recycling mechanism that prevents accumulation of IgG along the podocyte slit diaphragms [55]. However, the renal impairment has minor or no effect on the systemic clearance of therapeutic mAbs [55, 98]. Thus increasing FcRn expression in the kidneys of 10- and 42-day-old mice may not render any effect on the pharmacokinetics of AMG589.

Based on the current evidence in the literature and the results of the ontogeny of FcRn expression in **Chapter 4**, we hypothesized that the pharmacokinetics of AMG589 in different age groups of C57BL/6J mice would not be affected by the organ-specific ontogenic patterns of FcRn expression observed in mouse liver, lung, and kidney after accounting for the alteration in body size during postnatal development. To test this hypothesis, a population pharmacokinetic analysis approach was used to delineate the factors that influence the pharmacokinetics of AMG589 during the development of C57BL/6J mice.

Method

Animals

Nine timed-pregnant C57BL/6J mice were purchased from The Jackson Laboratory (Bar Harbor, ME) and were shipped to arrive on day 13 of gestation. All timed-pregnant mice were housed with free access to food and water in the animal facility at the University of Tennessee Health Science Center for 1 week. The day of birth

of the offspring was assigned as their first day of life (day 1). The offsprings were raised to pre-determined postnatal ages including 2, 10, and 21 days. All pups were weaned at 21 days. Male and female pups were separately housed in different cages at weaning.

Due to one mouse not being pregnant, only ten 21 day old mice were available. However, at least 18 mice in each age group were needed for the pharmacokinetic study in order to get at least three mice at each blood sampling point. As a result, eight additional 21 day old C57BL/6J mice (4 males and 4 females) were purchased from The Jackson Laboratory (Bar Harbor, ME). For the 42 and 70 day old groups, nine male and nine female C57BL/6J mice of each age group were also purchased from The Jackson Laboratory (Bar Harbor, ME). All animals were housed in standard laboratory cages throughout the study. The study was conducted according to the guidelines of the Animal Welfare Act and the Public Health Service Policy on Humane Care and Use of Laboratory Animals, and the protocol was approved by the Institutional Animal Care and Use Committee of the University of Tennessee Health Science Center. The number of animals in each age group and their demographic characteristics are shown in **Table 5-1**.

Pharmacokinetic Study

AMG 589, a fully-human monoclonal antibody, was kindly provided by Amgen Inc. (Thousand Oaks, CA) and was used as a model drug for studying the pharmacokinetics in different age groups of mice. AMG 589 was subcutaneously administered at 39 mg/kg in 2 day old mice and at 50 mg/kg in 10, 21, 42, and 70 day old C57BL/6J mice. Blood was collected by cardiac puncture from 3 or 4 mice in each age group at 2, 24, 72, 168, 336, and 504 hours post-dose, except 42 day old mice, in which 3 mice were sacrificed at 2, 24, 96, 168, 336, and 504 hours post-dose. All dosing and blood sampling schemes are shown in **Table 5-2**. Blood was kept in BD Vacutainer® Plus plastic serum tubes with additive clot activator and gel for serum separation (Franklin Lakes, NJ). Serum was separated by centrifugation for 16 minutes at 2500 × g at 4°C. All mouse serum samples were subsequently stored at -70°C before shipping to Amgen Inc. (Thousand Oaks, CA) for further analysis.

Quantification of AMG589 in Mouse Serum Samples

Courtesy of Amgen Inc (Thousand Oaks, CA), all mouse serum samples from the pharmacokinetic study were quantified for AMG589 using ELISA according to the company protocol. The variability of the assay was about 15%. The calibration range of the assay was 10 – 10,000 ng/mL, and LLOQ was 10 ng/mL. Due to the limited volume of serum acquired from one animal of the 2-day group at the 2-hour sampling time, only two samples were quantified at this time point.

Table 5-1. Demographic characteristics of C57BL/6J mice included in the pharmacokinetic study of AMG 589

Characteristics	Average weight (g) (Range)	Number of animals
Day 2[a]	0.9 (0.9 – 0.9)	20
Day 10		
Male	3.6 (2.9 – 4.3)	8
Female	3.6 (3.0 – 4.9)	11
Day 21		
Male	10.7 (2.5 – 16.1)	8
Female	9.6 (6.4 – 14.0)	10
Day 42		
Male	15.6 (13.0 – 19.0)	9
Female	12.7 (11.0 – 15.0)	9
Day 70		
Male	19.4 (16.3 – 23.5)	9
Female	15.1 (11.0 – 18.0)	9

[a] Based on mouse anatomy, sex determination was not possible in the day 2 age group.

Table 5-2. Dosing and blood collection scheme for the pharmacokinetic study of AMG589 in different age groups of C57BL/6J mice

Age at dosing (days)	Dose (mg/kg)	Total number of mice	Number of mice at each sampling time point					
			2 h	24 h	72 h/ 96 h	168 h	336 h	650 h
2	39	20	3	1 M	2 M	1 M	2 M	3 M
				2 F	1 F	2 F	2 F	1 F
10	50	19	1 M	1 M	1 M	2 M	1 M	2 M
			2 F	2 F	2 F	1 F	2 F	2 F
21	50	18	2 M	1 M	1 M	2 M	1 M	1 M
			1 F	2 F	2 F	1 F	2 F	2 F
42[a]	50	18	1 M	2 M	1 M[a]	2 M	1 M	2 M
			2 F	1 F	2 F[a]	1 F	2 F	1 F
70	50	18	2 M	1 M	2 M	1 M	2 M	1 M
			1 F	2 F	1 F	2 F	1 F	2 F

Note: M and F represent male and female, respectively.
[a] 42 day old mice were sacrificed at 96 hours instead of 72 hours after dosing.

Pharmacokinetic Data Analysis

The full dataset contained one observation from each mouse at each sampling time point. Due to insufficient serum obtained from one mouse in the day 2 age group, 92 observations were obtained in total. The sex of the mice in the 2 days old age group could not be identified at the 2-hour sampling time point. In this case, all animals in this group and time point were assigned to be male in the dataset. Weights of male and female mice in each age group at the time of dosing were imputed for each data record before data analysis.

In an exploratory data analysis that plotted the serum concentration-time profiles of AMG589 in different age groups of C57BL/6J mice, high variation at 24 hours in 42 day old mice (RSD ~87%) may have been caused by experimental error. Thus, two datasets were created—one with and one without these questionable data points. The dataset that excluded serum concentrations of AMG589 at the 24-hour time point was first analyzed and used for population model building. The full dataset that included the serum concentrations of AMG589 at the 24-hour sampling time was then subsequently analyzed with the same modeling approach as that used for the first data set.

Non-Compartmental Analysis

A non-compartmental pharmacokinetic analysis of the concentration-time data was performed using Phoenix™ WinNonlin® version 6.3. By this approach, the pharmacokinetic profiles of AMG589 were separately analyzed according to age group with uniform weighing in the two datasets--the one excluding serum concentration-time profile of AMG589 at the 24-hour time point and the full dataset.

Population Pharmacokinetic Analysis

To explore covariates that may affect the pharmacokinetics of AMG589 in different age groups of C57BL/6J mice, a population pharmacokinetic approach using nonlinear mixed effects modeling was applied using NONMEM software version 7.2 (ICON Development Solutions, Hanover, MD) with the Pirana version 2.9.0 platform (®Pirana Software & Consulting BV, http://www.pirana-software.com). R (The R Foundation for Statistical Computing) with Xpose and ggplot2 packages was used within Pirana version 2.9.0 for graphical visualization of the results [99]. The effects of body weight, age, and FcRn expression on the pharmacokinetics of AMG589 in different age groups of C57BL/6J mice were explored. The population pharmacokinetic model was developed using the dataset that excluded serum concentration-time data of AMG589 in C7BL/6J mice at the 24-hour time point. The final model was then applied to the full dataset.

Based on the serum concentration-time profiles of AMG589 in different age groups of C57BL/6J mice that exhibited a single phase of distribution and elimination,

along with the information that subcutaneous injection was the route of administration for AMG589, a one-compartment linear model with first-order absorption was chosen to build the structural model. The FOCE method within NONMEM was used throughout the model-building process.

Between-subject variability (η) for AMG589 pharmacokinetic parameters was assumed to follow a log-normal distribution with zero mean and variance ω^2. Thus, an exponential error model was applied for the estimation of η (**Equation 5-1**). A proportional error model was applied for the estimation of the residual error (ε_{ij}) that was assumed to be normally distributed with zero mean and variance σ^2 (**Equation 5-2**). The choice of the proportional residual error model is supported by the fact that all measured serum concentrations were far larger than the lower limit of quantification of the assay.

$$P_i = P \times e^{\eta}$$

(Eq. 5-1)

$$C_{ij,observed} = C_{ij,predicted} \times (1 + \varepsilon_{ij})$$

(Eq. 5-2)

The covariate effect was then explored and subsequently added to the structural model. Pharmacokinetic parameters such as clearance (CL) and volume of distribution (V) are usually functions of body size; thus the effect of body size can overlay and may potentially mask the effect of other covariates. To identify covariates other than body size, these pharmacokinetic parameters should first be adjusted to an appropriate body size measure [100]. According to this consideration, body weight was the first covariate incorporated into the structural model by the widely used allometric scaling approach [8, 100]. After accounting for the body size effect, other covariates such as age and FcRn expression were subsequently evaluated.

Rapid growth during the first phase of development in the C57BL/6J mice resulted in great relative changes in body weight throughout the sampling period, which potentially had an impact on the pharmacokinetics of AMG589 during the study period. As a result, mouse body weight was incorporated in the structural model with consideration of the incremental changes in mouse body weight during development. The first step was to explore the growth pattern of C57BL/6J mice by plotting the mean body weights of male and female mice against age at the time of dosing from each studied age group (**Figure 5-1**) and comparing them with the reported growth curves for C57BL/6J mice. The mean body weights of male and female mice at various time points were then derived from **Equation 5-3**.

$$BW_P = 0.9 + \frac{W_{max} \times (Age)^N}{Age_{50}{}^N + (Age)^N}$$

(Eq. 5-3)

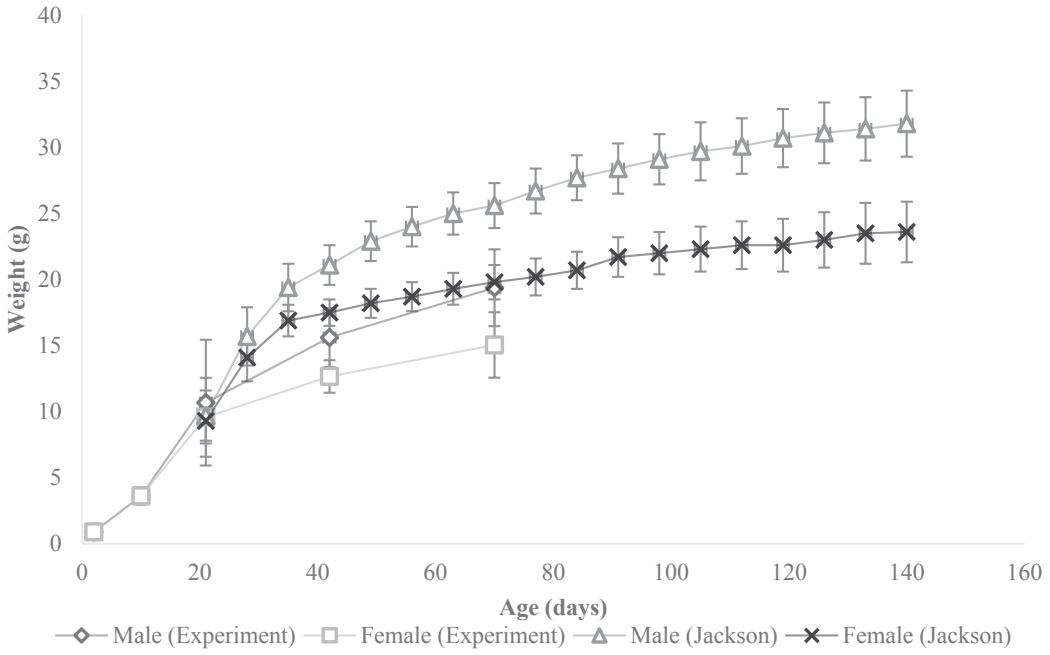

Figure 5-1. Growth curves of male and female C57BL/6J mice
Comparison of the actual growth curves of male and female C57BL/6J mice in the study and the growth curves of male and female C57BL/6J mice obtained from information at Jackson Laboratories

BW_P is the predicted body weight (g) of male or female C57BL/6J mice at various time points during the study period, 0.9 is the mean body weight (g) of 2 day old C57BL/6J mice in the study, W_{max} is the maximal body weight (g) of the male or female C57BL/6J mice presented in the growth curve, Age is the age of mice (days) at individual time points, N is the sex-specific hill coefficient that describes the growth curve of male or female C57BL/6J mice in the study, and Age_{50} is the age of male or female mice (days) at which they reach 50% of maximal body weight.

Age (days), which represents the age of C57BL/6J mice at individual time points, can be estimated from the age at dosing or AAD (days) and time after dosing, TAD (days), as shown in **Equation 5-4**.

$$\text{Age} = (\text{AAD}) + \text{TAD}$$

(Eq. 5-4)

When comparing the growth curves of C57BL/6J mice in this study to those of the same mouse species from the Jackson Laboratories, there was some deviation (**Figure 5-1**). To account for this deviation, nominal body weights of male and female mice at the time of dosing were first determined from the growth curve by **Equation 5-5** (similar to **Equation 5-3**).

$$BW_{AAD} = 0.9 + \frac{W_{max} \times AAD^N}{Age_{50}{}^N + AAD^N}$$

(Eq. 5-5)

By replacing the age of mice (days) at individual time points with the age of mice at the time of dosing (days), nominal body weights (g) of male and female C57BL/6J mice at the age of dosing can be determined from the growth curve. A multiplier, or correction factor (F), to account for the differences between nominal and actual body weights, was defined by dividing the actual body weight (Wt) of male and female mice at the time of dosing with the corresponding nominal body weight at the age of dosing, BW_{AAD} (**Equation 5-6**). The sex-specific multiplier (F) was then used to adjust the predicted body weights of male and female mice (BW) for their actual body weight at the time of dosing (**Equation 5-7**).

$$F = \frac{Wt}{BW_{AAD}}$$

(Eq. 5-6)

$$BW = F \times BW_P$$

(Eq. 5-7)

The body weight (BW) was subsequently incorporated into the structural model by the allometric scaling approach using **Equation 5-8**.

$$P = \theta_P \times \left(\frac{BW}{BW_{70d}}\right)^b$$

(Eq. 5-8)

P is the pharmacokinetic parameter that represents clearance (CL), or volume of distribution (V). θ_P is the typical value of each pharmacokinetic parameter. BW is the predicted mouse body weight at various time points, and BW_{70d} is the average body weight in g of a 70 day old male C57BL/6J mouse. b is the allometric exponent that describes the relationship between the pharmacokinetic parameter and body weight.

Due to the limited and sparse data in this study, the exponent (b) of the power function in allometric scaling may be inaccurately estimated [8]. Moreover, fixing the allometric exponent helps in delineating the size effect from other covariates which may show a high degree of collinearity with body size [8, 100]. Thus, the allometric exponent was fixed to 1 for the volume of distribution (V). Because of disagreement in the scientific literature over the appropriate exponent on CL for mAbs, the exponent on CL was tested and selected between two options, 0.75 and 0.85, before fixing [101].

After the effect of mouse body weight was accounted for and incorporated into the structural model, the effects of age and FcRn expression from various organs were subsequently explored. Different patterns of covariate effects were investigated (**Equations 5-9** to **5-13**).

$$P = \theta_P \times \left(\frac{BW}{BW_{70d}}\right)^b + \left(\theta_C \times \frac{COV}{COV_{70M}}\right)$$

(Eq. 5-9)

$$P = \theta_P \times \left(\frac{BW}{BW_{70d}}\right)^b \times \left[1 + \left(\theta_C \times \frac{COV}{COV_{70M}}\right)\right]$$

(Ep. 5-10)

$$P = \theta_P \times \left(\frac{BW}{BW_{70d}}\right)^b \times exp\left(\theta_C \times \frac{COV}{COV_{70M}}\right)$$

(Ep. 5-11)

$$P = \theta_P \times \left(\frac{BW}{BW_{70d}}\right)^b \times \theta_C^{\left(\frac{COV}{COV_{70M}}\right)}$$

(Eq. 5-12)

$$P = \theta_P \times \left(\frac{BW}{BW_{70d}}\right)^b \times \left(\frac{COV}{COV_{70M}}\right)^{\theta_C}$$

(Eq. 5-13)

P, θ_P, b, BW, and BW_{70d} represent the parameters that were already described. COV represents the covariate of interest including age and relative FcRn expression in various organs in different age groups of C57BL/6J mice. COV_{70M} is the mean value of the covariate of interest in 70 day old male C57BL/6J mice. θ_C is the parameter to be estimated that best describes the relationship between the pharmacokinetic parameter and the covariate.

Relative FcRn protein expression in various organs during postnatal development of C57BL/6J mice was obtained from the study described in **Chapter 4**. Mean FcRn expression results from the sample set with 20 μg protein loading were used for the investigation of covariate effects. (**Table 5-3**). Mean FcRn expression of mice in each age group was normalized to mean FcRn expression of 70 day old C57BL/6J mice in the model.

The covariate model was built using a stepwise forward addition/backward deletion modeling approach [102]. The criterion for inclusion of a covariate in the model was a decrease in objective function value (OFV) of 3.84 ($p < 0.05$). Due to the multiple comparisons inherent in the forward addition procedure, more stringent criteria with a change in OFV of 10.8 ($p < 0.001$) was required for a covariate to remain in the model during the backward deletion step [103]. Moreover, goodness-of-fit plots and changes in between-subject variability, along with the standard error of the parameter estimates, were considered criteria for model selection. The final model was subsequently applied to the full dataset that included the serum concentration-time data of AMG589 at the 24-hour time point.

Population Pharmacokinetic Model Evaluation

The precision and stability of the final model estimates were evaluated by nonparametric bootstrap analysis, and the ability of the final population pharmacokinetic model to adequately describe the observed data in the full dataset was determined by visual predictive check. The full dataset was used for model qualification, which was performed by using PsN (GNU General Public License, version 2) [104] using the Pirana version 2.9.0 platform (®Pirana Software & Consulting BV, http://www.pirana-software.com). Graphical visualization of the results was performed using the ggplot2 package in R (The R Foundation for Statistical Computing) via the Pirana version 2.9.0 platform.

Bootstrap Analysis

500 bootstrap datasets were created by repeatedly random sampling with replacement from the original full dataset. Each bootstrap dataset contained the same sample size as the original dataset. With the stratified sampling approach on age at dosing, the same ratio of samples in each age group as those in the original dataset were created. The population parameters were subsequently estimated for each bootstrap

Table 5-3. FcRn expression in various organs during development in C57BL/6J mice

Age (days)	FcRn expression (20 µg loading sample set)				
	Skin	Liver	Kidney	Lung	Spleen
2	0.68	0.66	0.63	0.75	1.17
10	0.57	1.45	2.29	1.93	0.96
21	0.80	0.81	1.15	1.10	0.39
42	0.75	0.81	2.29	1.12	0.59
70	0.46	0.71	0.94	0.70	0.43

dataset using the final population pharmacokinetic model. Based on 500 estimations, the median and 90% confidence intervals (CIs) for each parameter were derived and compared to the final estimates obtained from the original dataset.

Visual Predictive Check

1000 simulations were performed using the final population pharmacokinetic model with the final parameter estimates and their distributions. To preserve the data distribution in each age group of the original dataset, the simulations were stratified on age at dosing of mice. The median and 90% CIs of AMG589 plasma concentration at each time point were subsequently determined from the simulated plasma concentrations data. The median and 90% CIs obtained from simulated plasma concentrations data were plotted and overlaid with the observed concentrations.

Results

Serum concentration-time profiles of AMG589 following subcutaneous (SC) administration at 39 mg/kg in 2-day old mice, and at 50 mg/kg in 10, 21, 42, and 70 day old mice were similar across all age groups (**Figure 5-2**). A single phase of distribution and elimination was observed in the serum concentration-time profiles of AMG589 in all age groups of mice. Lower serum concentrations of AMG589 were observed in the 2 day old C57BL/6J mice. Scaling the SC dose administered in 2-day old mice from 39 mg/kg to 50 mg/kg (Day 2 (50 mg/mL) in **Figure 5-2**) showed a slight increase in AMG589 systemic exposure, but did not significantly change the non-compartmental pharmacokinetic analysis results (**Table 5-4**). Compared to other age groups, a slightly flatter terminal disposition phase was observed in the serum concentration-time profile of 42 day old C57BL/6J mice. The pharmacokinetic parameters obtained by standard non-compartmental analysis are listed in **Table 5-4**.

The results of the non-compartmental analysis revealed smaller values for apparent clearance (CL/F) and apparent volume of distribution (V/F) in the full dataset compared to those in the dataset that excluded serum concentration-time data of AMG589 at the 24-hour time point. However, both data sets showed the same pattern of changes in CL/F across all age groups of C57BL/6J mice. Decreasing CL/F was observed as mice aged, until the age of 42 days. 70 day old C57BL/6J mice showed increased CL/F of AMG589 compared to 42 day old mice. The value of CL/F in 70 day old mice was the same as that in 21-day old mice. V/F of AMG589 in both datasets also exhibited a similar pattern of change across all age groups of C57BL/6J mice. Decreased V/F of AMG589 was observed during the developmentof C57BL/6J mice until the age of 42 days. In the full dataset, V/F of AMG589 in 42 day old mice was of the same magnitude as that in 70 day old mice, whereas increased V/F was observed in 70 day old C57BL/6J mice in the dataset that excluded AMG589 serum concentration-time data at 24 hours.

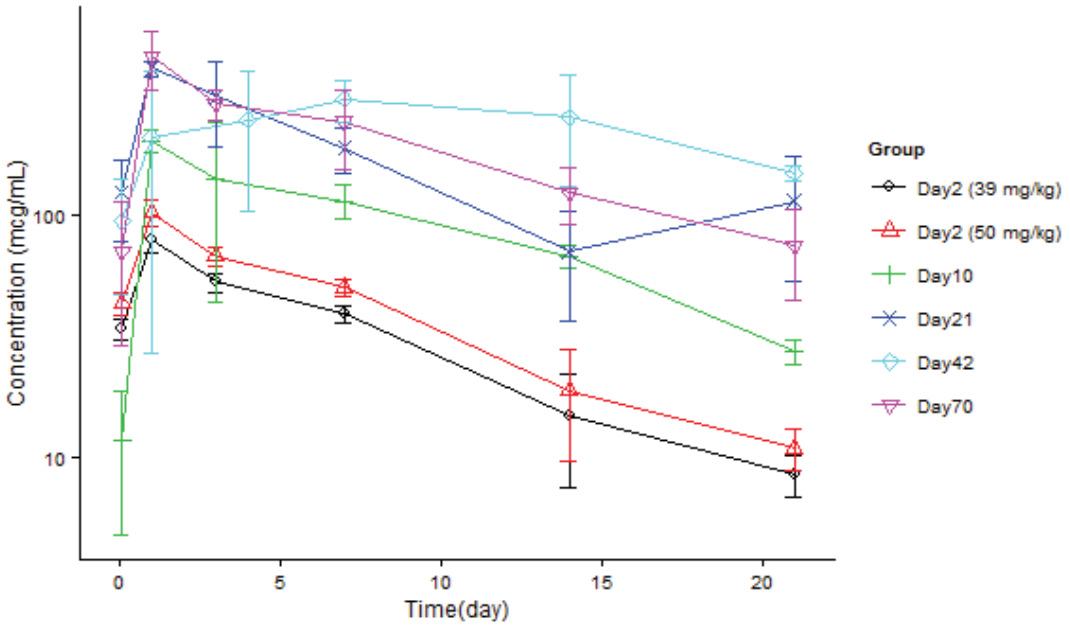

Figure 5-2. Serum concentration-time profiles of AMG 589 in different age groups of C57BL/6J mice (n = 3- 4) in the full dataset

Table 5-4. Non-compartmental pharmacokinetic parameters of AMG589 following SC administration in different age groups of C57BL/6J mice

Parameters	Units	Age					
		Day 2[a]	Day 2[b]	Day 10	Day 21	Day 42	Day 70
Exclusion of 24-hour data							
CL/F	mL/day/kg	58.4	60.0	24.8	9.85	6.34	11.0
V/F	mL/kg	550.	565	271	159	126	140.
λ_z	1/day	0.106	0.106	0.0913	0.0619	0.0501	0.0781
$t_{1/2}$	day	7	7	8	11	14	9
Full dataset							
CL/F	mL/day/kg	53.7	54.1	22.3	9.26	6.22	9.97
V/F	mL/kg	506	510.	245	150.	124	128
λ_z	1/day	0.106	0.106	0.0913	0.0619	0.0501	0.0781
$t_{1/2}$	day	7	7	8	11	14	9

[a] Instead of the 50 mg/kg SC dosing of AMG589, 39 mg/kg was SC administered in 2 day old mice.
[b] The pharmacokinetic parameters were derived from the plasma concentrations that were scaled to those after SC dosing at 50 mg/kg.

The elimination rate constants (λ_z) and half-lives ($t_{1/2}$) of AMG589 in C57BL/6J mice were the same between the two datasets. λ_z dropped from the first day of life until the age of 42 days and rose again in 70-day old mice. As a consequence, $t_{1/2}$ of AMG589 increased until the age of 42 days and then dropped in 70 day old C57BL/6J mice.

A one-compartment model with first-order absorption was applied to the structural model in the population pharmacokinetic modeling. Inclusion of body weight (BW) by the allometric scaling approach with fixed allometric exponent (b) (**Equation 5-8**) on CL (b = 0.75) and V (b = 1) resolved the problem that was encountered in the structural model regarding the estimates were near the boundary, decreased the objective function value (OFV) by approximately 50.8, and improved the goodness-of-fit plots. Comparison of the allometric exponent (b) on CL between 0.75 and 0.85 showed comparable results in the OFV and values of parameter estimates (**Table 5-5**). However, a b value of 0.75 yielded less %RSE of the parameter estimates compared to the b value of 0.85. Fixing the exponent at 0.75 seems to follow an underlying physiological principle [8, 100] and has been successfully used in the population pharmacokinetics of ciprofloxacin in pediatric patients [103]. Thus b was fixed at 0.75 for CL and at 1 for V before the next step in the modeling process.

The effects of the remaining covariates were subsequently explored. The plots of the between-subject variability (ETA) of each pharmacokinetic parameter (CL, V, and K_a) versus each covariate (sex, age, and FcRn expression in each organ) suggested a potential effect of age and FcRn expression on CL and V (**Figures C-1** to **C-4**). Between-subject variability of K_a seemed not to be explainable by any of these covariates (**Figures C-5** to **C-6**). Additional age effects on CL and V were first explored with the stepwise forward addition criteria (at $p < 0.05$, the decrease in OFV should be at least 3.84).Age was included in the model with a power effect on V, and resulted in a decrease in OFV about 11.7. After accounting for the age effect, the between-subject variability (BSV; ω^2) reduced from 0.198 to 0.175 for CL, and from 0.212 to 0.148 for V. However, the BSV for K_a slightly increased from 0.573 to 0.610. The parameter estimate for the age effect on V was -0.331, which indicated that volume of distribution decreased during development.

The effect of FcRn expression in various organs of different age groups of mice was then explored. During the screening with the criteria of the stepwise forward addition approach, relative FcRn expression in skin and kidney were found to have an influence on CL, whereas FcRn expressions in skin, liver, lung, and spleen were found to have an effect on V. The effect of FcRn expression in skin on CL was first included in the model due to the biggest reduction in OFV (-15.116). Accounting for the effect of skin FcRn expression on CL further reduced the BSV from 0.175 to 0.00608 for CL, from 0.148 to 0.0905 for V, and from 0.61 to 0.469 for K_a. After adding the effect of skin FcRn expression on CL, FcRn expression in the spleen was the only covariate that had a significant effect on V (change in OFV was -4.36). However, during the backward deletion step with stricter criteria (increase in OFV at least 10.8; $p < 0.001$), FcRn expression in the spleen was excluded in the final model.

Table 5-5. Comparison between two values of the allometric exponent (b) on CL

Parameters	b = 0.75 (OFV = 1708.13)		b = 0.85 (OFV = 1709.74)	
	Parameter estimate	%RSE	Parameter estimate	%RSE
CL (mL/day)				
θ_{CL}	0.135	11.9	0.142	12.3
V (mL)				
θ_{V}	3.37	15.9	3.44	14.5
K_a (day^{-1})				
θ_{Ka}	2.63	36.7	2.64	40.9
BSV				
ω^2_{CL}	0.198	65.2	0.221	92.3
ω^2_{V}	0.212	47.6	0.227	101
ω^2_{Ka}	0.573	87.6	0.618	152
Residual error				
σ^2_{ij}	0.0260		0.0179	

Due to the very low BSV for CL (0.006) with very high %RSE (1318.3), removing this parameter from the final model resulted in almost the same final parameter estimates with significantly reduced %RSE of BSV for V and for proportional error (decreasing from 179% to 63.5% and 118.8% to 30.5%, respectively) observed in the model-building dataset (results not shown). When we applied this approach to the full dataset, almost the same final parameter estimates with comparable %RSE were observed (results not shown). The final model thus contained only BSV for V and K_a. The parameter estimates obtained from the final model are shown in **Table 5-6** and the goodness-of-fit plots are shown in **Figure 5-3**.

The final model was successfully applied to the full dataset that included serum concentration-time data of AMG589 at the 24-hour time point. The parameter estimates obtained from the final model in the full dataset are presented in **Table 5-6**. The goodness-of-fit plots of the final model applied in the full dataset are depicted in **Figure C-7** in **Appendix C**. The final parameter estimates obtained from both datasets were comparable.

The precision of the final parameter estimates obtained from the final model was subsequently qualified by bootstrap analysis. The medians along with 90% CIs of the parameter estimates obtained from the nonparametric bootstrap are tabulated in **Table 5-6**. The median population parameter estimates from the bootstrap analysis were generally within 3% of the estimates from the final model applied to the full dataset, except for those of BSV on V and residual error, which showed larger deviations. These results confirm the stability and robustness of the final population pharmacokinetic model. The 90% CIs for the covariate effects did not include zero, supporting the statistical significance of the covariates included in the final model.

The predictive capability of the final model was further evaluated by visual predictive check plots (**Figure 5-4**). 1000 simulations with age stratification based on the final model showed the observations in the full dataset (dots) were reasonably-well predicted by the median (black line) and mostly captured within the simulated 90% prediction interval (red lines) in all age groups. Based on these qualification results, the final population pharmacokinetic model seems suitable to describe the observed pharmacokinetics of AMG589 in different age groups of C57BL/6J mice.

Discussion

The two objectives of this study were to explore the pharmacokinetics of mAbs in different age groups of mice and to determine the covariates that potentially have a significant impact on the pharmacokinetics of therapeutic mAbs during development and maturation. The effect of FcRn expression is of special interest due to published evidence that suggests a role for this recycling receptor in the pharmacokinetics of mAbs and the potential for postpartum ontogeny of FcRn expression. Thus AMG589, a fully-human mAb, was used as a model drug to study the changes in pharmacokinetics of mAbs in 2,

Table 5-6. Parameter estimates obtained from the final population pharmacokinetic model

Model	Parameters	Model building dataset			Full dataset			Bootstrap[a]	
		Parameter estimate	%RSE	%Shrinkage	Parameter estimate	%RSE	%Shrinkage	Parameter estimate	90%CI
CL (mL/day)									
$\theta_{CL} \times \left(\frac{BW}{19.4}\right)^{0.75} \times \left(\frac{FcRn_{skin}}{0.46}\right)^{\theta_{skin\_FcRn}}$	θ_{CL}	0.191	8.30		0.184	8.40		0.183	0.161-0.219
V (mL)									
$\theta_V \times \left(\frac{BW}{19.4}\right) \times \left(\frac{Age}{24 \times 70}\right)^{\theta_{Age}}$	θ_V	2.42	10.7		2.17	8.70		2.20	1.91-2.57
K_a (1/day)									
θ_{Ka}	θ_{Ka}	3.08	38.0		3.02	21.6		2.97	2.05-4.53
Covariates									
FcRn expression in mouse skin	θ_{skin_FcRn}	-1.36	23.8		-1.17	25.6		-1.18	(-1.87)-(-0.631)
Age	θ_{Age}	-0.336	24.2		-0.375	14.4		-0.368	(-0.445)-(-0.278)
Between-subject variability (BSV)									
$V_i = \theta_V \times e^{\eta_V}$	ω^2_V	0.0816	63.5	53	0.0341	120.	65	0.0479	0.00655-0.127
$K_{a_i} = \theta_{K_a} \times e^{\eta_{K_a}}$	ω^2_{Ka}	0.460	91.1	67	0.604	64.2	65	0.608	0.0760-1.95
Residual variability									
$C_{ij,observed} = C_{ij,predicted} \times (1 + \varepsilon_{ij})$	σ^2	0.0893	30.5	18	0.101	28.7	13	0.0853	0.0462-0.124

[a] Bootstrap analysis was performed on full dataset.
BW is mouse body weight calculated as described by **Equations 5-4** to **5-7**.

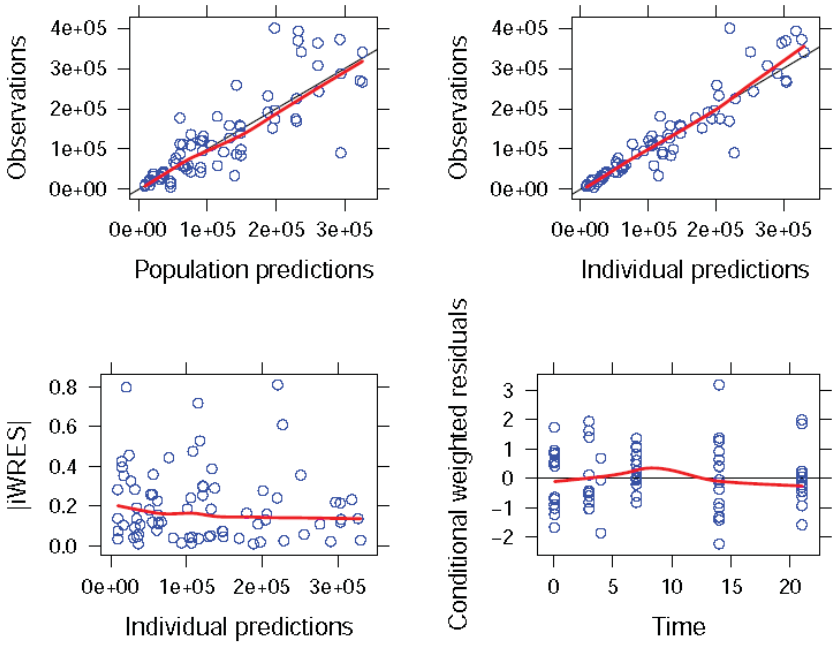

Figure 5-3. Goodness-of-fit plots of the final model applied to the model building data set

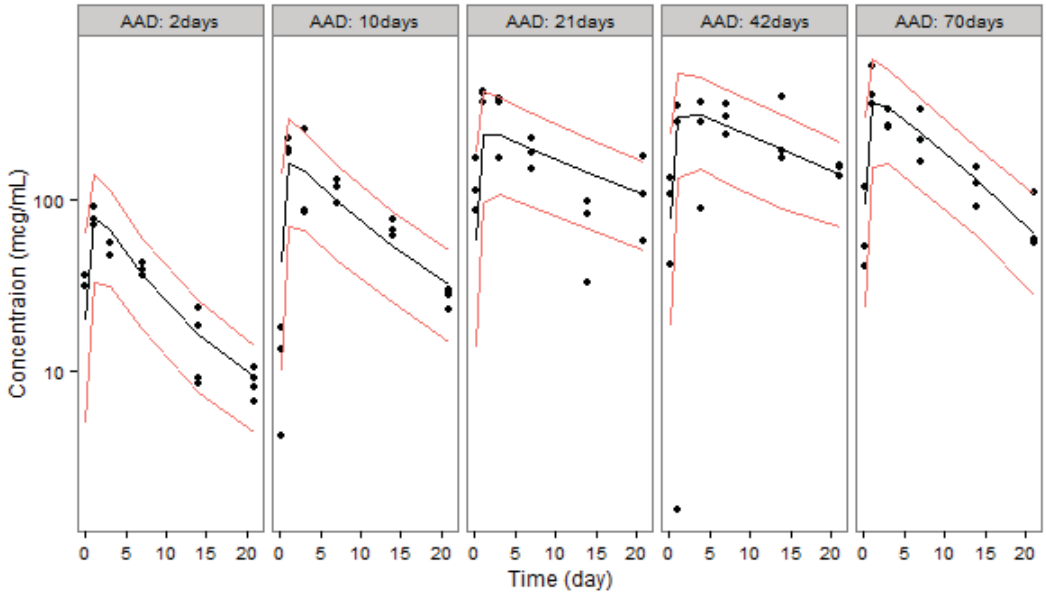

Figure 5-4. Visual predictive check for the final population pharmacokinetic model applied to the full dataset

10, 21, 42, and 70 day old C57BL/6J mice that were selected as representative age groups for neonates, infants, children, adolescents, and adults.

The results from the non-compartmental analysis of the pharmacokinetics of AMG589 in different age groups of C57BL/6J mice revealed comparable values for the parameter estimates with slightly lower values for apparent clearance (CL/F) and apparent volume of distribution (V/F) observed in the full dataset when compared to the dataset that excluded data at the 24-hour sampling time. The results of this analysis, however, should be interpreted with caution. The methodology for the non-compartmental analysis assumes a constant clearance during the sampling period, but due to weight and potential maturational changes this is clearly not the case in our analysis. In addition, some pharmacokinetic parameters are normalized for weight at dosing, but again, weight changes dramatically over the sampling interval, especially in the younger animals. Thus, the results of the non-compartmental analysis give a time-averaged estimate for initial comparisons between the age groups, but the subsequent model-based analysis provides a more precise assessment of the age-associated changes of AMG589 disposition in mice.

In the full dataset, CL/F and V/F across all age groups were 6.22 – 53.7 mL/day/kg and 124 – 506 mL/kg, respectively, whereas 6.34 – 58.4 mL/day/kg of CL/F and 126 – 550 mL/kg of V/F were observed in the dataset that excluded data at the 24-hour sampling time. Scaling the original SC dose of 39 mg/kg in two day old mice to 50 mg/kg yielded similar pharmacokinetic parameters. The highest values for CL/F and V/F were observed in the youngest age group. Both parameters had a tendency to decrease in value as the animals aged. Although these observations indicate that CL and V of the younger animals were higher than those of the adults, they could also suggest the possibility of low bioavailability (F) during the beginning of life. However, a potentially lower bioavailability occurring in neonates is difficult to mechanistically explain due to many potential factors, such as the thickness of skin and lymphatic supply at the injection site, which might have influenced the absorption process [8, 26].

CL/F and V/F of AMG589 in 70 day old mice were comparable to those of rituximab (CL ~ 13.8 mL/day/kg and V_{ss} ~ 156 mL/kg) after IV administration at 40 mg/kg in male C57BL/6J mice (average weight ~ 18 – 22 g) [105]. Terminal half-lives (λ_z) were the same in both datasets and ranged from 7 – 14 days. Half-life was shortest in the two youngest age groups (2- and 10- days old) and increased slightly in older groups until the age of 21 days. The half-life of AMG589 in 70 day old mice (9 days) was also comparable to that observed for rituximab (8 days) [105] and other mouse IgG1s (9 days) [106] in mice.

Although developmental changes in body composition with decreased total body water:body fat ratio during maturation have been suggested to not have any significant impact on the biodistribution of mAbs [8], decreasing volumes of distribution of AMG589 during development in mice seems to mimic what occurs with the pharmacokinetics of hydrophilic drugs [107]: a reduction in volume with decreasing percentage of body water during growth and maturation. However, alterations in the

biodistribution of AMG589 may also be affected by other changes in body composition and amount of circulating plasma proteins.

The longest half-life of AMG589 observed in 42 days old C57BL/6J mice suggests age-dependent pharmacokinetics, which may be the result of several factors. The drug disposition processes of AMG589 are most likely regulated by common factors and mechanisms for mAbs, such as their large size, charge, the degree and nature of glycosylation, and the Fc region [6, 55, 101, 105]. In many cases, mAb elimination is dominated by affinity for the FcRn receptor and their susceptibility to proteolysis. In contrast, the ontogeny of small molecular drug transporters in the liver and kidney, along with the alteration of hepatic drug-metabolizing enzymes during development [25, 107], should not have any effect on the pharmacokinetics of these macromolecules.

One of the factors that can influence the pharmacokinetics of mAbs is immunogenicity [4]. In this study, a fully-human mAb, AMG 589, was administered to mice. This xenogenic antibody can trigger an immune response that may lead to anti-drug antibody formation, immune complex formation, and ultimately alterations in the distribution and the elimination rate of AMG 589. This change in distribution and clearance might have an impact on the efficacy of therapy. However, immunogenicity seems unlikely in this study since serum concentration-time profiles of AMG589 did not show any pattern of abrupt decline in the terminal elimination phase, and therapy was limited to a single dose followed over 3 weeks

The ontogeny of FcRn expression is a major factor of interest since this recycling receptor contributes to the prolonged half-life of antibody-based therapeutic proteins [70, 88, 106, 108]. The results of our characterization of the ontogeny of FcRn expression in C57BL/6J mice described in **Chapter 4** revealed specific patterns of the ontogeny of FcRn expression in liver, kidney, and lungs. However, only FcRn expression in the kidney showed a 2-fold increase at the age of 42 days, which coincides with the prolonged half-life observed in this age group. The role of renal FcRn in regulating IgG homeostasis is not clear. Although FcRn has been shown to be involved in the recycling process of IgG in the kidneys, renal impairment seems to have only minor or no effect on the elimination of therapeutic mAbs [55, 98]. Thus, the ontogeny of FcRn expression in the kidneys may not have any impact on the pharmacokinetics of AMG589 in different age groups of mice.

To explore the covariate effect on the pharmacokinetics of AMG589 in different age groups of C57BL/6J mice, a population pharmacokinetic modeling approach was used. A one-compartment linear model with first-order absorption was selected as the structural model based on the serum concentration-time profile of AMG589 that showed in a log-linear plot a single terminal disposition phase, which is typical for a non-binding antibody [109]. Target receptor-mediated metabolism was assumed to be absent in the elimination of AMG589, a fully-human mAb, since it binds only to its human target antigen but not the murine homologue. Thus, a simple model such as the one-compartment linear model with first-order absorption rather than a target-mediated drug

disposition model seems to be a reasonable structural model for describing the pharmacokinetics of AMG589 in mice.

To account for the effect of body weight on the pharmacokinetics of AMG589, an allometric scaling approach was applied. One of the assumptions underlying this technique includes the absence of nonlinear pharmacokinetics, which might not hold true for most therapeutic antibodies [5]. However, this assumption should be applicable for the pharmacokinetics of AMG589 due to the lack of clearance through target receptor-mediated metabolism. Accounting for the body weight effect using the allometric scaling approach resulted in the reduction in OFV and a better goodness-of-fit plot, which coincides with reports that reveal body size as the most frequently-identified and clinically-relevant covariate that influences the pharmacokinetics of antibody-based therapeutic proteins [8].

Even though several reports have shown that after accounting for the effect of body size, age has rarely been identified as a covariate that influences the pharmacokinetics of therapeutic proteins [8], the results in the present study suggested otherwise. After accounting for the effect of body weight, age was found to affect the volume of distribution. During development, the volume of distribution of AMG589 seemed to decrease. This finding corresponds to the results obtained from the non-compartmental analysis. As already discussed, this may due to decreasing the percentage of body water during maturation or it may due to other changes in body composition and the amount of circulating plasma proteins. Surprisingly, FcRn expression in the skin was found to be a covariate that affects clearance of AMG589 even though there was no significant difference in FcRn expression across age groups of C57BL/6J mice (Results are described and discussed in **Chapter 4**). With increasing level of FcRn in the skin, clearance decreased. This result agrees with another study that shows that functional FcRn receptors are expressed in endothelial cells of the small arterioles and capillaries in the skin which principally contribute to the homeostasis of IgG [68]. Thus, the discrepancies between the results of the ontogeny of FcRn expression and population pharmacokinetic results may disappear when FcRn expression is quantified from the extracted endothelial cells in skin or the amount of endothelial cells in the skin is taken into account during data analysis. The population pharmacokinetic results suggested that the effect of skin FcRn expression and age can cause clearance and volume of distribution to change by 0 – 29% and 69 - 279%, respectively.

Although using a fully-human mAb in this pharmacokinetic study may raise concern regarding the species differences in FcRn binding affinity [5, 6], the half-life of a fully-human mAb in rodents had been shown to be comparable to that of mouse mAb versions [55]. However, the 2.5-fold higher binding affinity of human IgG to mouse FcRn compared to mouse IgG to mouse FcRn [19] may result in masking the potential effect of FcRn expression in other organs on the pharmacokinetics of AMG589 in different age groups of mice. To account for species differences in FcRn binding affinity, a human FcRn transgenic mouse model may potentially be used as a surrogate for pharmacokinetic studies of humanized or fully-human mAbs [106]. Alternatively, mouse IgGs could be used as model drugs for the pharmacokinetic study in wild-type mice.

A sparse dataset with limited observations per individual as analyzed in the present study has not surprisingly resulted in parameter estimates with relatively high values of shrinkage for between-subject variability (53 - 67% and 65% shrinkage in model-building dataset and full dataset, respectively). As a consequence, the final model derived by the stepwise model-building procedure may suffer from model selection bias, especially when model selection is based on the graphical evaluation of the goodness-of-fit plots. However, the final model showed reasonable goodness-of-fit. Moreover, the final model did not show the perfect fit phenomenon in which the values of individual predictions shrink towards the actual observations [110, 111] which may result from high shrinkage (over 20 – 30%). Although high shrinkage may lead to bias in the model selection, this selection bias may be of minor importance in the present study because the purpose of the population modeling was to explore and determine covariates that have significant influence on the pharmacokinetics of mAbs during the developmental process in mice, rather than the assessment of between-animal variability.

The findings in this study suggest that body weight along with age are significant factors that should be considered for dose optimization of therapeutic mAbs in different age populations. Current practice has also shown that the successful dose extrapolation from adults to pediatric patients for most therapeutic proteins can be achieved using body weight or body surface area-adjusted strategies [8, 26]. Using body weight and body surface area-adjusted dosing strategies, the pharmacokinetics are comparable between pediatric patients and adults once maturation of drug disposition processes has been completed. Therefore, the decreasing volume of distribution during maturation may be a maturation-related factor to consider for the application of therapeutic mAbs in different age populations. In addition, inter-individual differences in skin FcRn expression accounted for some of the observed between-subject variability, although no age-associated changes for skin FcRn expression were observed, at least in mice.

The age groups of mice that were used in this study might not truly represent the human developmental age; since human newborns are most comparable to 7-day-old mice in term of immunological development [112]. However, the effect of body weight on the pharmacokinetics of therapeutic mAbs should be emphasized in pediatrics due to differential growth rates at young ages that results in a much larger variability in body size for children than for adults [8, 100]. Moreover, unlike AMG589, many antibody-based therapeutic proteins generally include target receptor-mediated metabolism as a major elimination pathway. In that case, the prediction of pharmacokinetics in different age populations becomes more challenging since target antigen levels may be an additional covariate that influences the pharmacokinetics of the therapeutic mAb. Thus, differences in target antigen levels between pediatric patients and adults should be considered during dose optimization in pediatrics for therapeutic proteins that are eliminated via this saturable disposition process [8].

In conclusion, this study revealed age-dependent pharmacokinetics of AMG589 during the developmental process in mice with the longest exposure observed in 42-day old animals. The study revealed the effect of body weight, age, and FcRn expression in the skin as factors that influenced the observed age-dependent pharmacokinetics of

AMG589 in mice. The importance of body weight adjusted dosing should be emphasized, especially in pediatrics, since body size rapidly changes during the early period of life.

CHAPTER 6. SUMMARY OF DISSERTATION RESEARCH

Advancements in biotechnology have transitioned therapeutic modality from the use of small chemically-defined molecules to biological macromolecules. Consequently, a large and increasing number of therapeutic macromolecules are being launched in the market. Similar to what is necessary with the therapeutic application of small-molecule therapeutic agents, successful therapy with biotechnologically-derived therapeutic agents can be achieved by rational therapeutic regimens that are designed based on the understanding of their pharmacokinetics and pharmacodynamics. However, their complex structure endows these therapeutic macromolecules with a complicated disposition pattern that depends on various factors and results in many challenges with regard to their pharmacokinetic assessment and interpretation. Two challenges that need to be considered during the interpretation of pharmacokinetic results and the design of dosage regimens for therapeutic proteins and monoclonal antibodies (mAbs) were explored in **Chapters 3** to **5** of this dissertation: 1) The error of bioavailability assessment, by using the conventional bioavailability estimation that can be observed during subcutaneous (SC) administration of therapeutic macromolecules that undergo target-mediated drug disposition (TMDD) and 2) the ontogeny of FcRn expression along with its effect on the pharmacokinetics of mAbs during development.

One advantage of therapeutic macromolecules over conventional small-molecule drugs is their high affinity and specific binding, which result in limited off-target toxicities. Due to high specificity and affinity of binding to the target receptor, receptor-mediated metabolism is often the dominant pathway of clearance. This receptor-mediated metabolism is usually well described by TMDD. However, the limited availability of target receptors leads to saturation of binding upon dosing, which results in saturation of the clearance process. The saturation of target receptors under therapeutic concentrations, along with the high contribution of this process to the overall elimination pathways, can result in the observed nonlinear pharmacokinetics with decreasing clearance upon increasing the dose. The nonlinear pharmacokinetics observed for many therapeutic proteins can have an impact on bioavailability estimation. Bioavailability estimation based on the classic AUC approach can be erroneous, which is mainly due to the assumption of dose-independent constant clearance that cannot be applied to therapeutic proteins that undergo TMDD. To shed light on this issue, we hypothesized that there is a dose-dependent error in the bioavailability assessment for therapeutic proteins that undergo TMDD if the classical approach of dose-normalized AUCs is used. The error becomes apparent when different doses of IV and SC administration are used for bioavailability estimations, since the clearances at different IV and SC doses are not equal and change over time, which is dependent on the achieved concentrations.

The results in **Chapter 3** support this first hypothesis. Various degrees of error in the bioavailability estimation were observed after the bioavailability of filgrastim and denosumab were estimated by a conventional method, using different combinations of simulated dose-normalized AUCs at various IV and SC doses (0.01 – 10000 μg/kg for filgrastim and 0.66 – 210 mg for denosumab). The error became obvious when

significantly different IV and SC doses were used for the evaluation of bioavailability. The overestimations were extreme when high SC and low IV doses of both protein drugs were used for the estimations, whereas the underestimations were exactly the reverse. The error in the bioavailability estimation originated from different dose-normalized AUCs observed at various doses.

These variations of dose-normalized AUCs indicated disproportional characteristic changes in drug plasma concentration-time profiles, which resulted from changes in clearance upon dose alteration. The transition from low plasma concentration (at low dose) to high plasma concentration (at high dose) shifted the major elimination pathway from TMDD to the linear clearance pathways. At low plasma concentration of the therapeutic protein target receptors have full capacity for elimination; thus TMDD is the dominant elimination pathway. In contrast, high plasma concentrations at high doses of protein drugs saturate all target receptors and shift the main elimination pathway to be governed by linear clearance. The relationship between the simulated plasma concentrations at different IV doses to the corresponding clearances of both protein drugs were investigated. The dynamics of the alteration of clearances and dose-normalized AUCs was parallel and very obvious in the dose range of 0.1 – 5 μg/kg for filgrastim and below 60 mg for denosumab; thus care should be taken when bioavailability of these two therapeutic proteins is estimated in these dose ranges. To minimize the error that occurs when using conventional bioavailability estimation, the bioavailability should be estimated using dose-normalized AUCs at similar IV and SC doses, or the assessment should be performed in dose ranges that yield constant dose-normalized AUCs that may result from concentration-independent clearance (0.01 – 0.1 μg/kg or 5 – 10000 μg/kg for filgrastim, and 60 – 210 mg for denosumab). Moreover, an alternative approximation method could be applied that determines the ratio of IV and SC doses that generate equal AUCs, as suggested by Gibiansky et al. [51]. Overall, model-based bioavailability assessment seems to be the most precise approach for therapeutic proteins that undergo TMDD.

The second challenge related to the ontogeny of FcRn expression and its effect on the pharmacokinetics of mAbs in different age populations should be of special concern if therapeutic mAbs are used in pediatric populations. Currently, the dosing regimens for therapeutic proteins in pediatrics have been generalized from the clinical practice in adults [8, 26]. Physiological differences in body composition and organ function between pediatric patients and adults may lead to the age-dependent pharmacokinetics and pharmacodynamics. The understanding of the developmental changes in the physiological factors that cause age-dependent pharmacokinetics and pharmacodynamics are prerequisites for developing effective dosage regimens with maximal efficacy and low toxicity.

FcRn has been considered a salvage pathway from lysosomal clearance for mAbs and Fc conjugated proteins [4-7]. This salvage pathway functions through a pH-dependent binding process, and can prolong the existence of therapeutic proteins in systemic circulations. The influence and contribution of the FcRn receptor to the elimination of mAbs and Fc-conjugated proteins have been shown in many publications

and have been applied in molecular engineering to generate improved versions of mAbs and Fc-conjugated proteins with desirable half-lives. The influence of the ontogeny of FcRn expression on the pharmacokinetics of therapeutic proteins, however, has never been investigated. The age-dependent expression of FcRn was observed in mouse intestine with detectable amounts observed up to 3 weeks postpartum [62, 74]. Reduced expression of FcRn during early developmental stages may result in alterations of the pharmacokinetics of mAbs upon dosing. Thus, a second hypothesis was established that the down-regulation of FcRn expression levels during development would result in a shortened half-life of AMG589 in mice. To test this second hypothesis, three experimental aims were framed. In the first aim, the levels of FcRn expression in organs of C57BL/6J mice from postnatal days 2 through 70 were examined. In the second aim, the pharmacokinetics of AMG589 were studied in different age groups of C57BL/6J mice. Finally, in the third aim the FcRn expression levels and pharmacokinetics of AMG589 in the different age groups of mice were correlated using a nonlinear-mixed effects modeling-based population pharmacokinetic approach.

The findings on the ontogeny of FcRn expression in C57BL/6J mice in **Chapter 4** and the results of the pharmacokinetics of AMG589 in various age groups of C57BL/6J mice in **Chapter 5** led to conclusions that negated the second hypothesis. Although FcRn expression showed an ontogenic pattern, its occurrence was significant in only three organs: liver, lungs, and kidneys. Moreover, the age-associated expression of FcRn revealed organ-specific patterns of ontogeny. Two-fold increases in FcRn expression were observed in liver and lungs of 10 days old mice, whereas the FcRn expression in kidneys was doubled in 10- and 42-days old mice. This ontogeny of FcRn expression could not be correlated with the prolonged half-life of AMG589 that was observed in 42 day old mice. Although a doubling of FcRn expression was observed in mouse kidneys at this age, the contribution of this organ to the overall elimination processes of mAbs seems to be limited. Moreover, the function of FcRn expressed in kidneys is still controversial. The negligible influence of the ontogeny of FcRn expression on the pharmacokinetics of AMG589 in various age groups of mice was confirmed by the population pharmacokinetic analysis. The population pharmacokinetic analysis revealed that after the effect of body weight was adjusted by allometric scaling, age and FcRn expression in skin were the additional factors that influenced the pharmacokinetics of AMG589 in different age groups of mice. The volume of distribution of AMG589 was affected by age with decreasing volume of distribution during development. Interestingly, variability in the clearance of AMG589 could be partially explained by the expression of FcRn in the skin, even though FcRn expression in skin did not show any ontogeny. Although the experimental results in mice suggested three significant factors (body weight, age, and FcRn expression in the skin) that should be considered during dosage regimen design for mAbs, there are several limitations that might limit the generalization of this finding to humans. One of these limitations is potential species differences in developmental growth rate and the ontogenic pattern of FcRn expression. Regardless of the species difference in physiology, however, body weight should be taken into account during the dosage regimen design, especially for pediatric patients who usually exhibit an expeditious increase in body size at an early age.

The findings in this dissertation have highlighted some challenges and determinants that should be considered during the pharmacokinetic interpretation and the dosage regimen design for therapeutic proteins. To explore the error in the conventional bioavailability estimation of therapeutic proteins that undergo TMDD, potential effects of FcRn were considered to have a negligible effect on the pharmacokinetics of the model drugs used. Similarly, TMDD was not considered to be a relevant pharmacokinetic process in the disposition of AMG589 in mice. In reality, however, these two factors may affect some therapeutic proteins, depending on the contribution of each process to the overall pharmacokinetics. Moreover, other processes and determinants of drug disposition of therapeutic proteins, such as immunogenicity and clearance through Fcγ-receptors and other proteolytic processes, may affect and further complicate the pharmacokinetic behavior of proteins. Although a thorough understanding of the role and limitations of each of these processes is necessary to fully understand the disposition of individual therapeutic proteins, the findings in the studies presented in this dissertation should be able to be generalized to other therapeutic proteins with similar pharmacokinetic properties.

LIST OF REFERENCES

1. Leader, B., Q.J. Baca, and D.E. Golan, *Protein therapeutics: a summary and pharmacological classification.* Nat Rev Drug Discov, 2008. **7**(1): p. 21-39.
2. Tang, L., A.M. Persky, G. Hochhaus, and B. Meibohm, *Pharmacokinetic aspects of biotechnology products.* J Pharm Sci, 2004. **93**(9): p. 2184-204.
3. Meibohm, B. and R. Braeckman, *Pharmacokinetics and Pharmacodynamics of Peptide and Protein Drugs*, in *Pharmaceutical Biotechnology*, D. Crommelin, R. Sindelar, and B. Meibohm, Editors. 2008, Informa Healthcare USA, Inc.: New York.
4. Keizer, R.J., A.D. Huitema, J.H. Schellens, and J.H. Beijnen, *Clinical pharmacokinetics of therapeutic monoclonal antibodies.* Clin Pharmacokinet, 2010. **49**(8): p. 493-507.
5. Wang, W., E.Q. Wang, and J.P. Balthasar, *Monoclonal antibody pharmacokinetics and pharmacodynamics.* Clin Pharmacol Ther, 2008. **84**(5): p. 548-58.
6. Lobo, E.D., R.J. Hansen, and J.P. Balthasar, *Antibody pharmacokinetics and pharmacodynamics.* J Pharm Sci, 2004. **93**(11): p. 2645-68.
7. Lin, J.H., *Pharmacokinetics of biotech drugs: peptides, proteins and monoclonal antibodies.* Curr Drug Metab, 2009. **10**(7): p. 661-91.
8. Xu, Z., H.M. Davis, and H. Zhou, *Rational development and utilization of antibody-based therapeutic proteins in pediatrics.* Pharmacol Ther, 2013. **137**(2): p. 225-47.
9. Kurlander, R.J., D.M. Ellison, and J. Hall, *The blockade of Fc receptor-mediated clearance of immune complexes in vivo by a monoclonal antibody (2.4G2) directed against Fc receptors on murine leukocytes.* J Immunol, 1984. **133**(2): p. 855-62.
10. Ternant, D., M. Buchler, M. Beneton, G. Alvan, M. Ohresser, G. Touchard*, et al.*, *Interindividual variability in the concentration-effect relationship of antilymphocyte globulins - a possible influence of FcgammaRIIIa genetic polymorphism.* Br J Clin Pharmacol, 2008. **65**(1): p. 60-8.
11. Abuqayyas, L. and J.P. Balthasar, *Application of knockout mouse models to investigate the influence of FcgammaR on the tissue distribution and elimination of 8C2, a murine IgG1 monoclonal antibody.* Int J Pharm, 2012. **439**(1-2): p. 8-16.
12. Abuqayyas, L. and J.P. Balthasar, *Investigation of the role of FcgammaR and FcRn in mAb distribution to the brain.* Mol Pharm, 2013. **10**(5): p. 1505-13.
13. Mortensen, D.L., S. Prabhu, E.G. Stefanich, S. Kadkhodayan-Fischer, T.R. Gelzleichter, D. Baker*, et al.*, *Effect of antigen binding affinity and effector function on the pharmacokinetics and pharmacodynamics of anti-IgE monoclonal antibodies.* MAbs, 2012. **4**(6): p. 724-31.
14. Clarkson, S.B., R.P. Kimberly, J.E. Valinsky, M.D. Witmer, J.B. Bussel, R.L. Nachman*, et al.*, *Blockade of clearance of immune complexes by an anti-Fc gamma receptor monoclonal antibody.* J Exp Med, 1986. **164**(2): p. 474-89.

15. Mager, D.E. and W.J. Jusko, *General pharmacokinetic model for drugs exhibiting target-mediated drug disposition.* J Pharmacokinet Pharmacodyn, 2001. **28**(6): p. 507-32.
16. Andersen, J.T. and I. Sandlie, *The versatile MHC class I-related FcRn protects IgG and albumin from degradation: implications for development of new diagnostics and therapeutics.* Drug Metab Pharmacokinet, 2009. **24**(4): p. 318-32.
17. Jin, F. and J.P. Balthasar, *Mechanisms of intravenous immunoglobulin action in immune thrombocytopenic purpura.* Hum Immunol, 2005. **66**(4): p. 403-10.
18. Getman, K.E. and J.P. Balthasar, *Pharmacokinetic effects of 4C9, an anti-FcRn antibody, in rats: implications for the use of FcRn inhibitors for the treatment of humoral autoimmune and alloimmune conditions.* J Pharm Sci, 2005. **94**(4): p. 718-29.
19. Ober, R.J., C.G. Radu, V. Ghetie, and E.S. Ward, *Differences in promiscuity for antibody-FcRn interactions across species: implications for therapeutic antibodies.* Int Immunol, 2001. **13**(12): p. 1551-9.
20. Andersen, J.T., M.B. Daba, G. Berntzen, T.E. Michaelsen, and I. Sandlie, *Cross-species binding analyses of mouse and human neonatal Fc receptor show dramatic differences in immunoglobulin G and albumin binding.* J Biol Chem, 2010. **285**(7): p. 4826-36.
21. Vaccaro, C., R. Bawdon, S. Wanjie, R.J. Ober, and E.S. Ward, *Divergent activities of an engineered antibody in murine and human systems have implications for therapeutic antibodies.* Proc Natl Acad Sci U S A, 2006. **103**(49): p. 18709-14.
22. Petkova, S.B., S. Akilesh, T.J. Sproule, G.J. Christianson, H. Al Khabbaz, A.C. Brown*, et al.*, *Enhanced half-life of genetically engineered human IgG1 antibodies in a humanized FcRn mouse model: potential application in humorally mediated autoimmune disease.* Int Immunol, 2006. **18**(12): p. 1759-69.
23. Roopenian, D.C., G.J. Christianson, and T.J. Sproule, *Human FcRn transgenic mice for pharmacokinetic evaluation of therapeutic antibodies.* Methods Mol Biol, 2010. **602**: p. 93-104.
24. Proetzel, G. and D.C. Roopenian, *Humanized FcRn mouse models for evaluating pharmacokinetics of human IgG antibodies.* Methods, 2014. **65**(1): p. 148-53.
25. Kearns, G.L., S.M. Abdel-Rahman, S.W. Alander, D.L. Blowey, J.S. Leeder, and R.E. Kauffman, *Developmental pharmacology--drug disposition, action, and therapy in infants and children.* N Engl J Med, 2003. **349**(12): p. 1157-67.
26. Zhang, Y., X. Wei, G. Bajaj, J.S. Barrett, B. Meibohm, A. Joshi*, et al.*, *Challenges and considerations for development of therapeutic proteins in pediatric patients.* J Clin Pharmacol, 2015. **55 Suppl 3**: p. S103-15.
27. Levy, G., *Pharmacologic target-mediated drug disposition.* Clin Pharmacol Ther, 1994. **56**(3): p. 248-52.
28. Meibohm, B., ed. *The Role of Pharmacokinetics and Pharmacodynamics in the Development of Biotech Drugs*. Pharmacokinetics and Pharmacodynamics of Biotech Drugs, ed. B. Meibohm. 2006, Wiley-VCH Verlag GmpH & co. KGaA: Weinheim, Germany.
29. Dirks, N.L. and B. Meibohm, *Population pharmacokinetics of therapeutic monoclonal antibodies.* Clin Pharmacokinet, 2010. **49**(10): p. 633-59.

30. Mager, D.E., *Target-mediated drug disposition and dynamics.* Biochem Pharmacol, 2006. **72**(1): p. 1-10.
31. Mager, D.E., B. Neuteboom, C. Efthymiopoulos, A. Munafo, and W.J. Jusko, *Receptor-mediated pharmacokinetics and pharmacodynamics of interferon-beta1a in monkeys.* J Pharmacol Exp Ther, 2003. **306**(1): p. 262-70.
32. Yang, B.B., P. Lum, A. Chen, R. Arends, L. Roskos, B. Smith*, et al.*, *Pharmacokinetic and pharmacodynamic perspectives on the clinical drug development of panitumumab.* Clin Pharmacokinet, 2010. **49**(11): p. 729-40.
33. Wang, B., T.M. Ludden, E.N. Cheung, G.G. Schwab, and L.K. Roskos, *Population pharmacokinetic-pharmacodynamic modeling of filgrastim (r-metHuG-CSF) in healthy volunteers.* J Pharmacokinet Pharmacodyn, 2001. **28**(4): p. 321-42.
34. Sutjandra, L., R.D. Rodriguez, S. Doshi, M. Ma, M.C. Peterson, G.R. Jang*, et al.*, *Population pharmacokinetic meta-analysis of denosumab in healthy subjects and postmenopausal women with osteopenia or osteoporosis.* Clin Pharmacokinet, 2011. **50**(12): p. 793-807.
35. Gibiansky, L., L. Sutjandra, S. Doshi, J. Zheng, W. Sohn, M.C. Peterson*, et al.*, *Population pharmacokinetic analysis of denosumab in patients with bone metastases from solid tumours.* Clin Pharmacokinet, 2012. **51**(4): p. 247-60.
36. Mager, D.E. and W. Krzyzanski, *Quasi-equilibrium pharmacokinetic model for drugs exhibiting target-mediated drug disposition.* Pharm Res, 2005. **22**(10): p. 1589-96.
37. Grimm, H.P., *Gaining insights into the consequences of target-mediated drug disposition of monoclonal antibodies using quasi-steady-state approximations.* J Pharmacokinet Pharmacodyn, 2009. **36**(5): p. 407-20.
38. Gibiansky, L., E. Gibiansky, T. Kakkar, and P. Ma, *Approximations of the target-mediated drug disposition model and identifiability of model parameters.* J Pharmacokinet Pharmacodyn, 2008. **35**(5): p. 573-91.
39. Yan, X., D.E. Mager, and W. Krzyzanski, *Selection between Michaelis-Menten and target-mediated drug disposition pharmacokinetic models.* J Pharmacokinet Pharmacodyn, 2010. **37**(1): p. 25-47.
40. Peletier, L.A. and J. Gabrielsson, *Dynamics of target-mediated drug disposition.* Eur J Pharm Sci, 2009. **38**(5): p. 445-64.
41. Peletier, L.A. and J. Gabrielsson, *Dynamics of target-mediated drug disposition: characteristic profiles and parameter identification.* J Pharmacokinet Pharmacodyn, 2012. **39**(5): p. 429-51.
42. Wiczling, P., P. Lowe, E. Pigeolet, F. Ludicke, S. Balser, and W. Krzyzanski, *Population pharmacokinetic modelling of filgrastim in healthy adults following intravenous and subcutaneous administrations.* Clin Pharmacokinet, 2009. **48**(12): p. 817-26.
43. Amgen, *Neupogen(R) (filgrastim)*, in *Product information*, Amgen, Editor. 2012: Thousand Oaks, California.
44. Amgen, *Xgeva(R) (denosumab)*, in *Product information*, Amgen, Editor. 2012.
45. Kakkar, T., C. Sung, L. Gibiansky, T. Vu, A. Narayanan, S.L. Lin*, et al.*, *Population PK and IgE pharmacodynamic analysis of a fully human monoclonal antibody against IL4 receptor.* Pharm Res, 2011. **28**(10): p. 2530-42.

46. Frey, N., S. Grange, and T. Woodworth, *Population pharmacokinetic analysis of tocilizumab in patients with rheumatoid arthritis.* J Clin Pharmacol, 2010. **50**(7): p. 754-66.
47. Betts, A.M., T.H. Clark, J.X. Yang, J.L. Treadway, M. Li, M.A. Giovanelli*, et al.*, *The Application of Target Information and Preclinical Pharmacokinetic/Pharmacodynamic Modeling in Predicting Clinical Doses of a Dickkopf-1 Antibody for Osteoporosis.* Journal of Pharmacology and Experimental Therapeutics, 2010. **333**(1): p. 2-13.
48. Agerso, H., R.V. Overgaard, M.B. Petersen, L. Hansen, M.B. Hermit, M.H. Sorensen*, et al.*, *Pharmacokinetics of an anti-TFPI monoclonal antibody (concizumab) blocking the TFPI interaction with the active site of FXa in Cynomolgus monkeys after iv and sc administration.* Eur J Pharm Sci, 2014. **56**: p. 65-9.
49. Ulrichts, H., K. Silence, A. Schoolmeester, P. de Jaegere, S. Rossenu, J. Roodt*, et al.*, *Antithrombotic drug candidate ALX-0081 shows superior preclinical efficacy and safety compared with currently marketed antiplatelet drugs.* Blood, 2011. **118**(3): p. 757-65.
50. Zhao, L., P. Ji, Z. Li, P. Roy, and C.G. Sahajwalla, *The antibody drug absorption following subcutaneous or intramuscular administration and its mathematical description by coupling physiologically based absorption process with the conventional compartment pharmacokinetic model.* J Clin Pharmacol, 2013. **53**(3): p. 314-25.
51. Gibiansky, L., Gibiansky, E., *Bioavailability of drugs with nonlinear pharmacokinetics (PK) can be approximated by the ratio of doses that provide equal areas under the concentration-time curves (AUCs).* in *National Biotechnology Conference 2012*. 2012.
52. Roopenian, D.C. and S. Akilesh, *FcRn: the neonatal Fc receptor comes of age.* Nat Rev Immunol, 2007. **7**(9): p. 715-25.
53. Kuo, T.T., K. Baker, M. Yoshida, S.W. Qiao, V.G. Aveson, W.I. Lencer*, et al.*, *Neonatal Fc receptor: from immunity to therapeutics.* J Clin Immunol, 2010. **30**(6): p. 777-89.
54. Roopenian, D.C. and V.Z. Sun, *Clinical ramifications of the MHC family Fc receptor FcRn.* J Clin Immunol, 2010. **30**(6): p. 790-7.
55. Giragossian, C., T. Clark, N. Piche-Nicholas, and C.J. Bowman, *Neonatal Fc receptor and its role in the absorption, distribution, metabolism and excretion of immunoglobulin G-based biotherapeutics.* Curr Drug Metab, 2013. **14**(7): p. 764-90.
56. Ghetie, V. and E.S. Ward, *Multiple roles for the major histocompatibility complex class I- related receptor FcRn.* Annu Rev Immunol, 2000. **18**: p. 739-66.
57. Martin, W.L., A.P. West, Jr., L. Gan, and P.J. Bjorkman, *Crystal structure at 2.8 A of an FcRn/heterodimeric Fc complex: mechanism of pH-dependent binding.* Mol Cell, 2001. **7**(4): p. 867-77.
58. Mezo, A.R., V. Sridhar, J. Badger, P. Sakorafas, and V. Nienaber, *X-ray crystal structures of monomeric and dimeric peptide inhibitors in complex with the human neonatal Fc receptor, FcRn.* J Biol Chem, 2010. **285**(36): p. 27694-701.

59. Rodewald, R., *pH-dependent binding of immunoglobulins to intestinal cells of the neonatal rat.* J Cell Biol, 1976. **71**(2): p. 666-9.
60. Wallace, K.H. and A.R. Rees, *Studies on the immunoglobulin-G Fc-fragment receptor from neonatal rat small intestine.* Biochem J, 1980. **188**(1): p. 9-16.
61. Rodewald, R. and J.P. Kraehenbuhl, *Receptor-mediated transport of IgG.* J Cell Biol, 1984. **99**(1 Pt 2): p. 159s-164s.
62. Jakoi, E.R., J. Cambier, and S. Saslow, *Transepithelial transport of maternal antibody: purification of IgG receptor from newborn rat intestine.* J Immunol, 1985. **135**(5): p. 3360-4.
63. Blumberg, R.S., T. Koss, C.M. Story, D. Barisani, J. Polischuk, A. Lipin*, et al.*, *A major histocompatibility complex class I-related Fc receptor for IgG on rat hepatocytes.* J Clin Invest, 1995. **95**(5): p. 2397-402.
64. Cauza, K., G. Hinterhuber, R. Dingelmaier-Hovorka, K. Brugger, G. Klosner, R. Horvat*, et al.*, *Expression of FcRn, the MHC class I-related receptor for IgG, in human keratinocytes.* J Invest Dermatol, 2005. **124**(1): p. 132-9.
65. Zhu, X., G. Meng, B.L. Dickinson, X. Li, E. Mizoguchi, L. Miao*, et al.*, *MHC class I-related neonatal Fc receptor for IgG is functionally expressed in monocytes, intestinal macrophages, and dendritic cells.* J Immunol, 2001. **166**(5): p. 3266-76.
66. Akilesh, S., G.J. Christianson, D.C. Roopenian, and A.S. Shaw, *Neonatal FcR expression in bone marrow-derived cells functions to protect serum IgG from catabolism.* J Immunol, 2007. **179**(7): p. 4580-8.
67. Cianga, P., C. Cianga, P. Plamadeala, D. Branisteanu, and E. Carasevici, *The neonatal Fc receptor (FcRn) expression in the human skin.* Virchows Arch, 2007. **451**(4): p. 859-60.
68. Borvak, J., J. Richardson, C. Medesan, F. Antohe, C. Radu, M. Simionescu*, et al.*, *Functional expression of the MHC class I-related receptor, FcRn, in endothelial cells of mice.* Int Immunol, 1998. **10**(9): p. 1289-98.
69. Cianga, C., P. Cianga, P. Plamadeala, and C. Amalinei, *Nonclassical major histocompatibility complex I-like Fc neonatal receptor (FcRn) expression in neonatal human tissues.* Hum Immunol, 2011. **72**(12): p. 1176-87.
70. Ghetie, V., J.G. Hubbard, J.K. Kim, M.F. Tsen, Y. Lee, and E.S. Ward, *Abnormally short serum half-lives of IgG in beta 2-microglobulin-deficient mice.* Eur J Immunol, 1996. **26**(3): p. 690-6.
71. Haymann, J.P., J.P. Levraud, S. Bouet, V. Kappes, J. Hagege, G. Nguyen*, et al.*, *Characterization and localization of the neonatal Fc receptor in adult human kidney.* J Am Soc Nephrol, 2000. **11**(4): p. 632-9.
72. Spiekermann, G.M., P.W. Finn, E.S. Ward, J. Dumont, B.L. Dickinson, R.S. Blumberg*, et al.*, *Receptor-mediated immunoglobulin G transport across mucosal barriers in adult life: functional expression of FcRn in the mammalian lung.* J Exp Med, 2002. **196**(3): p. 303-10.
73. Cianga, P., C. Medesan, J.A. Richardson, V. Ghetie, and E.S. Ward, *Identification and function of neonatal Fc receptor in mammary gland of lactating mice.* Eur J Immunol, 1999. **29**(8): p. 2515-23.

74. Martin, M.G., S.V. Wu, and J.H. Walsh, *Ontogenetic development and distribution of antibody transport and Fc receptor mRNA expression in rat intestine.* Dig Dis Sci, 1997. **42**(5): p. 1062-9.
75. Simister, N.E. and A.R. Rees, *Isolation and characterization of an Fc receptor from neonatal rat small intestine.* Eur J Immunol, 1985. **15**(7): p. 733-8.
76. Simister, N.E. and K.E. Mostov, *An Fc receptor structurally related to MHC class I antigens.* Nature, 1989. **337**(6203): p. 184-7.
77. Israel, E.J., S. Taylor, Z. Wu, E. Mizoguchi, R.S. Blumberg, A. Bhan*, et al.*, *Expression of the neonatal Fc receptor, FcRn, on human intestinal epithelial cells.* Immunology, 1997. **92**(1): p. 69-74.
78. Shah, U., B.L. Dickinson, R.S. Blumberg, N.E. Simister, W.I. Lencer, and W.A. Walker, *Distribution of the IgG Fc receptor, FcRn, in the human fetal intestine.* Pediatr Res, 2003. **53**(2): p. 295-301.
79. Hornby, P.J., P.R. Cooper, C. Kliwinski, E. Ragwan, J.R. Mabus, B. Harman*, et al.*, *Human and non-human primate intestinal FcRn expression and immunoglobulin G transcytosis.* Pharm Res, 2014. **31**(4): p. 908-22.
80. Schlachetzki, F., C. Zhu, and W.M. Pardridge, *Expression of the neonatal Fc receptor (FcRn) at the blood-brain barrier.* J Neurochem, 2002. **81**(1): p. 203-6.
81. Deane, R., A. Sagare, K. Hamm, M. Parisi, B. LaRue, H. Guo*, et al.*, *IgG-assisted age-dependent clearance of Alzheimer's amyloid beta peptide by the blood-brain barrier neonatal Fc receptor.* J Neurosci, 2005. **25**(50): p. 11495-503.
82. Kim, H., R.N. Fariss, C. Zhang, S.B. Robinson, M. Thill, and K.G. Csaky, *Mapping of the neonatal Fc receptor in the rodent eye.* Invest Ophthalmol Vis Sci, 2008. **49**(5): p. 2025-9.
83. Vidarsson, G., A.M. Stemerding, N.M. Stapleton, S.E. Spliethoff, H. Janssen, F.E. Rebers*, et al.*, *FcRn: an IgG receptor on phagocytes with a novel role in phagocytosis.* Blood, 2006. **108**(10): p. 3573-9.
84. Antohe, F., L. Radulescu, A. Gafencu, V. Ghetie, and M. Simionescu, *Expression of functionally active FcRn and the differentiated bidirectional transport of IgG in human placental endothelial cells.* Hum Immunol, 2001. **62**(2): p. 93-105.
85. Simister, N.E., C.M. Story, H.L. Chen, and J.S. Hunt, *An IgG-transporting Fc receptor expressed in the syncytiotrophoblast of human placenta.* Eur J Immunol, 1996. **26**(7): p. 1527-31.
86. Story, C.M., J.E. Mikulska, and N.E. Simister, *A major histocompatibility complex class I-like Fc receptor cloned from human placenta: possible role in transfer of immunoglobulin G from mother to fetus.* J Exp Med, 1994. **180**(6): p. 2377-81.
87. Leach, J.L., D.D. Sedmak, J.M. Osborne, B. Rahill, M.D. Lairmore, and C.L. Anderson, *Isolation from human placenta of the IgG transporter, FcRn, and localization to the syncytiotrophoblast: implications for maternal-fetal antibody transport.* J Immunol, 1996. **157**(8): p. 3317-22.
88. Telleman, P. and R.P. Junghans, *The role of the Brambell receptor (FcRB) in liver: protection of endocytosed immunoglobulin G (IgG) from catabolism in hepatocytes rather than transport of IgG to bile.* Immunology, 2000. **100**(2): p. 245-51.

89. Montoyo, H.P., C. Vaccaro, M. Hafner, R.J. Ober, W. Mueller, and E.S. Ward, *Conditional deletion of the MHC class I-related receptor FcRn reveals the sites of IgG homeostasis in mice.* Proc Natl Acad Sci U S A, 2009. **106**(8): p. 2788-93.
90. Hempstead, B.L., C.W. Parker, and A. Kulczycki, Jr., *The cell surface receptor for immunoglobulin E. Effect of tunicamycin on molecular properties of receptor from rat basophilic leukemia cells.* J Biol Chem, 1981. **256**(20): p. 10717-23.
91. Rodewald, R., *Distribution of immunoglobulin G receptors in the small intestine of the young rat.* J Cell Biol, 1980. **85**(1): p. 18-32.
92. Cooper, P.R., C.M. Kliwinski, R.A. Perkinson, E. Ragwan, J.R. Mabus, G.D. Powers*, et al.*, *The contribution of cell surface FcRn in monoclonal antibody serum uptake from the intestine in suckling rat pups.* Front Pharmacol, 2014. **5**: p. 225.
93. Rodewald, R., *Selective antibody transport in the proximal small intestine of the neonatal rat.* J Cell Biol, 1970. **45**(3): p. 635-40.
94. Morris, B. and R. Morris, *The absorption of 125I-labelled immunoglobulin G by different regions of the gut in young rats.* J Physiol, 1974. **241**(3): p. 761-70.
95. Tiwari, B. and R.P. Junghans, *Functional analysis of the mouse Fcgrt 5′ proximal promoter.* Biochim Biophys Acta, 2005. **1681**(2-3): p. 88-98.
96. Martin, M.G., S.V. Wu, and J.H. Walsh, *Hormonal control of intestinal Fc receptor gene expression and immunoglobulin transport in suckling rats.* J Clin Invest, 1993. **91**(6): p. 2844-9.
97. Kouadjo, K.E., Y. Nishida, J.F. Cadrin-Girard, M. Yoshioka, and J. St-Amand, *Housekeeping and tissue-specific genes in mouse tissues.* BMC Genomics, 2007. **8**: p. 127.
98. Meibohm, B. and H. Zhou, *Characterizing the impact of renal impairment on the clinical pharmacology of biologics.* J Clin Pharmacol, 2012. **52**(1 Suppl): p. 54S-62S.
99. Keizer, R.J., M.O. Karlsson, and A. Hooker, *Modeling and Simulation Workbench for NONMEM: Tutorial on Pirana, PsN, and Xpose.* CPT Pharmacometrics Syst Pharmacol, 2013. **2**: p. e50.
100. Meibohm, B., S. Laer, J.C. Panetta, and J.S. Barrett, *Population pharmacokinetic studies in pediatrics: issues in design and analysis.* AAPS J, 2005. **7**(2): p. E475-87.
101. Deng, R., S. Iyer, F.P. Theil, D.L. Mortensen, P.J. Fielder, and S. Prabhu, *Projecting human pharmacokinetics of therapeutic antibodies from nonclinical data: what have we learned?* MAbs, 2011. **3**(1): p. 61-6.
102. Wahlby, U., E.N. Jonsson, and M.O. Karlsson, *Comparison of stepwise covariate model building strategies in population pharmacokinetic-pharmacodynamic analysis.* AAPS PharmSci, 2002. **4**(4): p. E27.
103. Rajagopalan, P. and M.R. Gastonguay, *Population pharmacokinetics of ciprofloxacin in pediatric patients.* J Clin Pharmacol, 2003. **43**(7): p. 698-710.
104. Lindbom, L., P. Pihlgren, and E.N. Jonsson, *PsN-Toolkit--a collection of computer intensive statistical methods for non-linear mixed effect modeling using NONMEM.* Comput Methods Programs Biomed, 2005. **79**(3): p. 241-57.

105. Kagan, L., J. Zhao, and D.E. Mager, *Interspecies pharmacokinetic modeling of subcutaneous absorption of rituximab in mice and rats.* Pharm Res, 2014. **31**(12): p. 3265-73.
106. Roopenian, D.C., G.J. Christianson, T.J. Sproule, A.C. Brown, S. Akilesh, N. Jung*, et al.*, *The MHC class I-like IgG receptor controls perinatal IgG transport, IgG homeostasis, and fate of IgG-Fc-coupled drugs.* J Immunol, 2003. **170**(7): p. 3528-33.
107. Anderson, G.D. and A.M. Lynn, *Optimizing pediatric dosing: a developmental pharmacologic approach.* Pharmacotherapy, 2009. **29**(6): p. 680-90.
108. Junghans, R.P. and C.L. Anderson, *The protection receptor for IgG catabolism is the beta2-microglobulin-containing neonatal intestinal transport receptor.* Proc Natl Acad Sci U S A, 1996. **93**(11): p. 5512-6.
109. Hansen, L., L.C. Petersen, B. Lauritzen, J.T. Clausen, S.N. Grell, H. Agerso*, et al.*, *Target-mediated clearance and bio-distribution of a monoclonal antibody against the Kunitz-type protease inhibitor 2 domain of Tissue Factor Pathway Inhibitor.* Thromb Res, 2014. **133**(3): p. 464-71.
110. Karlsson, M.O. and R.M. Savic, *Diagnosing model diagnostics.* Clin Pharmacol Ther, 2007. **82**(1): p. 17-20.
111. Savic, R.M. and M.O. Karlsson, *Importance of shrinkage in empirical bayes estimates for diagnostics: problems and solutions.* AAPS J, 2009. **11**(3): p. 558-69.
112. Adkins, B., C. Leclerc, and S. Marshall-Clarke, *Neonatal adaptive immunity comes of age.* Nat Rev Immunol, 2004. **4**(7): p. 553-64.

APPENDIX A. CHAPTER 3 SUPPLEMENTAL RESULTS

Table A-1. Dose effect on the bioavailability estimation of filgrastim with reference bioavailability (F_{ref}) equals to 1.0[a]

IV dose	SC dose (µg/kg)														
(µg/kg)	**0.01**	**0.05**	**0.1**	**0.5**	**1**	**2.5**	**5**	**10**	**50**	**100**	**500**	**1000**	**1500**	**5000**	**10000**
0.01	**0.991**	1.01	1.05	1.59	2.29	3.07	3.44	3.66	3.89	3.92	3.95	3.96	3.96	3.96	3.96
	(-0.936)	(1.49)	(5.21)	(59.4)	(129)	(207)	(244)	(266)	(289)	(292)	(295)	(296)	(296)	(296)	(296)
0.05	0.961	**0.985**	1.02	1.55	2.22	2.98	3.34	3.55	3.77	3.80	3.84	3.84	3.84	3.85	3.85
	(-3.87)	**(-1.52)**	(2.09)	(54.7)	(122)	(198)	(234)	(255)	(277)	(280.)	(284)	(284)	(284)	(285)	(285)
0.1	0.909	0.931	**0.965**	1.46	2.10	2.82	3.15	3.36	3.56	3.60	3.63	3.63	3.63	3.64	3.64
	(-9.13)	(-6.91)	**(-3.49)**	(46.2)	(110.)	(182)	(215)	(236)	(256)	(260.)	(263)	(263)	(263)	(264)	(264)
0.5	0.500	0.512	0.531	0.804	**1.16**	1.55	1.73	1.85	1.96	1.98	1.99	2.00	2.00	2.00	2.00
	(-50.0)	(-48.8)	(-46.9)	(-19.6)	**(15.6)**	(55.0)	(73.4)	(84.7)	(96.0)	(97.8)	(99.4)	(99.7)	(99.8)	(99.9)	(99.9)
1	0.378	0.387	0.402	0.608	**0.875**	1.17	1.31	1.40	1.48	1.50	1.51	1.51	1.51	1.51	1.51
	(-62.2)	(-61.3)	(-59.8)	(-39.2)	**(-12.5)**	(17.3)	(31.3)	(39.8)	(48.3)	(49.7)	(50.9)	(51.1)	(51.2)	(51.3)	(51.3)
2.5	0.306	0.313	0.325	0.492	0.708	**0.949**	1.06	1.13	1.20	1.21	1.22	1.22	1.22	1.22	1.22
	(-69.4)	(-68.7)	(-67.5)	(-50.8)	(-29.2)	**(-5.12)**	(6.20)	(13.1)	(20.0)	(21.1)	(22.1)	(22.3)	(22.3)	(22.4)	(22.4)
5	0.281	0.288	0.298	0.452	0.650	0.871	**0.974**	1.04	1.10	1.11	1.12	1.12	1.12	1.12	1.12
	(-71.9)	(-71.2)	(-70.2)	(-54.8)	(-35.0)	(-12.9)	**(-2.57)**	(3.77)	(10.1)	(11.1)	(12.0)	(12.2)	(12.2)	(12.3)	(12.3)
10	0.267	0.273	0.284	0.430	0.618	0.828	0.927	**0.987**	1.05	1.06	1.07	1.07	1.07	1.07	1.07
	(-73.3)	(-72.7)	(-71.6)	(-57.0)	(-38.2)	(-17.2)	(-7.33)	**(-1.30)**	(4.72)	(5.67)	(6.55)	(6.68)	(6.73)	(6.79)	(6.81)
50	0.254	0.260	0.270	0.409	0.588	0.788	0.882	0.940	**0.997**	1.01	1.01	1.02	1.02	1.02	1.02
	(-74.6)	(-74.0)	(-73.0)	(-59.1)	(-41.2)	(-21.2)	(-11.8)	(-6.03)	**(-0.292)**	(0.613)	(1.45)	(1.57)	(1.62)	(1.69)	(1.70)
100	0.252	0.258	0.268	0.406	0.584	0.782	0.876	0.932	0.989	**0.998**	1.01	1.01	1.01	1.01	1.01
	(-74.8)	(-74.2)	(-73.2)	(-59.4)	(-41.6)	(-21.8)	(-12.4)	(-6.75)	(-1.06)	**(-0.164)**	(0.668)	(0.790)	(0.834)	(0.900)	(0.916)
500	0.250	0.257	0.266	0.403	0.580	0.777	0.869	0.926	0.982	0.991	**0.999**	1.00	1.00	1.00	1.00
	(-75.0)	(-74.3)	(-73.4)	(-59.7)	(-42.0)	(-22.3)	(-13.1)	(-7.42)	(-1.78)	(-0.884)	**(-0.0584)**	(0.0632)	(0.106)	(0.172)	(0.187)
1000	0.250	0.256	0.266	0.402	0.579	0.776	0.868	0.925	0.981	0.990	0.998	1.00	**1.00**	1.00	1.00
	(-75.0)	(-74.4)	(-73.4)	(-59.8)	(-42.1)	(-22.4)	(-13.2)	(-7.52)	(-1.88)	(-0.990)	(-0.165)	(-0.0437)	**(0.000581)**	(0.0648)	(0.0803)
1500	0.250	0.256	0.266	0.402	0.579	0.775	0.868	0.924	0.981	0.990	0.998	0.999	1.00	**1.00**	1.00
	(-75.0)	(-74.4)	(-73.4)	(-59.8)	(-42.1)	(-22.5)	(-13.2)	(-7.56)	(-1.92)	(-1.03)	(-0.203)	(-0.0819)	(-0.0388)	**(0.0266)**	(0.0421)
5000	0.250	0.256	0.265	0.402	0.578	0.775	0.867	0.924	0.980	0.989	0.997	0.999	0.999	1.00	**1.00**
	(-75.0)	(-74.4)	(-73.5)	(-59.8)	(-42.2)	(-22.5)	(-13.3)	(-7.61)	(-1.97)	(-1.09)	(-0.261)	(-0.140)	(-0.0969)	(-0.0316)	**(-0.0161)**
10000	0.250	0.256	0.265	0.402	0.578	0.775	0.867	0.924	0.980	0.989	0.997	0.998	0.999	1.00	**1.00**
	(-75.0)	(-74.4)	(-73.5)	(-59.8)	(-42.2)	(-22.5)	(-13.3)	(-7.62)	(-1.99)	(-1.10)	(-0.275)	(-0.154)	(-0.111)	(-0.0455)	**(-0.0299)**

[a] %Prediction errors are reported in the brackets. Bioavailabilities with minimum bias are reported in bold.
Light gray area demonstrates overestimated bioavailability with prediction error exceeds 20%.
Dark gray area demonstrates underestimated bioavailability with prediction error exceeds 20%.

Table A-2. Dose effect on the bioavailability estimation of denosumab with the reference bioavailability (F_{ref}) equals to 1.0[a]

IV dose	SC dose (mg)													
(mg)	**0.66**	**1.98**	**6**	**6.6**	**14**	**15**	**19.8**	**30**	**60**	**66**	**100**	**120**	**198**	**210**
0.66	**0.919**	1.70	6.57	7.18	11.8	12.2	13.7	15.6	17.9	18.2	19.1	19.4	20.2	20.3
	(-8.13)	(70.1)	(557)	(618)	(1084)	(1123)	(1269)	(1457)	(1691)	(1716)	(1809)	(1843)	(1919)	(1926)
1.98	0.440	**0.815**	3.15	3.44	5.67	5.86	6.56	7.46	8.58	8.70	9.14	9.31	9.67	9.70
	(-56.0)	**(-18.5)**	(215)	(244)	(467)	(486)	(556)	(646)	(758)	(770.)	(814)	(831)	(867)	(870.)
6	0.129	0.239	0.921	**1.01**	1.66	1.71	1.92	2.18	2.51	2.55	2.68	2.72	2.83	2.84
	(-87.1)	(-76.1)	(-7.87)	**(0.649)**	(66.0)	(71.5)	(92.0)	(118)	(151)	(155)	(168)	(172)	(183)	(184)
6.6	0.119	0.220	0.851	**0.930**	1.53	1.58	1.77	2.02	2.32	2.35	2.47	2.52	2.62	2.63
	(-88.1)	(-78.0)	(-14.9)	**(-6.99)**	(53.4)	(58.4)	(77.4)	(102)	(132)	(135)	(147)	(152)	(162)	(163)
14	0.0754	0.140	0.539	0.589	0.972	**1.00**	1.12	1.28	1.47	1.49	1.57	1.60	1.66	1.66
	(-92.5)	(-86.0)	(-46.1)	(-41.1)	(-2.79)	**(0.398)**	(12.4)	(27.9)	(47.1)	(49.1)	(56.8)	(59.5)	(65.8)	(66.4)
15	0.0732	0.136	0.523	0.572	0.943	**0.974**	1.09	1.241	1.43	1.45	1.52	1.55	1.61	1.61
	(-92.7)	(-86.4)	(-47.7)	(-42.8)	(-5.67)	**(-2.58)**	(9.10)	(24.1)	(42.7)	(44.7)	(52.1)	(54.8)	(60.9)	(61.5)
19.8	0.0658	0.122	0.471	0.514	0.848	0.876	**0.981**	1.12	1.283	1.30	1.37	1.39	1.45	1.45
	(-93.4)	(-87.8)	(-52.9)	(-48.6)	(-15.2)	(-12.4)	**(-1.88)**	(11.6)	(28.3)	(30.1)	(36.8)	(39.2)	(44.7)	(45.2)
30	0.0583	0.108	0.417	0.455	0.751	0.776	0.869	**0.988**	1.14	1.15	1.21	1.23	1.28	1.29
	(-94.2)	(-89.2)	(-58.3)	(-54.5)	(-24.9)	(-22.4)	(-13.1)	**(-1.20)**	(13.6)	(15.2)	(21.1)	(23.3)	(28.1)	(28.6)
60	0.0510	0.0944	0.365	0.398	0.657	0.678	0.760	0.864	**0.994**	1.01	1.06	1.08	1.12	1.12
	(-94.9)	(-90.6)	(-63.5)	(-60.2)	(-34.3)	(-32.2)	(-24.0)	(-13.6)	**(-0.621)**	(0.773)	(5.94)	(7.81)	(12.0)	(12.4)
66	0.0503	0.0931	0.360	0.393	0.648	0.669	0.750	0.853	0.981	**0.994**	1.05	1.06	1.11	1.11
	(-95.0)	(-90.7)	(-64.0)	(-60.7)	(-35.2)	(-33.1)	(-25.0)	(-14.7)	(-1.95)	**(-0.572)**	(4.53)	(6.37)	(10.5)	(10.9)
100	0.0479	0.0887	0.343	0.374	0.618	0.638	0.714	0.812	0.934	0.947	**0.996**	1.01	1.05	1.06
	(-95.2)	(-91.1)	(-65.7)	(-62.6)	(-38.2)	(-36.2)	(-28.6)	(-18.8)	(-6.57)	(-5.26)	**(-0.407)**	(1.35)	(5.32)	(5.70)
120	0.0471	0.0872	0.337	0.368	0.607	0.627	0.702	0.799	0.919	0.932	0.979	**0.997**	1.04	1.04
	(-95.3)	(-91.3)	(-66.3)	(-63.2)	(-39.3)	(-37.3)	(-29.8)	(-20.1)	(-8.14)	(-6.85)	(-2.07)	**(-0.342)**	(3.56)	(3.94)
198	0.0454	0.0841	0.325	0.355	0.585	0.604	0.677	0.770	0.885	0.898	0.944	0.960	0.998	**1.00**
	(-95.5)	(-91.6)	(-67.5)	(-64.5)	(-41.5)	(-39.6)	(-32.3)	(-23.0)	(-11.5)	(-10.2)	(-5.63)	(-3.96)	(-0.202)	**(0.162)**
210	0.0453	0.0838	0.324	0.354	0.583	0.602	0.674	0.767	0.882	0.894	0.940	0.957	0.994	**0.998**
	(-95.5)	(-91.6)	(-67.6)	(-64.6)	(-41.7)	(-39.8)	(-32.6)	(-23.3)	(-11.8)	(-10.6)	(-5.97)	(-4.30)	(-0.560)	**(-0.197)**

[a] %Prediction errors are reported in the brackets. Bioavailabilities with minimum bias are reported in bold.
Light gray area demonstrates overestimated bioavailability with prediction error exceeds 20%.
Dark gray area demonstrates underestimated bioavailability with prediction error exceeds 20%.

APPENDIX B. CHAPTER 4 SUPPLEMENTAL RESULTS

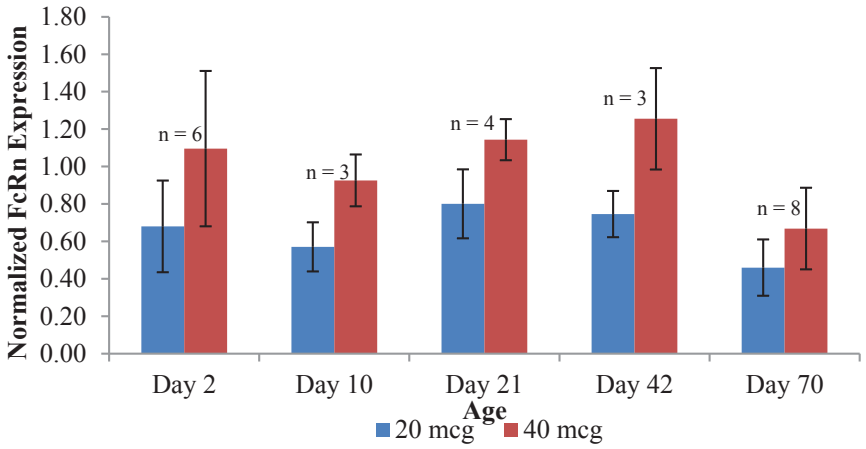

Figure B-1. Ontogeny of FcRn protein expression in mouse skin
No significant difference in the relative FcRn protein expression was observed in the skin of 2-, 10-, 21-, 42-, and 70-day old mice. The difference of relative FcRn protein expression between 20 µg and 40 µg loading sample sets was statistically significant ($p < 0.0001$).

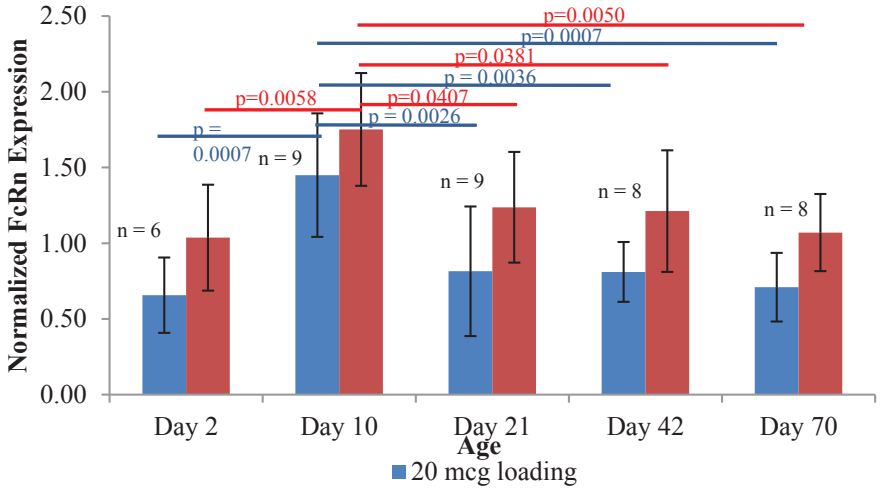

Figure B-2. Ontogeny of FcRn protein expression in mouse liver
Relative expression of FcRn protein in mouse liver was significantly increased in 10-day old mice compared to other age groups. The statistical p-values are reported above the line associated with each pair of comparison. The difference of relative FcRn protein expression between 20 µg and 40 µg loading sample sets was statistically significant ($p < 0.0001$).

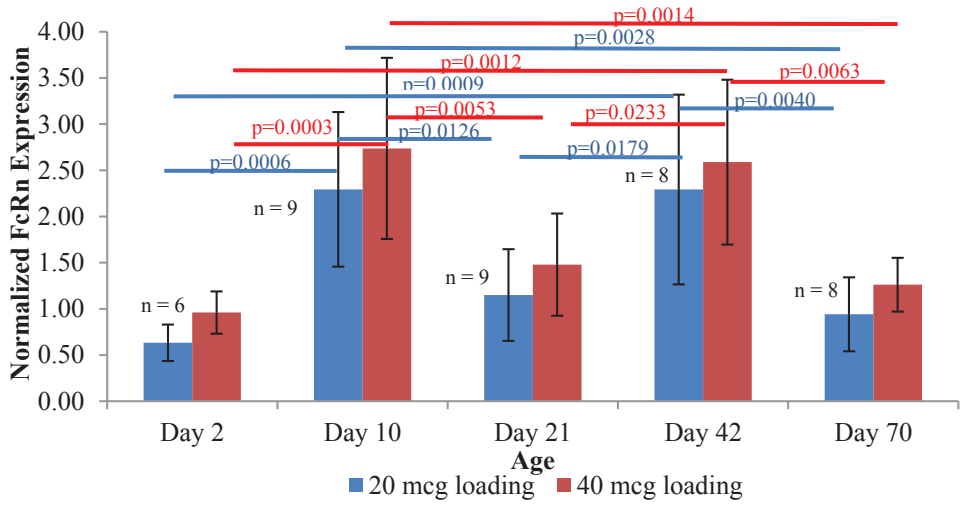

Figure B-3. Ontogeny of FcRn protein expression in mouse kidney
Relative expression of FcRn protein in mouse kidney was significantly increased in 10- and 42-day old mice compared to other age groups. The significant statistical p-values are reported above the line associated with each pair of comparison. The relative FcRn protein expressions in 20 µg and 40 µg loading sample sets were statistically significantly different (p = 0.0240).

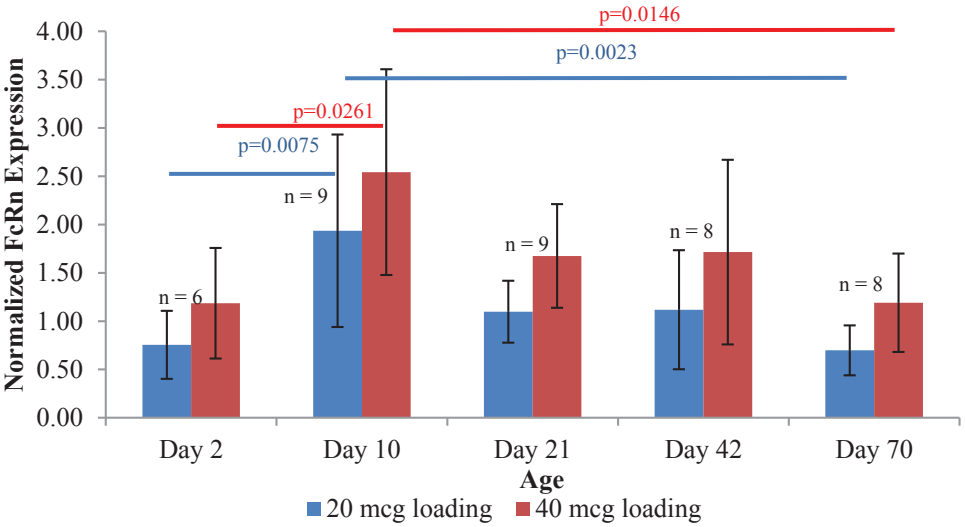

Figure B-4. Ontogeny of FcRn protein expression in mouse lung
Relative expression of FcRn protein in mouse lung was significantly increased in 10-day old mice compared to 2- and 70-day old animals. The significant statistical p-values are reported above the line associated with each pair of comparison. The relative FcRn protein expressions in 20 µg and 40 µg loading sample sets were statistically significantly different (p = 0.0005).

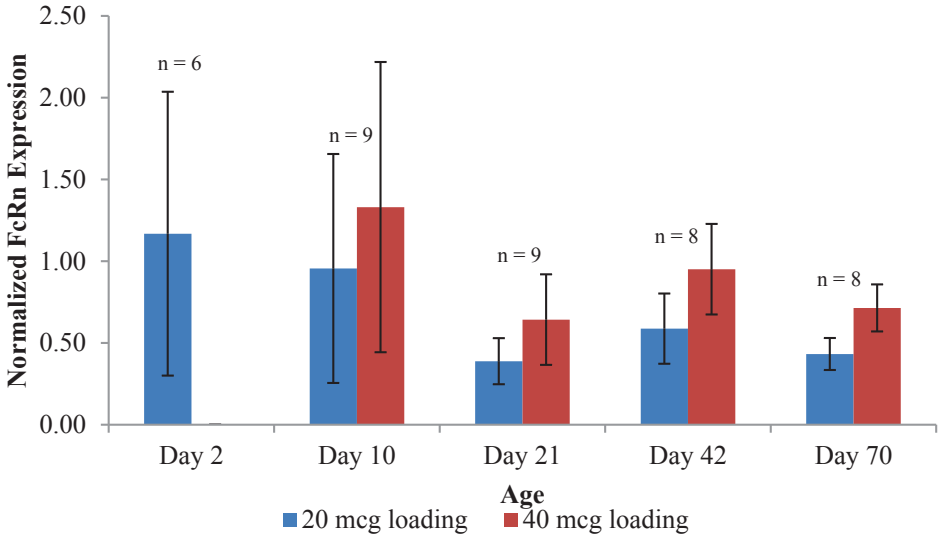

Figure B-5. Ontogeny of FcRn protein expression in mouse spleen
There was no significant difference in the relative expression of FcRn protein in mouse spleen among all age groups. The difference of relative FcRn protein expressions between 20 µg and 40 µg loading sample sets was statistically significant ($p = 0.008$). There was no result of 40 µg loading set in spleen from 2-day old mice.

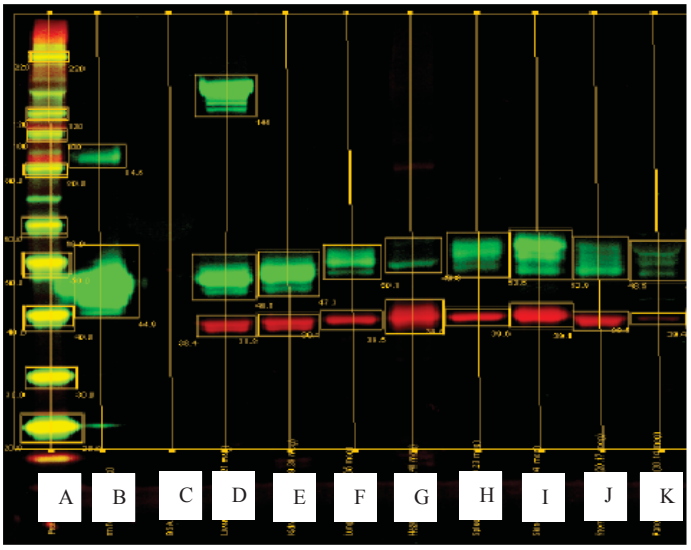

Figure B-6. Protein expression of FcRn and GAPDH in various organs of a 70 days old mouse
Protein that was loaded in each lane were protein ladder (A), recombinant mouse FcRn (positive control; B), Bovine serum albumin (negative control; C), total protein extracts from liver (D), kidney (E), lung (F), heart (G), spleen (H), skin (I), stomach (J), and pancreas (K) of a 70 days old C57BL/6J mouse.

Table B-1. Expression ratio of FcRn monomer and dimer per total FcRn protein expression and total FcRn expression in mouse liver across different age groups

Age	Monomer		Complex		Monomer + Complex	
	Mean	%RSD	Mean	%RSD	Mean	%RSD
Day 2	0.84	15.58	0.16	83.57	0.73	36.96
Day 10	0.93	7.37	0.07[a]	103.11	1.57	31.08
Day 21	0.71	22.91	0.29	56.30	1.13	42.64
Day 42	0.70	24.80	0.30	58.07	1.19	28.99
Day 70	0.68	23.88	0.32	51.13	1.02	34.19

[a] $p < 0.005$ when compared to mice from day 21, and 70 age groups

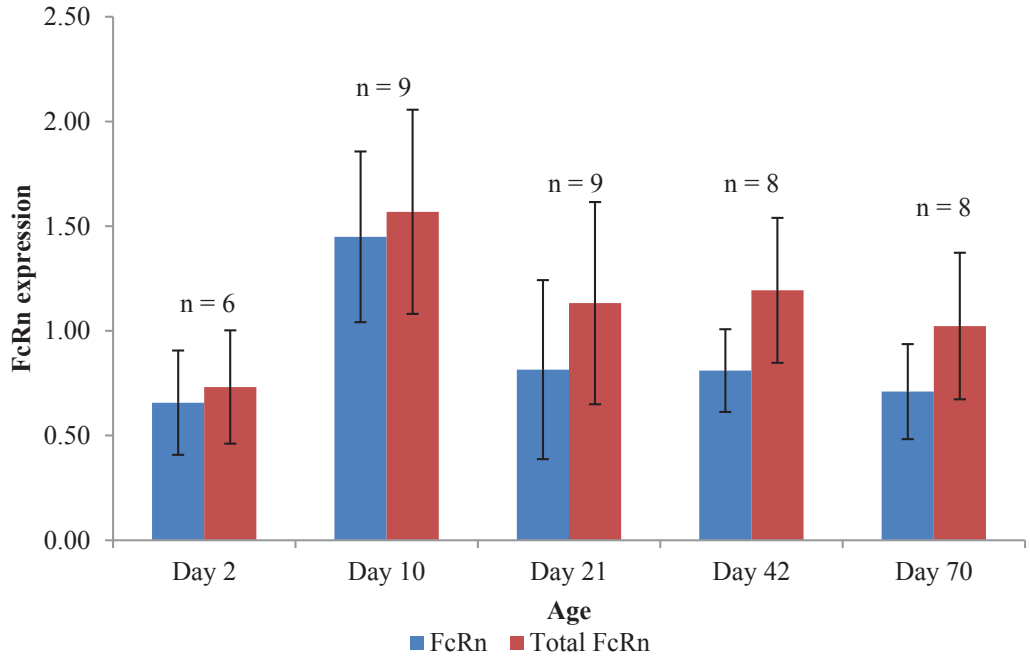

Figure B-7. Expression of FcRn monomer and total FcRn protein in mouse liver across all age groups

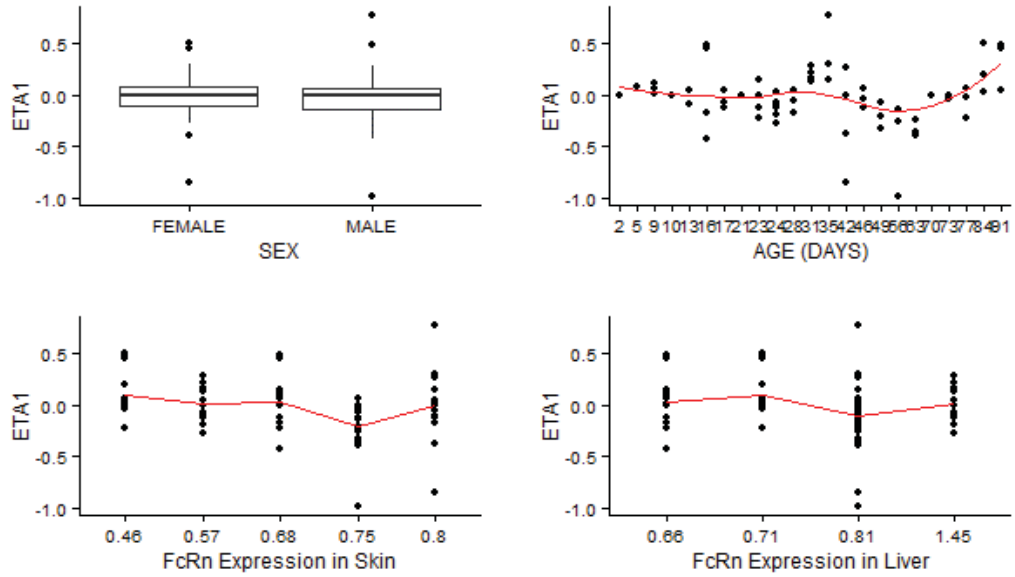

Figure C-1. Correlation between inter-subject variability on CL (ETA1) and covariates (sex, age, FcRn expression in skin, and FcRn expression in liver)

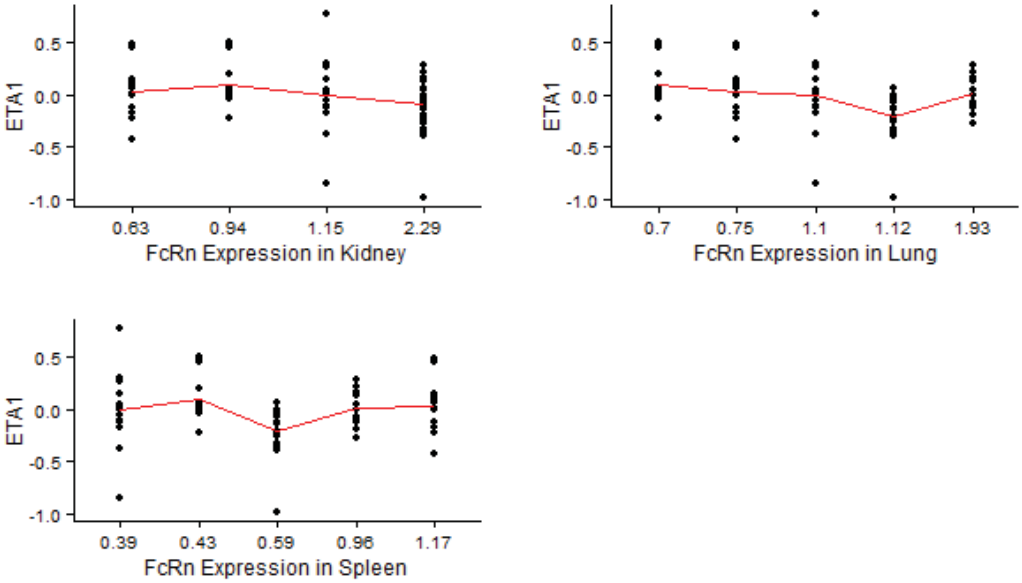

Figure C-2. Correlation between inter-subject variability on CL (ETA1) and covariates (FcRn expressions in kidney, lung, and spleen)

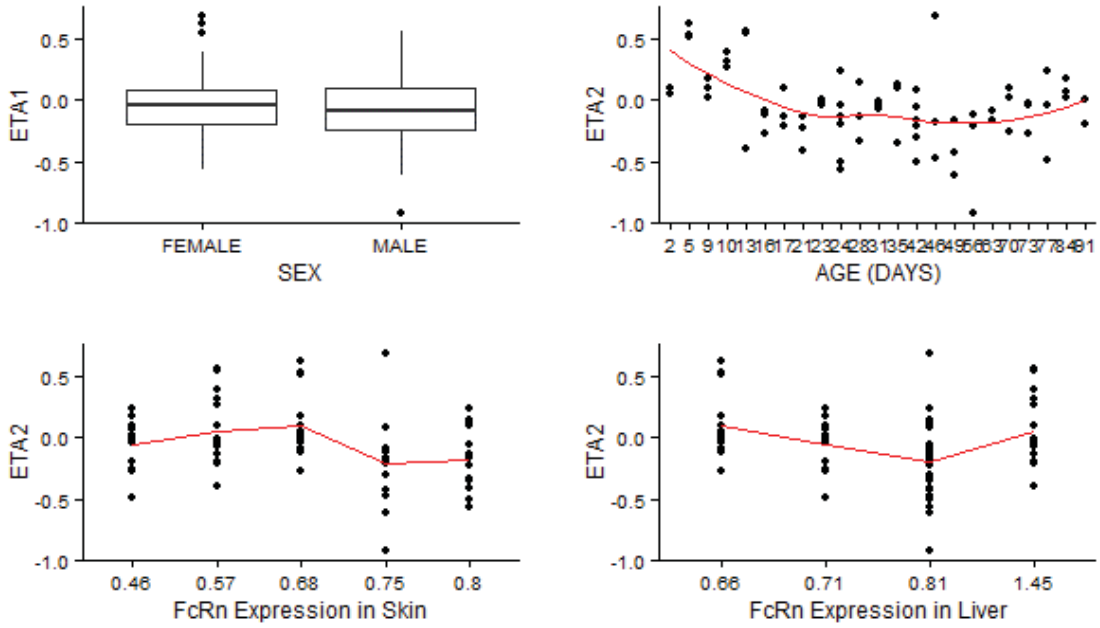

Figure C-3. Correlation between inter-subject variability on V (ETA2) and covariates (sex, age, FcRn expression in skin, and FcRn expression in liver)

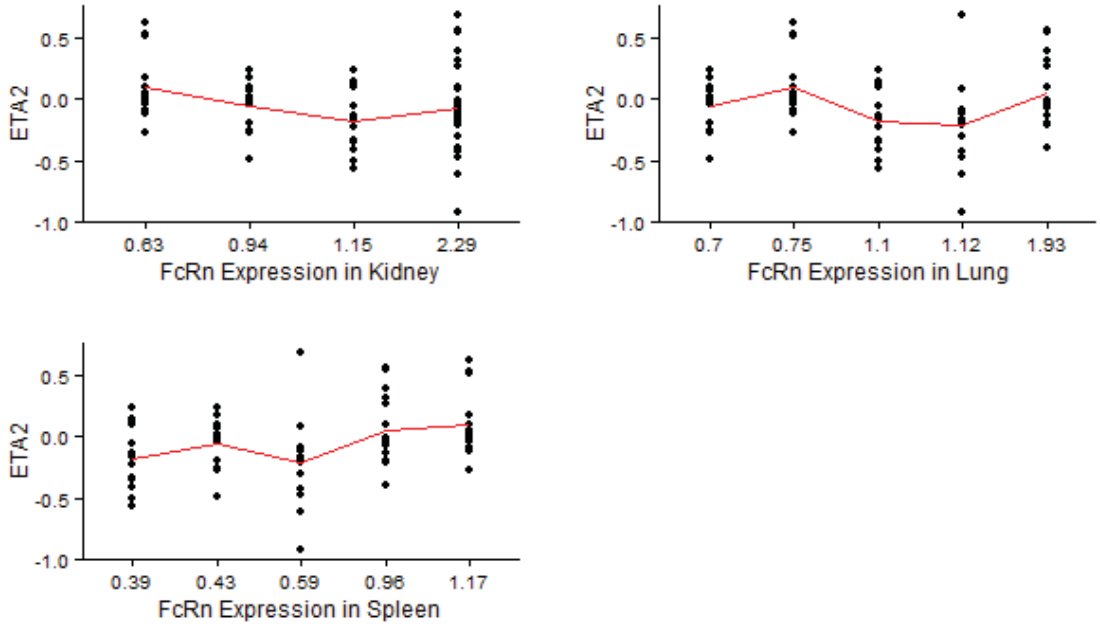

Figure C-4. Correlation between inter-subject variability on V (ETA2) and covariates (FcRn expressions in kidney, lung, and spleen)

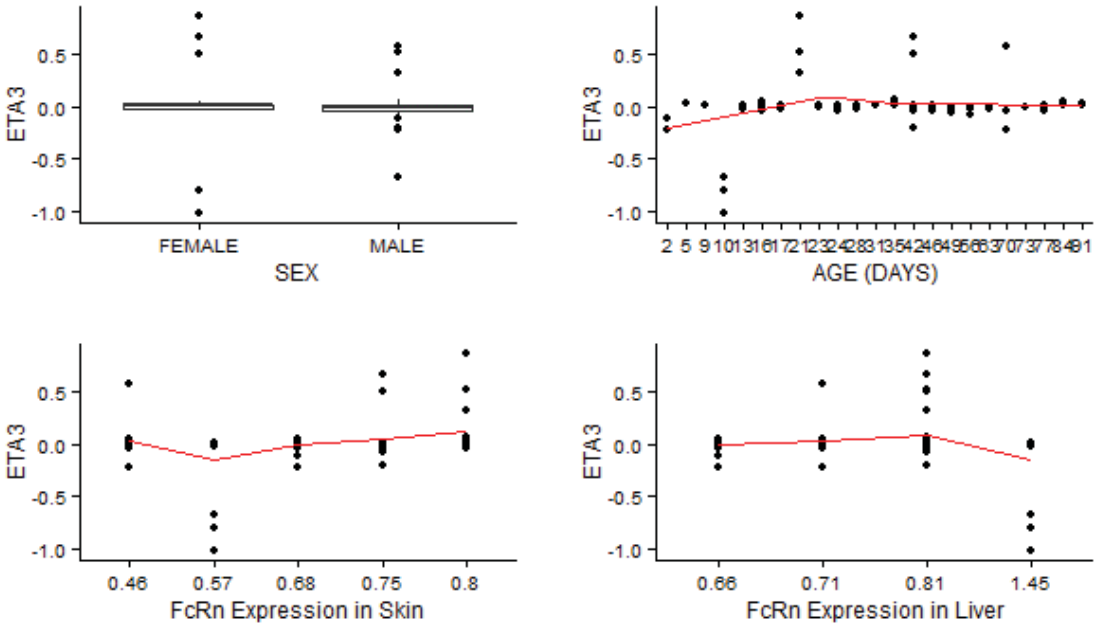

Figure C-5. Correlation between inter-subject variability on K_a (ETA3) and covariates (sex, age, FcRn expression in skin, and FcRn expression in liver)

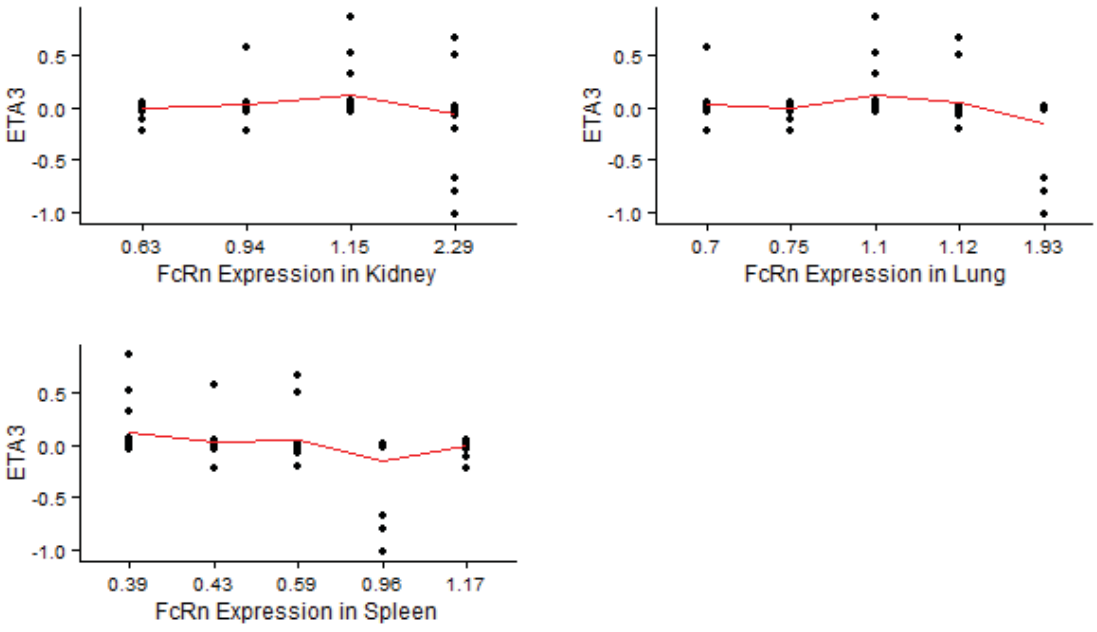

Figure C-6. Correlation between inter-subject variability on K_a (ETA3) and covariates (FcRn expressions in kidney, lung, and spleen)

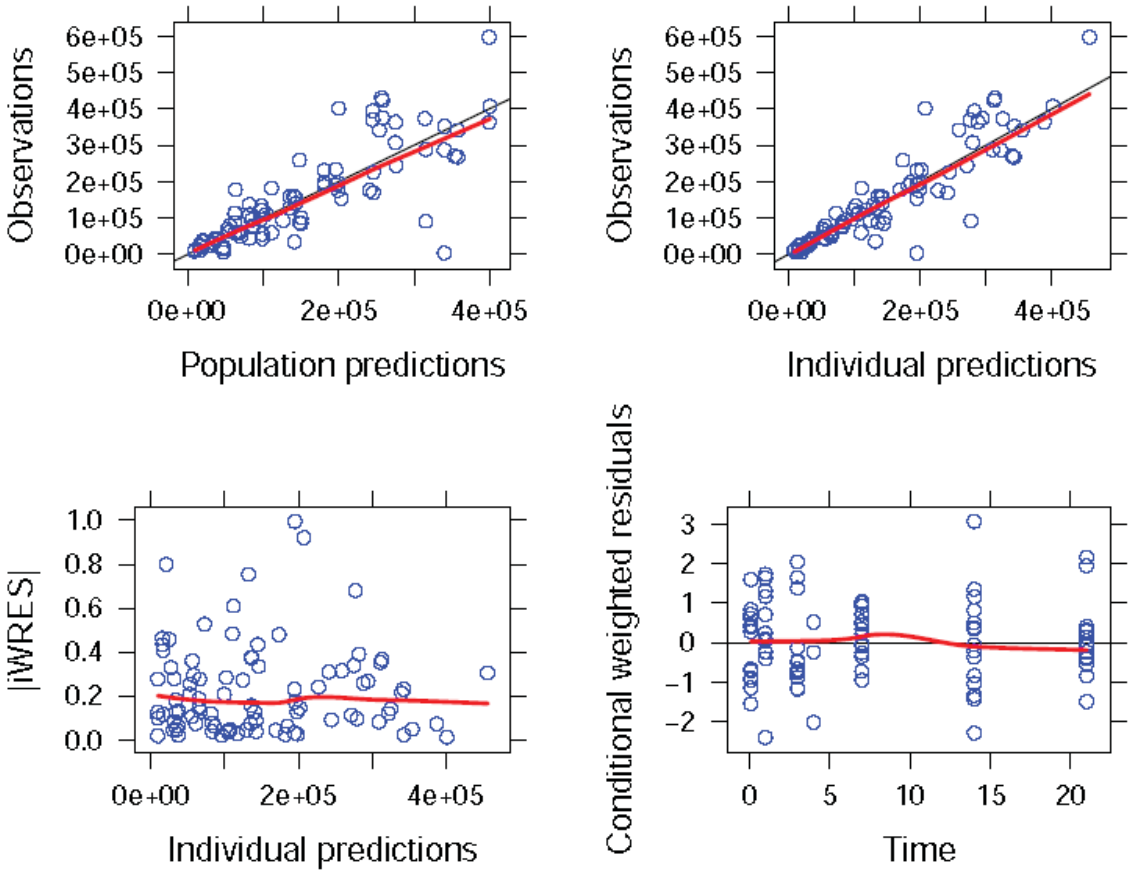

Figure C-7. Goodness-of-fit plots of the final model applied in full dataset

VITA

Wararat Limothai, daughter of Mr. Sirichai Limothai and Mrs. Narumon Sae-Ung, was born in 1981 in Bangkok, Thailand. She graduated from Faculty of Pharmaceutical Sciences, Chulalongkorn University with B.Sc. degree in 2004. After graduation, she worked as a researcher in Research and Development Institute, The Government Pharmaceutical Organization (GPO) in Thailand. After working for 4 years, she received a scholarship from GPO for pursuing a Ph.D. degree. In 2008, she enrolled in the Ph.D. program at the University of Tennessee Health Science Center under the direction of Dr. Bernd Meibohm in the Department of Pharmaceutical Sciences. In 2014, she moved back to Thailand and started working as a senior researcher in R&D Institute, GPO. She anticipates completing her Ph.D. by December 2015.